Magnetism to Spintronics

Dr. Shang-Fan Lee
Institute of Physics, Academia Sinica

Introduction to Solid State Physics
Kittel 8th ed
Chap. 11-13,

Solid State Physics
Ashcroft and Mermin
Chap. 31-33,

Condensed Matter Physics
Marder 2nd ed
Chap. 24-26,

Why do most broken permanent magnets repel each other?

Cooperative phenomena

- Elementary excitations in solids describe the response of a solid to a perturbation
  - Quasiparticles

    usually fermions, resemble the particles that make the system, e.g. quasi-electrons

  - Collective excitations

    usually bosons, describe collective motions

    use second quantization with Fermi-Dirac or Bose-Einstein statistics
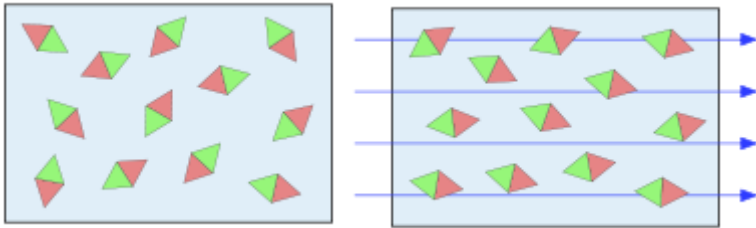
Magnetism

- the Bohr–van Leeuwen theorem

    when statistical mechanics and classical mechanics are applied consistently, the thermal average of the magnetization is always zero.
- Magnetism in solids is solely a quantum mechanical effect
- Origin of the magnetic moment:
    - Electron spin $\vec{S}$
    - Electron orbital momentum $\vec{L}$
- From (macroscopic) response to external magnetic field $\vec{H}$
    - Diamagnetism $\chi < 0, \chi \sim 1 \times 10^{-6}$, insensitive to temperature
    - Paramagnetism $\chi > 0$, $\chi = \dfrac{C}{T}$ Curie law

      $\chi = \dfrac{C}{T+\Delta}$ Curie-Weiss law
    - Ferromagnetism exchange interaction (quantum)
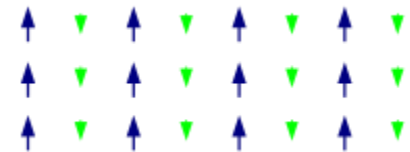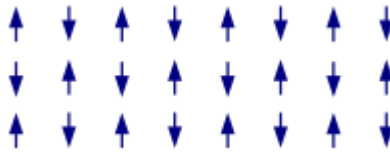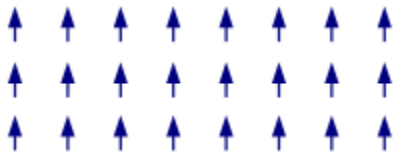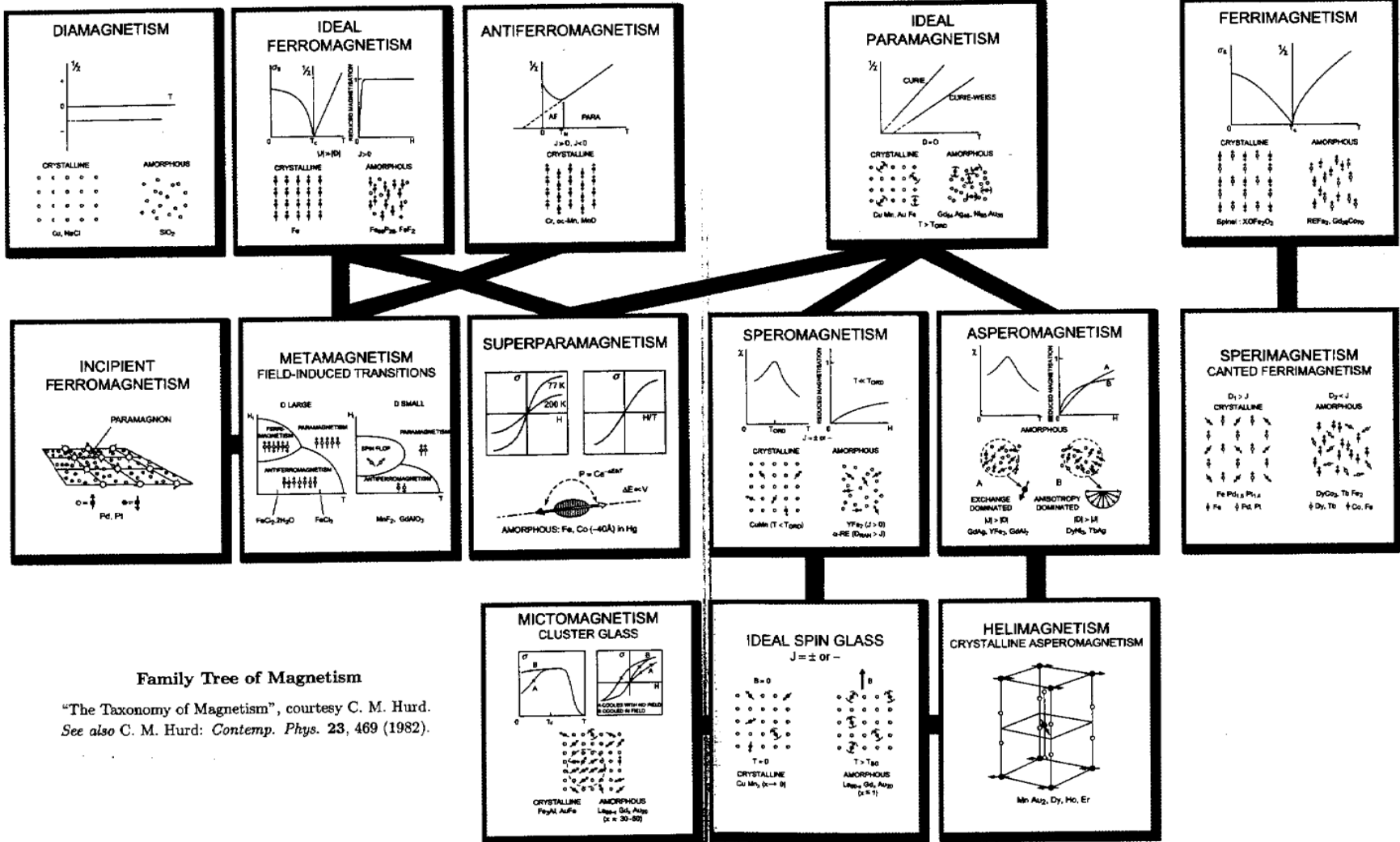
Magnetism

巨觀： 順磁性
Paramagnetism

逆磁性
diamagnetism

微觀： 鐵磁性
Ferromagnetism

反鐵磁性
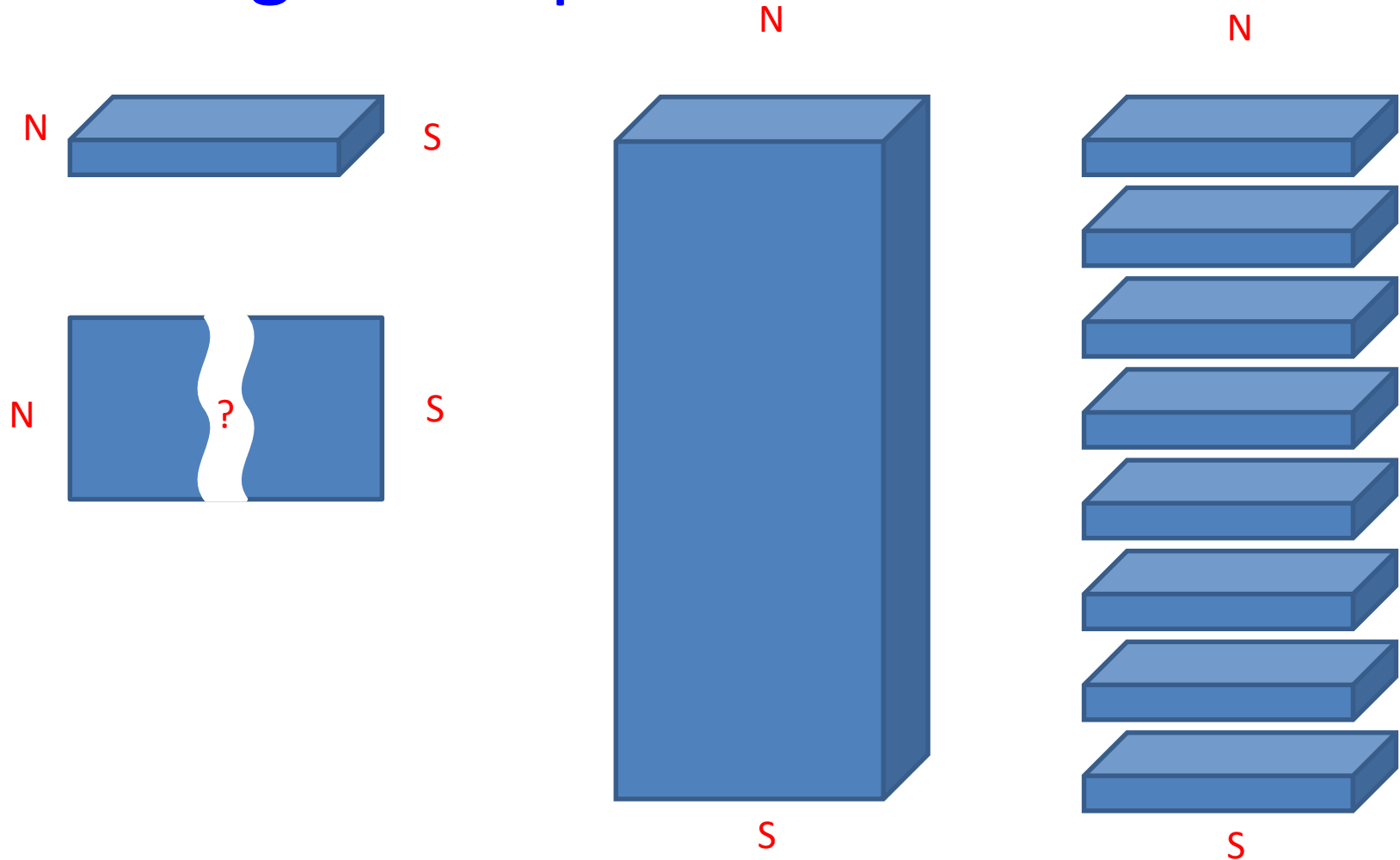**Antiferromagnetism**

亞鐵磁性
Ferrimagnetism

Family Tree of Magnetism

Family Tree of Magnetism

"The Taxonomy of Magnetism", courtesy C. M. Hurd.
See also C. M. Hurd: *Contemp. Phys.* **23**, 469 (1982).

Why do most broken permanent magnets repel each other?

- Classical and quantum theory for diamagnetism
  - Calculate $\langle r^2 \rangle$
- Classical and quantum theory for paramagnetism
  - Superparamagnetism, Langevin function
  - Hund's rules
  - Magnetic state $^{2S+1}L_J$
  - Crystal field
  - Quenching of orbital angular momentum L_z
    - **Angular momentum operator**
    - **Spherical harmonics**
  - Jahn-Teller effect
 - Paramagnetic susceptibility of conduction electrons

- Ferromagnetism
  - Microscopic – ferro, antiferro, ferri magnetism
  - Exchange interaction
  - Exchange splitting – source of magnetization
    two-electron system spin-independent Schrodinger equation
  - Type of exchange: direct exchange, super exchange, indirect exchange, itinerant exchange
  - Spin Hamiltonian and Heisenberg model
  - Molecular-field (mean-field) approximation

Critical phenomena

Universality. Divergences near the critical point are identical in a variety of apparently different physical systems and also in a collection of simple models.
Scaling. The key to understanding the critical point lies in understanding the relationship between systems of different sizes. Formal development of this idea led to the *renormalization group* of Wilson (1975).
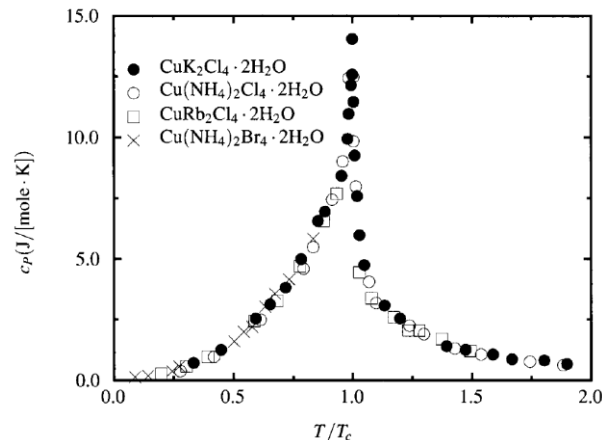
Landau Free Energy
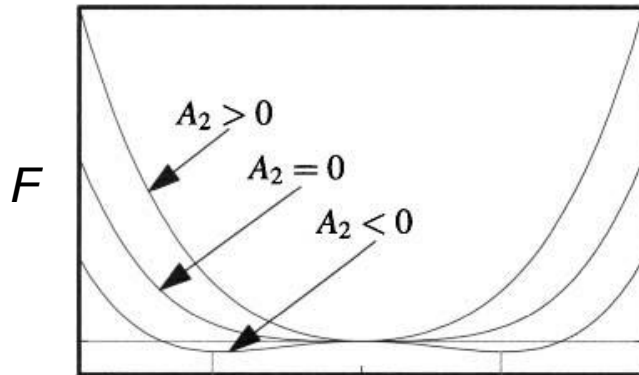
$$F(M, T) = A_0(T) + A_2(T)M^2 + A_4(T)M^4 + HM.$$

$$t \equiv \frac{T - T_C}{T_C}$$

$$F = a_2tM^2 + a_4M^4 + HM.$$

Molar heat capacities of four ferromagnetic copper salts versus scaled temperature T/T_c. [Source Jongh and Miedema (1974).]

Correspondence between Liquids and Magnets

- **Specific Heat—** α
- **Magnetization and Density—** β
- **Compressibility and** *Susceptibility—* γ
- **Critical Isotherm—** δ
- **Correlation Length —** ν
- **Power-Law Decay at Critical Point—** η

Summary of critical exponents, showing correspondence between fluid-gas systems, magnetic systems, and the three-dimensional Ising model.

Exponent	Fluid	Magnet	Mean Field Theory	Experiment	3d Ising
α	$C_V \sim |t|^{-\alpha}$	$C_V \sim |t|^{-\alpha}$	discontinuity	0.11–0.12	0.110
β	$\Delta n \sim |t|^{\beta}$	$M \sim |t|^{\beta}$	$\frac{1}{2}$	0.35–0.37	0.325
γ	$K_T \sim |t|^{-\gamma}$	$\chi \sim |t|^{-\gamma}$	1	1.21–1.35	1.241
δ	$P \sim |\Delta n|^{\delta}$	$|H| \sim |M|^{\delta}$	3	4.0–4.6	4.82
ν	$\xi \sim |t|^{-\nu}$	$\xi \sim |t|^{-\nu}$		0.61–0.64	0.63
η	$g(r) \sim r^{-1-\eta}$	$g(r) \sim r^{-1-\eta}$		0.02–0.06	0.032

Source: Vicentini-Missoni (1972) p. 67, Cummins (1971), p. 417, and Goldenfeld (1992) p. 384.

Relations Among Exponents

$$\alpha + 2\beta + \gamma = 2 \qquad\qquad (2 - \eta)\nu = \gamma$$

$$\delta = 1 + \frac{\gamma}{\beta} \qquad\qquad 2 - \alpha = 3\nu$$

- # Stoner band ferromagnetism

Teodorescu, C. M.; Lungu, G. A. (November 2008). "Band ferromagnetism in systems of variable dimensionality". *Journal of Optoelectronics and Advanced Materials* **10** (11): 3058–3068.

$$\mathcal{E} = \int_0^{\mathcal{E}_F - \Delta} d\mathcal{E}' \, D(\mathcal{E}')\mathcal{E}' + \frac{1}{2} \int_{\mathcal{E}_F - \Delta}^{\mathcal{E}_F + \Delta} d\mathcal{E}' \, D(\mathcal{E}')\mathcal{E}' - \frac{1}{2}nJ \langle S \rangle^2$$

$$\langle S \rangle = \frac{1}{2n} \int_{\mathcal{E}_F - \Delta}^{\mathcal{E}_F + \Delta} d\mathcal{E}' \, \frac{1}{2}D(\mathcal{E}') = \frac{1}{2n}D(\mathcal{E}_F)\Delta$$

$$\frac{\partial \mathcal{E}}{\partial \Delta}\bigg|_{\mathcal{E}_F} = \Delta D(\mathcal{E}_F) - \frac{J}{4n}D(\mathcal{E}_F)^2\Delta$$

$$\frac{\partial \mathcal{E}}{\partial \Delta}\bigg|_{\mathcal{E}_F} = 0 \Rightarrow \frac{J}{n}D(\mathcal{E}_F) = 4$$

Ferromagnetic elements: 鐵 Fe, 鈷 Co, 鎳 Ni, 釓 Gd, 鏑 Dy, 錳 Mn, 鈀 Pd ??

Elements with ferromagnetic properties
合金, alloys
錳氧化物 MnOx, ……

Platonic solid

   In **geometry**, a Platonic solid is a **convex polyhedron** that is **regular**, in the sense of a **regular polygon**. Specifically, the faces of a Platonic solid are **congruent** regular polygons, with the same number of faces meeting at each **vertex**; thus, all its edges are congruent, as are its vertices and angles. There are precisely five Platonic solids (shown below):

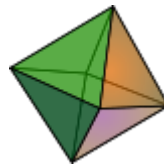   The name of each figure is derived from its number of faces: respectively 4, 6, 8, 12, and 20.

   The **aesthetic beauty** and **symmetry** of the Platonic solids have made them a favorite subject of **geometers** for thousands of years. They are named for the **ancient Greek philosopher** **Plato** who theorized that the **classical elements** were constructed from the regular solids.

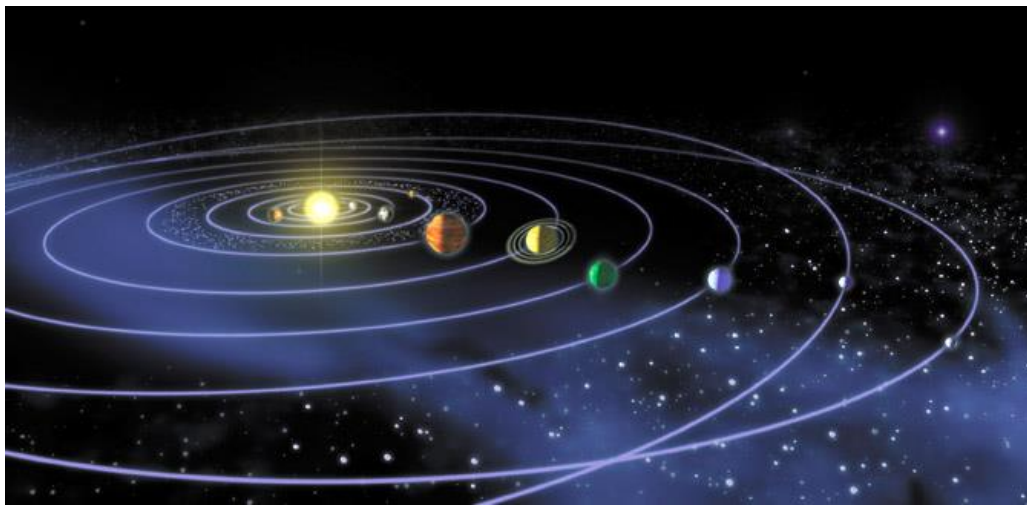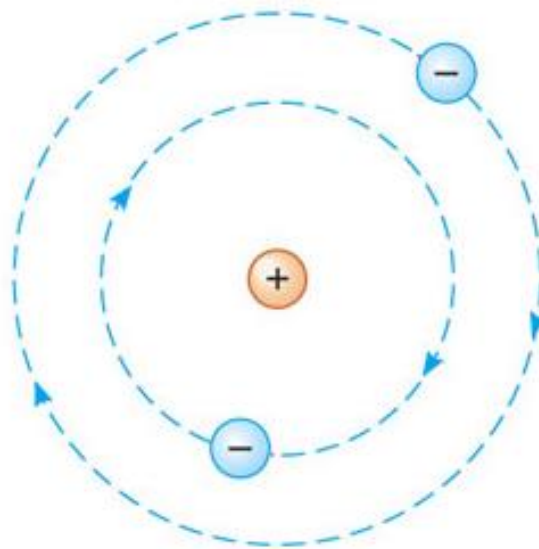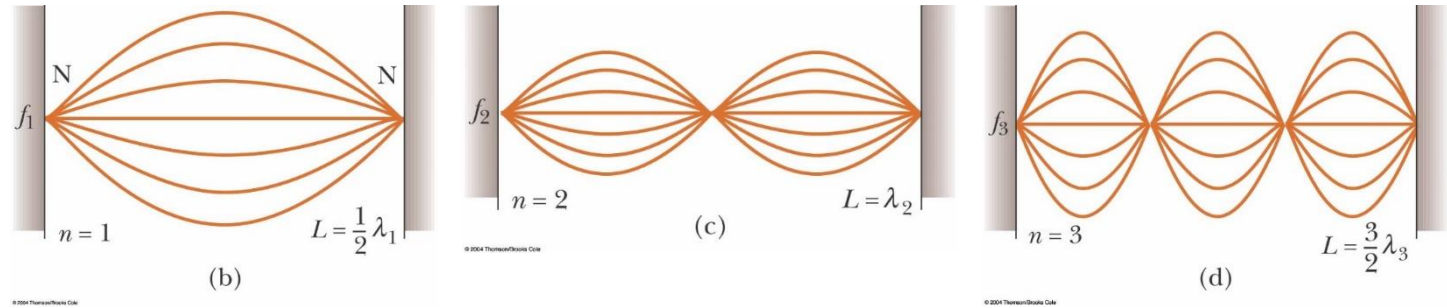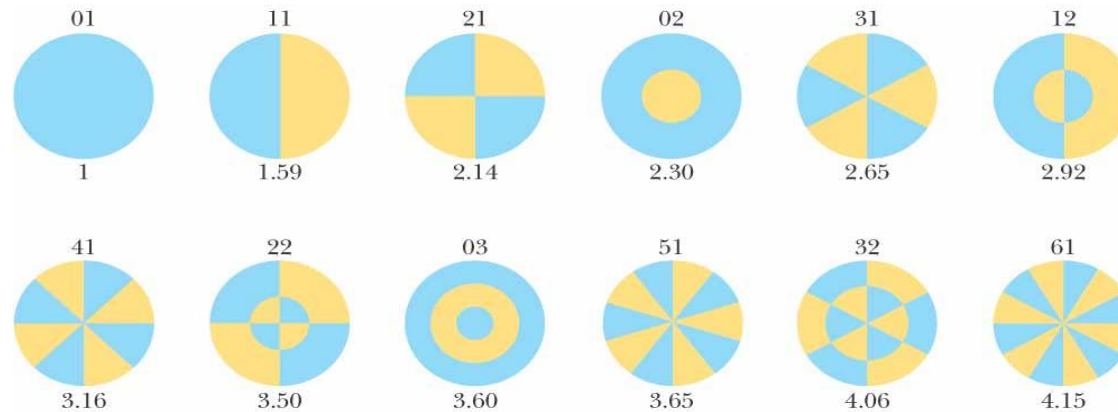|				
Tetrahedron	Cube hexahedron	Octahedron	Dodecahedron	Icosahedron

Solar system

Electronic orbit

s, p electron orbits
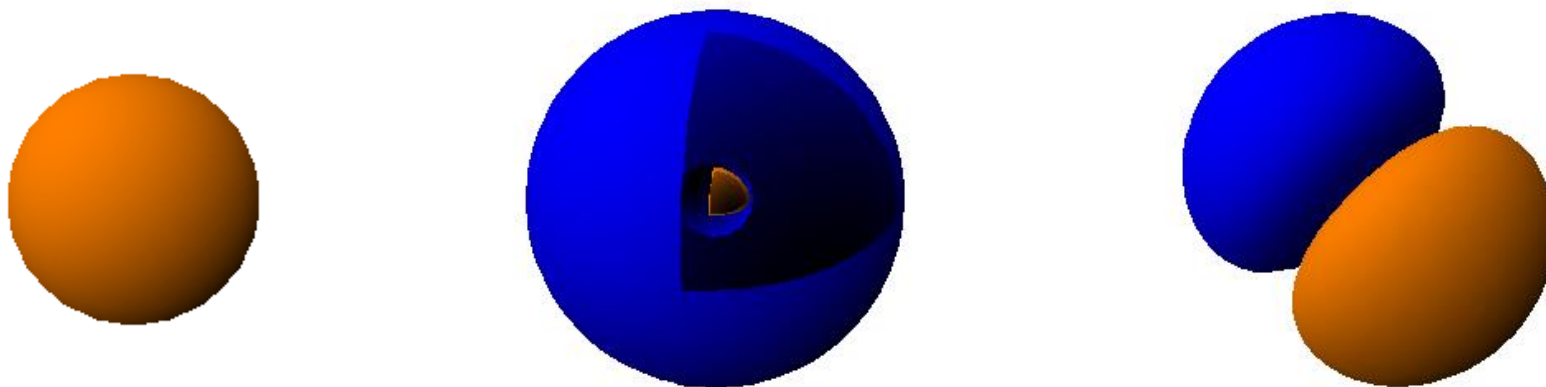
Resonance

One-dimensional

Two-dimensional

Three-dimensional   Hydrogen atom

f_1 N   N $n = 1$ $L = \frac{1}{2}\lambda_1$ (b)

f_2 $n = 2$ $L = \lambda_2$ (c)

f_3 $n = 3$ $L = \frac{3}{2}\lambda_3$ (d)

01   11   21   02   31   12
1   1.59   2.14   2.30   2.65   2.92

41   22   03   51   32   61
3.16   3.50   3.60   3.65   4.06   4.15

Elements of the medium moving out of the page at an instant of time.

Elements of the medium moving into the page at an instant of time.
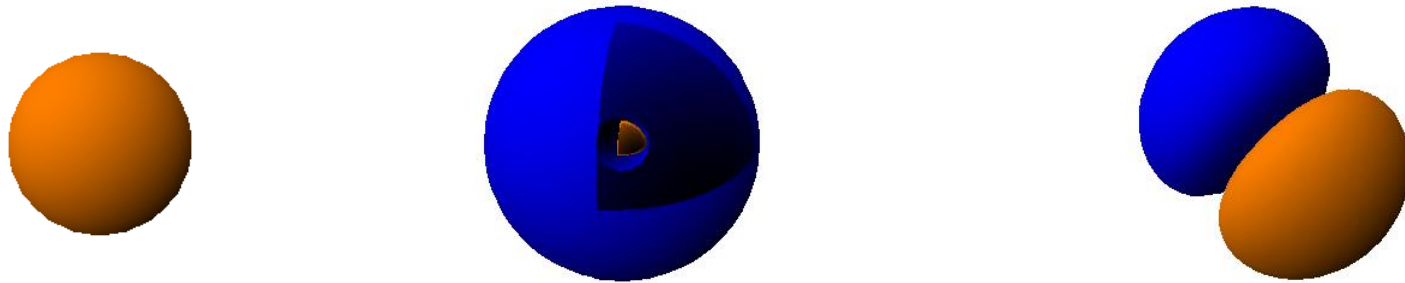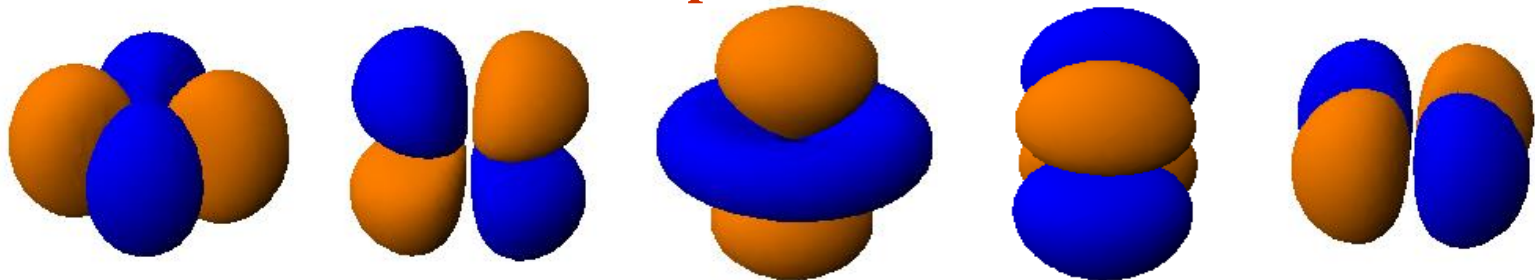
© 2004 Thomson/Brooks Cole

3d transition metals:

Mn atom has 5 d ↑ electrons   Bulk Mn is NOT magnetic

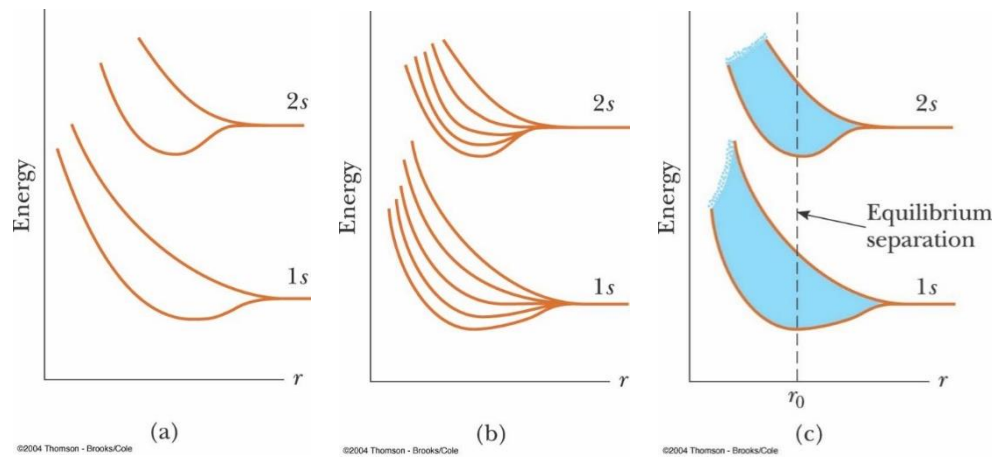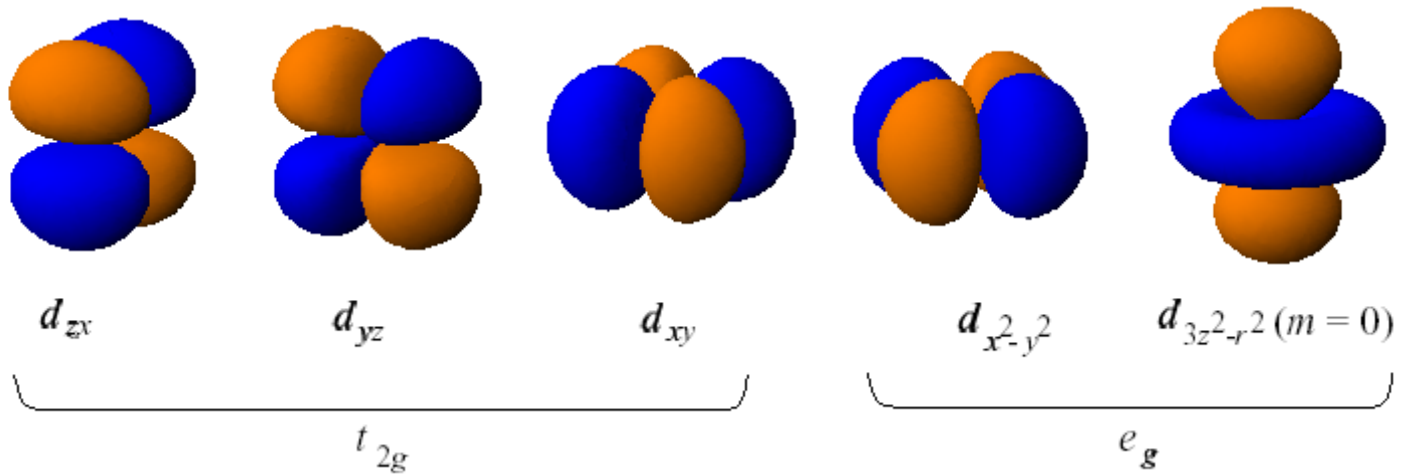**s, p electron orbital**

3d electron distribution in real space

**Co atom has 5 d ↑electrons and 2 d ↓ electrons
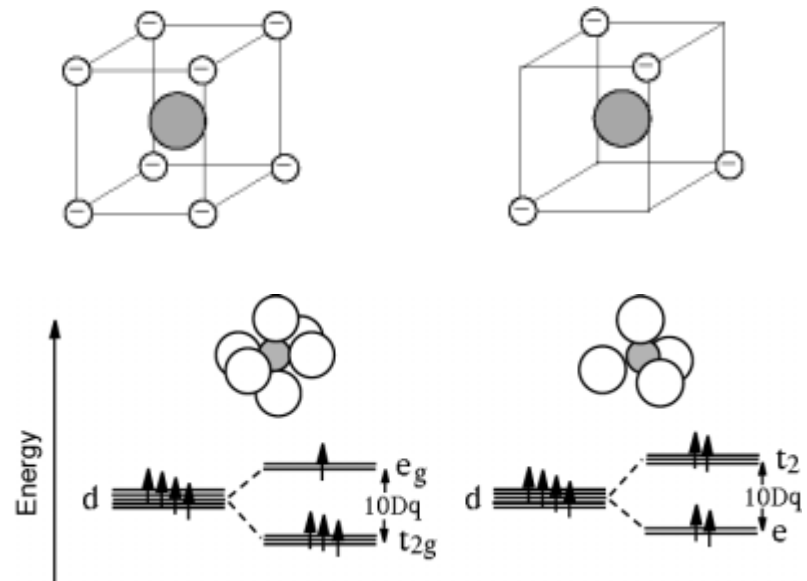Bulk Co is magnetic.**

Orbital viewer

d orbitals

$l = 2$

d_{zx} d_{yz} d_{xy} $d_{x^2-y^2}$ $d_{3z^2-r^2}\ (m = 0)$

t_{2g} e_g

Energy

2s

1s

(a)

©2004 Thomson - Brooks/Cole

Energy

2s

1s

(b)

©2004 Thomson - Brooks/Cole

Energy

2s

1s

Equilibrium separation

r_0

(c)

©2004 Thomson - Brooks/Cole

Crystal-field splitting

Energy

d

e_g

t_{2g}

10Dq

d

t_2

e

10Dq

Stern-Gerlach Experiment

Beam of
silver atoms

Oven

Photographic
plate

Nonuniform
magnetic field

Classical
pattern

Actual
pattern
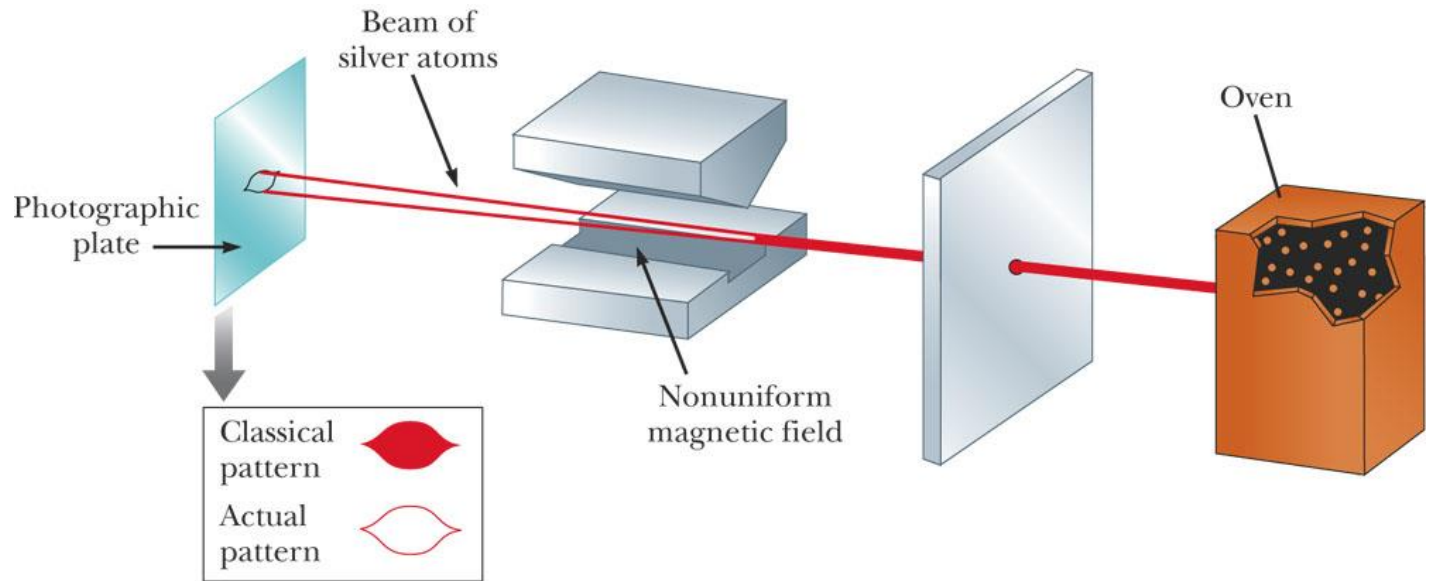
© 2006 Brooks/Cole - Thomson

z
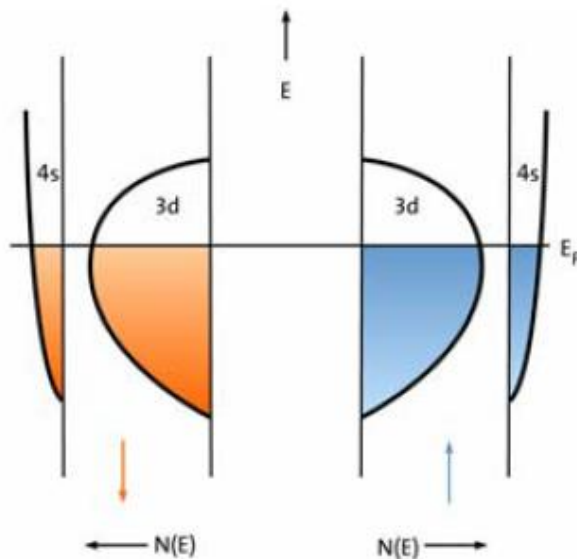
$\vec{S}$

z

$\vec{S}$

(a)

(b)
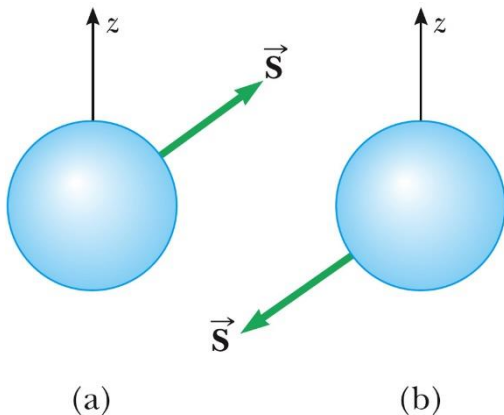
There are two kinds of electrons: spin-up and spin-down.

Stern and Gerlach: How a Bad Cigar Helped Reorient Atomic Physics
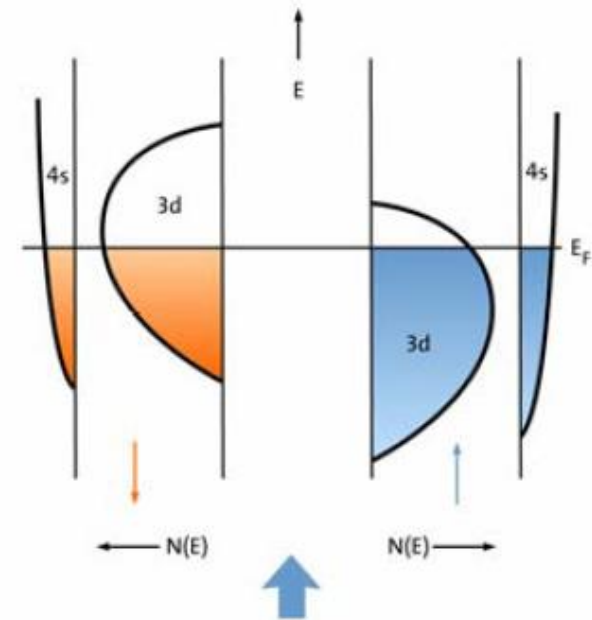Physics Today 56, 53 (2003) 10.1063/1.1650229

Stoner criterion for ferromagnetism:

I N(E_F) > 1, I is the **Stoner exchange parameter** and N(E_F) is the density of states at the Fermi energy.

For the non-magnetic state there are identical density of states for the two spins.

For a ferromagnetic state, N↑ > N↓. The polarization is indicated by the thick blue arrow.

Schematic plot for the energy band structure of 3d transition metals.

Teodorescu and Lungu, "Band ferromagnetism in systems of variable dimensionality".
J Optoelectronics and Adv. Mat. **10,** 3058–3068 (2008).

- # Stoner band ferromagnetism

Teodorescu, C. M.; Lungu, G. A. (November 2008). "Band ferromagnetism in systems of variable dimensionality". *Journal of Optoelectronics and Advanced Materials* **10** (11): 3058–3068.

$$\mathcal{E} = \int_0^{\mathcal{E}_F - \Delta} d\mathcal{E}' \, D(\mathcal{E}')\mathcal{E}' + \frac{1}{2} \int_{\mathcal{E}_F - \Delta}^{\mathcal{E}_F + \Delta} d\mathcal{E}' \, D(\mathcal{E}')\mathcal{E}' - \frac{1}{2} nJ \, \langle S \rangle^2$$

$$\langle S \rangle = \frac{1}{2n} \int_{\mathcal{E}_F - \Delta}^{\mathcal{E}_F + \Delta} d\mathcal{E}' \, \frac{1}{2} D(\mathcal{E}') = \frac{1}{2n} D(\mathcal{E}_F)\Delta$$

$$\left. \frac{\partial \mathcal{E}}{\partial \Delta} \right|_{\mathcal{E}_F} = \Delta D(\mathcal{E}_F) - \frac{J}{4n} D(\mathcal{E}_F)^2 \Delta$$

$$\left. \frac{\partial \mathcal{E}}{\partial \Delta} \right|_{\mathcal{E}_F} = 0 \Rightarrow \frac{J}{n} D(\mathcal{E}_F) = 4$$

Exchange interaction

Exchange Interactions between localized electron magnetic moments [edit]

Quantum mechanical particles are classified as bosons or fermions. The spin–statistics theorem of quantum field theory demands that all particles with half-integer spin behave as fermions and all particles with integer spin behave as bosons. Multiple bosons may occupy the same quantum state; by the Pauli exclusion principle, however, no two fermions can occupy the same state. Since electrons have spin 1/2, they are fermions. This means that the overall wave function of a system must be antisymmetric when two electrons are exchanged, i.e. interchanged with respect to both spatial and spin coordinates. First, however, exchange will be explained with the neglect of spin.

Exchange of spatial coordinates [edit]

Taking a hydrogen molecule-like system (i.e. one with two electrons), we may attempt to model the state of each electron by first assuming the electrons behave independently, and taking wave functions in position space of $\Phi_a(r_1)$ for the first electron and $\Phi_b(r_2)$ for the second electron. We assume that Φ_a and Φ_b are orthogonal, and that each corresponds to an energy eigenstate of its electron. Now, we may construct a wave function for the overall system in position space by using an antisymmetric combination of the product wave functions in position space:

$$\Psi_A(\vec{r}_1, \vec{r}_2) = \frac{1}{\sqrt{2}}[\Phi_a(\vec{r}_1)\Phi_b(\vec{r}_2) - \Phi_b(\vec{r}_1)\Phi_a(\vec{r}_2)] \tag{1}$$

Alternatively, we may also construct the overall position–space wave function by using a symmetric combination of the product wave functions in position space:

$$\Psi_S(\vec{r}_1, \vec{r}_2) = \frac{1}{\sqrt{2}}[\Phi_a(\vec{r}_1)\Phi_b(\vec{r}_2) + \Phi_b(\vec{r}_1)\Phi_a(\vec{r}_2)] \tag{2}$$

Treating the exchange interaction in the hydrogen molecule by the perturbation method, the overall Hamiltonian is:

$$\mathcal{H} = \mathcal{H}^{(0)} + \mathcal{H}^{(1)}$$

where $\mathcal{H}^{(0)} = -\frac{\hbar^2}{2m}\left(\nabla_1^2 + \nabla_2^2\right) - \frac{e^2}{r_1} - \frac{e^2}{r_2}$ and $\mathcal{H}^{(1)} = \left(\frac{e^2}{R_{ab}} + \frac{e^2}{r_{12}} - \frac{e^2}{r_{a1}} - \frac{e^2}{r_{b2}}\right)$

Two eigenvalues for the system energy are found:

$$E_{+/-} = E_{(0)} + \frac{C \pm J_{ex}}{1 \pm B^2} \tag{3}$$

where the E_+ is the spatially symmetric solution and E_- is the spatially antisymmetric solution. A variational calculation yields similar results. $\mathcal{H}$ can be diagonalized by using the position–space functions given by Eqs. (1) and (2). In Eq. (3), C is the **Coulomb integral**, B is the **overlap integral**, and J_{ex} is the **exchange integral**. These integrals are given by:

$$C = \int \Phi_a(\vec{r}_1)^2 \left(\frac{1}{R_{ab}} + \frac{1}{r_{12}} - \frac{1}{r_{a1}} - \frac{1}{r_{b2}}\right) \Phi_b(\vec{r}_2)^2 \, d^3r_1 \, d^3r_2 \tag{4}$$

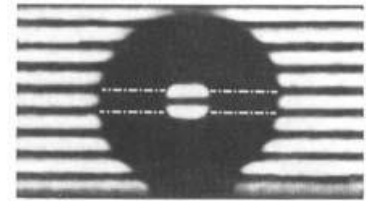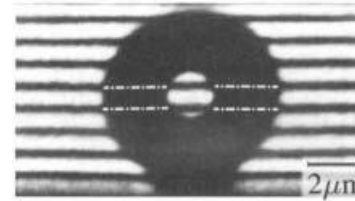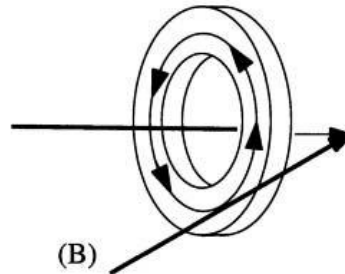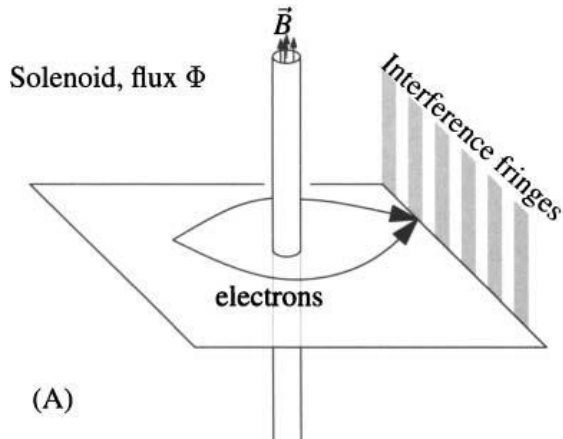$$B = \int \Phi_b(\vec{r}_2)\Phi_a(\vec{r}_2) \, d^3r_2 \tag{5}$$

$$J_{ex} = \int \Phi_a(\vec{r}_1)\Phi_b(\vec{r}_2) \left(\frac{1}{R_{ab}} + \frac{1}{r_{12}} - \frac{1}{r_{a1}} - \frac{1}{r_{b2}}\right) \Phi_b(\vec{r}_1)\Phi_a(\vec{r}_2) \, d^3r_1 \, d^3r_2 \tag{6}$$

The terms in parentheses in Eqs. (4) and (6) correspond to: proton–proton repulsion (R_{ab}), electron–electron repulsion (r_{12}), and electron–proton attraction ($r_{a1/a2/b1/b2}$). All quantities are assumed to be real.

Although in the hydrogen molecule the exchange integral, Eq. (6), is negative, Heisenberg first suggested that it changes sign at some critical ratio of internuclear distance to

Berry Phase

Aharonov-Bohm Effect

Electrons traveling around a flux tube suffer a phase change and can interfere with themselves even if they only travel through regions where B = 0.
(B) An open flux tube is not experimentally realizable, but a small toroidal magnet with no flux leakage can be constructed instead.
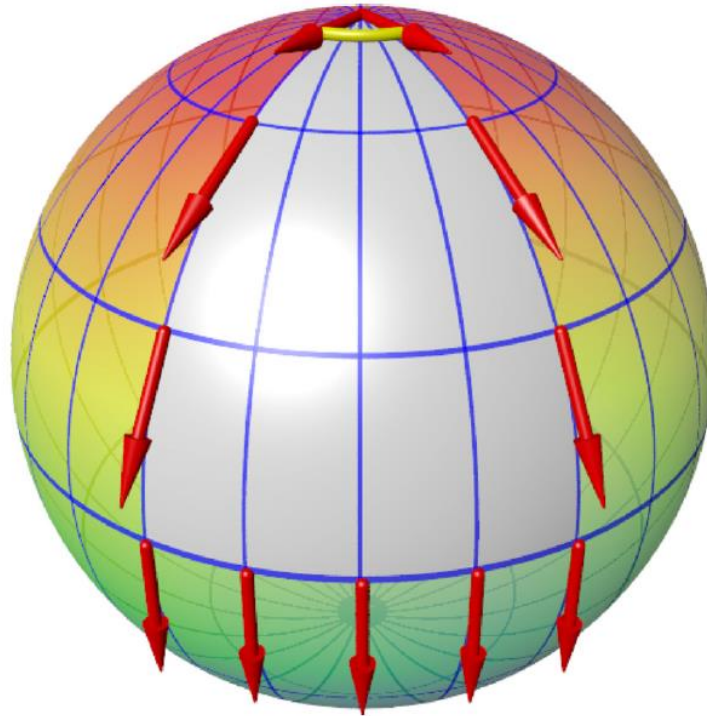
Electron hologram showing interference fringes of electrons passing through small toroidal magnet. The magnetic flux passing through the torus is quantized so as to produce an integer multiple of π phase change in the electron wave functions. The electron is completely screened from the magnetic induction in the magnet. In (A) the phase change is 0, while in (B) the phase change is π. [Source: Tonomura (1993), p. 67.]

$$\Phi = \int d^2r \, B_z = \oint d\vec{r} \cdot \vec{A}$$

$$A_\phi = \frac{\Phi}{2\pi r}$$

Parallel transport of a vector along a closed path on the sphere S_2 leads to a geometric phase between initial and final state.

Berry phase formalism for intrinsic Hall effects

Berry phase

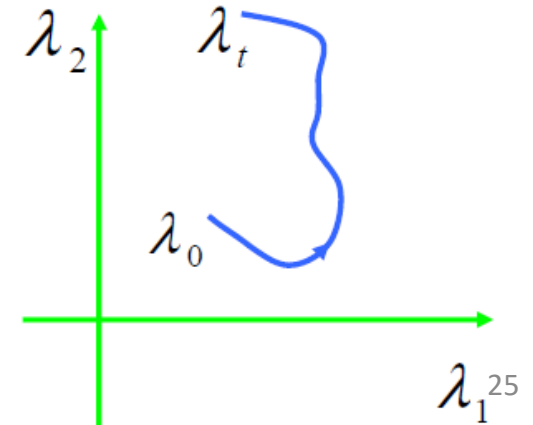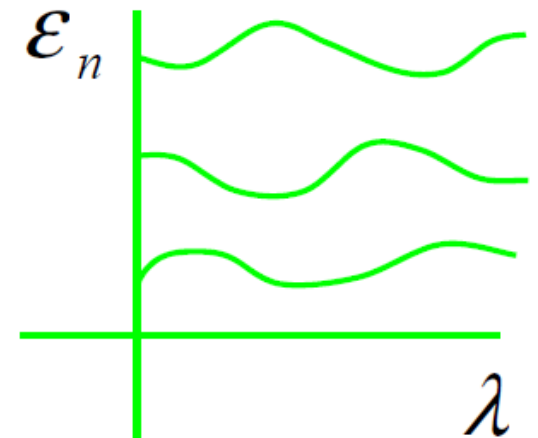[Berry, Proc. Roy. Soc. London A 392, 451 (1984)]

Parameter dependent system:

$$\{ \varepsilon_n(\lambda), \ \psi_n(\lambda) \}$$

Adiabatic theorem:

$$\Psi(t) = \psi_n(\lambda(t)) \ e^{-i\int_0^t dt\, \varepsilon_n/\hbar} \ e^{-i\gamma_n(t)}$$

Geometric phase:

$$\gamma_n = \int_{\lambda_0}^{\lambda_t} d\lambda \left\langle \psi_n \left| i\frac{\partial}{\partial\lambda} \right| \psi_n \right\rangle$$

Well defined for a closed path

From Prof. Guo Guang-Yu

$$\gamma_n = \oint_C d\lambda \left\langle \psi_n \left| i \frac{\partial}{\partial \lambda} \right| \psi_n \right\rangle$$

Stokes theorem

$$\gamma_n = \iint d\lambda_1 d\lambda_2 \, \Omega$$

λ_2

C

λ_1
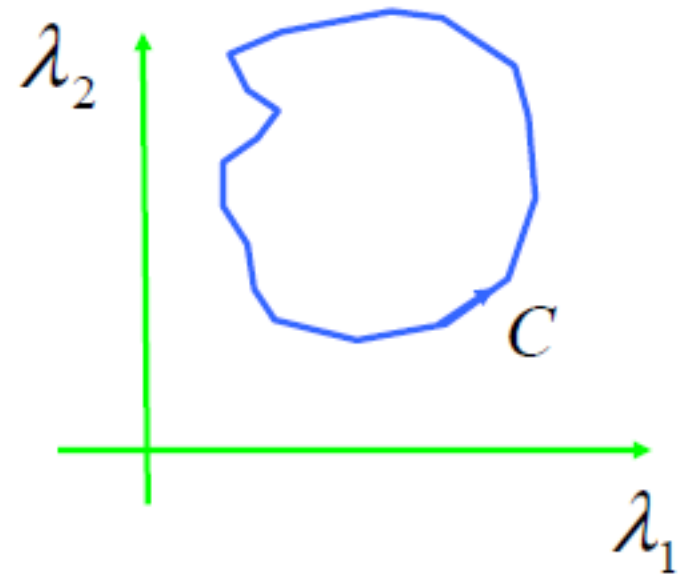
Berry Curvature

$$\Omega = i \frac{\partial}{\partial \lambda_1} \left\langle \psi \left| \frac{\partial}{\partial \lambda_2} \right| \psi \right\rangle - i \frac{\partial}{\partial \lambda_2} \left\langle \psi \left| \frac{\partial}{\partial \lambda_1} \right| \psi \right\rangle$$

Analogies

From Prof. Guo Guang-Yu

Berry curvature

$$\Omega(\vec{\lambda})$$

Magnetic field

$$B(\vec{r})$$

Berry connection

$$\langle \psi | i \frac{\partial}{\partial \lambda} | \psi \rangle$$

Vector potential

$$A(\vec{r})$$

Geometric phase

$$\oint d\lambda \langle \psi | i \frac{\partial}{\partial \lambda} | \psi \rangle = \iint d^2\lambda \ \Omega(\vec{\lambda})$$

Aharonov-Bohm phase

$$\oint dr \ A(\vec{r}) = \iint d^2r \ B(\vec{r})$$

Chern number

$$\oiint d^2\lambda \ \Omega(\vec{\lambda}) = \text{integer}$$

Dirac monopole

$$\oiint d^2r \ B(\vec{r}) = \text{integer} \ h/e$$

Semiclassical dynamics of Bloch electrons

From Prof. Guo Guang-Yu

Old [... 1976]

$$\dot{\mathbf{x}}_c = \frac{1}{\hbar}\frac{\partial \varepsilon_n(\mathbf{k})}{\partial \mathbf{k}},$$

$$\dot{\mathbf{k}} = -\frac{e}{\hbar}\mathbf{E} - \frac{e}{\hbar}\dot{\mathbf{x}}_c \times \mathbf{B} = \frac{e}{\hbar}\frac{\partial \varphi(\mathbf{r})}{\partial \mathbf{r}} - \frac{e}{\hbar}\dot{\mathbf{x}}_c \times \mathbf{B}$$

New version [Marder, 2000]

Berry phase correction [Chang & Niu, PRL (1995), PRB (1996)]

$$\dot{\mathbf{x}}_c = \frac{1}{\hbar}\frac{\partial \varepsilon_n(\mathbf{k})}{\partial \mathbf{k}} - \dot{\mathbf{k}} \times \mathbf{\Omega}_n(\mathbf{k}),$$

$$\dot{\mathbf{k}} = \frac{e}{\hbar}\frac{\partial \varphi(\mathbf{r})}{\partial \mathbf{r}} - \frac{e}{\hbar}\dot{\mathbf{x}}_c \times \mathbf{B},$$

$$\mathbf{\Omega}_n(\mathbf{k}) = -\mathrm{Im}\left\langle \frac{\partial u_{n\mathbf{k}}}{\partial \mathbf{k}} \Big| \times \Big| \frac{\partial u_{n\mathbf{k}}}{\partial \mathbf{k}} \right\rangle \qquad \text{(Berry curvature)}$$

Demagnetization factor D

can be solved analytically in some cases, numerically in others

For an ellipsoid $D_x + D_y + D_z = 1$ (SI units) $D_x + D_y + D_z = 4\pi$ (cgs units)

Solution for Spheroid $a = b \neq c$

1. Prolate spheroid (football shape) $c/a = r > 1$; $a = b$, In cgs units

$$D_c = \frac{4\pi}{r^2-1}\left[\frac{r}{\sqrt{r^2-1}}\ln\left(r + \sqrt{r^2-1}\right) - 1\right]$$

$$D_a = D_b = \frac{4\pi - D_c}{2}$$
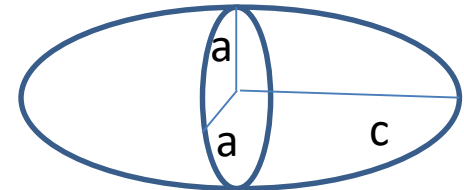
Limiting case r >> 1 (long rod)

$$D_c = \frac{4\pi}{r^2}\left[\ln(2r) - 1\right] \ll 1$$

$$D_a = D_b = 2\pi$$

Note: you measure $2\pi M$ *without* knowing the sample

2. Oblate Spheroid (pancake shape) $c/a = r < 1$; $a = b$

$$D_c = \frac{4\pi}{1-r^2}\left[1 - \frac{r}{\sqrt{1-r^2}}\cos^{-1}r\right] \qquad D_a = D_b = \frac{4\pi - D_c}{2}$$

Limiting case r >> 1 (flat disk)

$$D_c = 4\pi$$

$$D_a = D_b = \pi^2 r \ll 1$$

Note: you measure $4\pi M$ *without* knowing the sample
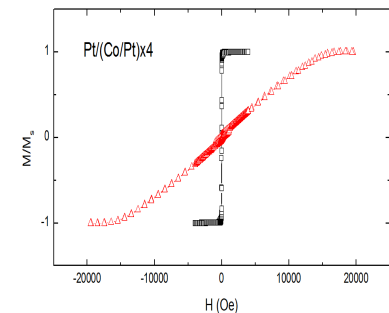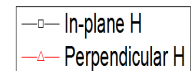
Surface anisotropy

$$E = E_{exchange} + E_{Zeeman} + E_{mag} + E_{anisotropy} + \cdots$$

- $E_{ex} : \sum 2J\vec{S_i} \cdot \vec{S_j}$

- $E_{Zeeman} : \vec{M} \cdot \vec{H}$

- $E_{mag} : \frac{1}{8\pi} \int B^2 dV$

- $E_{anisotropy}$

  For hcp Co= $K_1' \sin^2 \theta + K_2' \sin^4 \theta$
  For bcc Fe $= K_1(\alpha_1^2 \alpha_2^2 + \alpha_2^2 \alpha_3^2 + \alpha_3^2 \alpha_1^2) + K_2(\alpha_1^2 \alpha_2^2 \alpha_3^2)$
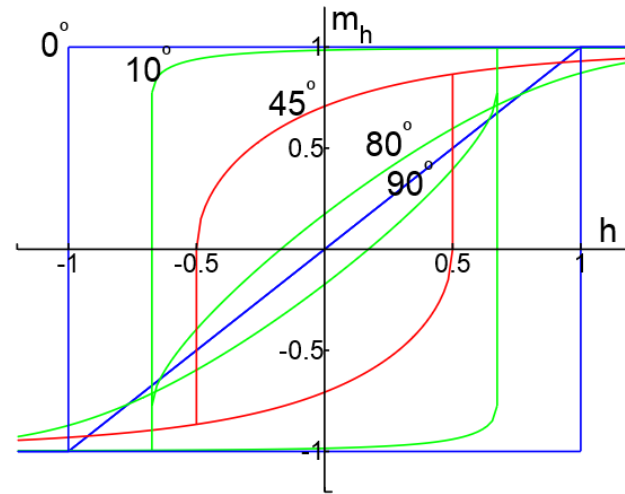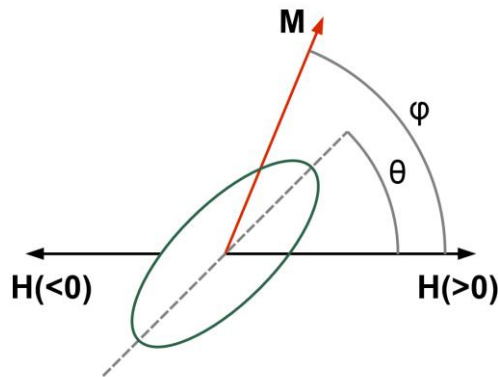
$$\alpha_i : \text{directional cosines}$$

Surface anisotropy $K_{\text{eff}} = \frac{2K_S}{t} + K_V$ ➜ $K_{\text{eff}} \cdot t = 2K_S + K_V \cdot t$
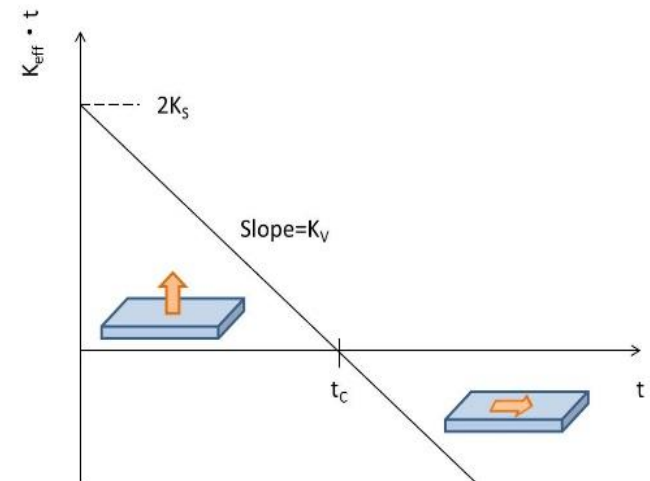
Stoner–Wohlfarth model

A widely used model for the magnetization of single-domain ferromagnets. It is a simple example of magnetic hysteresis and is useful for modeling small magnetic particles

$$E = K_u V \sin^2 (\phi - \theta) - \mu_0 M_s V H \cos \phi,$$

where K_u is the uniaxial anisotropy parameter, V is the volume of the magnet, M_s is the saturation magnetization.

Ferromagnetic domains

– competition between exchange, anisotropy, and magnetic energies.

– Bloch wall: rotation out of the plane of the two spins

– Neel wall: rotation within the plane of the two spins

For a 180° Bloch wall rotated in N+1 atomic planes $\quad N\Delta E_{ex} = N(JS^2 \left(\dfrac{\pi}{N}\right)^2)$

Wall energy density $\quad \sigma_w = \sigma_{ex} + \sigma_{anis} \approx JS^2\pi^2/(Na^2) + KNa \qquad a$: lattice constant

$\partial\sigma_w/\partial N \equiv 0, \qquad\qquad N = \sqrt{[JS^2\pi^2/(Ka^3)]} \approx 300 \qquad$ in Fe

$\sigma_w = 2\pi\sqrt{KJS^2/a} \approx \quad$ 1 erg/cm² in Fe

Wall width $\quad Na = \pi\sqrt{JS^2/Ka} \equiv \pi\sqrt{\dfrac{A}{K}}\ , \quad A = JS^2/a \quad$ Exchange stiffness constant

Domain wall energy γ versus thickness D of $Ni_{80}Fe_{20}$ thin films
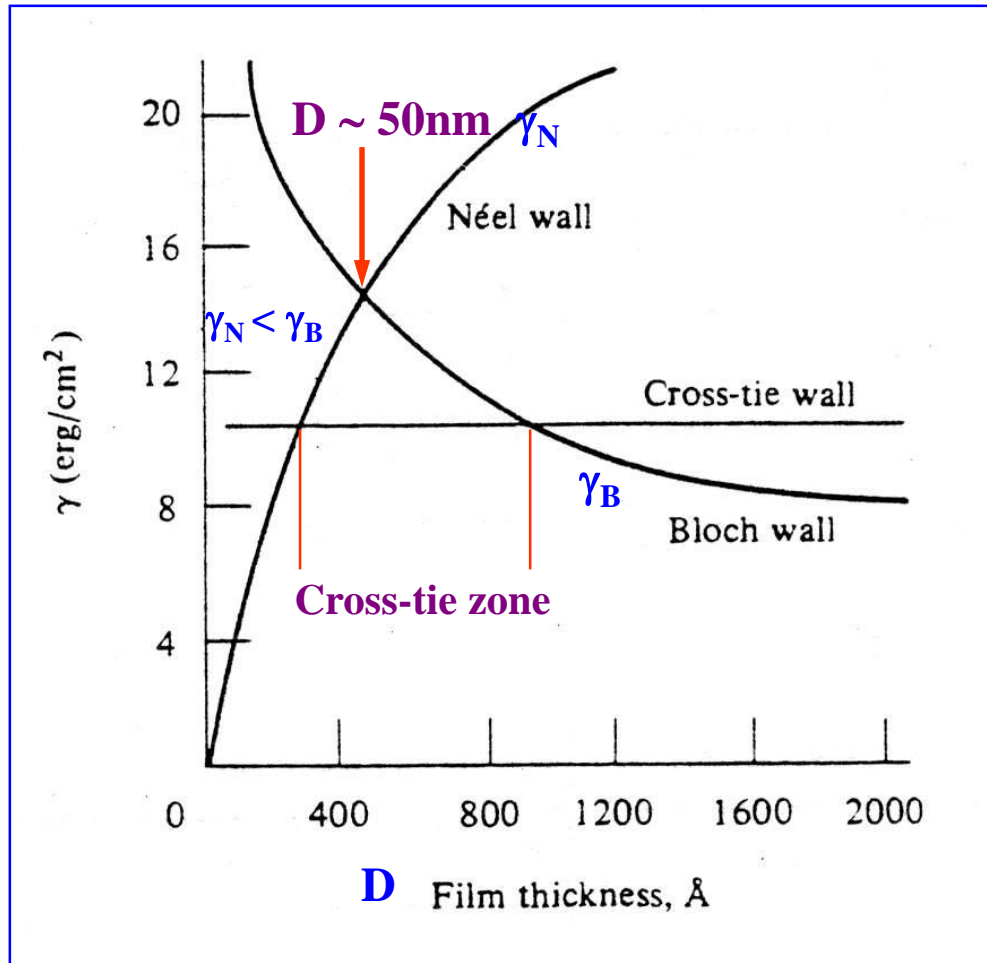
$\gamma_N < \gamma_B \sim$ **50nm**

Thick films have Bloch walls
Thin films have Neel walls

Cross-tie walls show up in between.

$A = 10^{-6}$ **erg/cm**

$K = 1500$ **erg/cm^3**

Further reference: Antonio DeSimone, Hans Knupfer, and Felix Otto, Calculus of Variations 27, 233–253 (2006) 2-d stability of the Neel wall

Magnetic Resonance

- Nuclear Magnetic Resonance (NMR)
  - Line width
  - Hyperfine Splitting, Knight Shift
  - Nuclear Quadrupole Resonance (NQR)
- Ferromagnetic Resonance (FMR)
  - Shape Effect
  - Spin Wave resonance (SWR)
- Antiferromagnetic Resonance (AFMR)
- Electron Paramagnetic Resonance (EPR or ESR)
  - Exchange narrowing
  - Zero-field Splitting
- Maser

What we can learn:
- From absorption fine structure ➔ electronic structure of single defects
- From changes in linewidth ➔ relative motion of the spin to the surroundings
- From resonance frequency ➔ internal magnetic field
- Collective spin excitations

FMR

Equation of motion of a magnetic moment $\boldsymbol{\mu}$ in an external field B_0

$$\frac{\hbar d\boldsymbol{I}}{dt} = \boldsymbol{\mu} \times \boldsymbol{B} \qquad \boldsymbol{\mu} = \gamma\hbar\boldsymbol{I} \qquad \frac{d\boldsymbol{\mu}}{dt} = \gamma\boldsymbol{\mu} \times \boldsymbol{B} \qquad \frac{d\boldsymbol{M}}{dt} = \gamma\boldsymbol{M} \times \boldsymbol{B}$$

Shape effect:

internal magnetic field

Landau-Lifshitz-Gilbert (LLG) equation

$$\frac{d\boldsymbol{M}}{dt} = -\gamma\boldsymbol{M} \times \boldsymbol{H}_{\text{eff}} + \alpha\boldsymbol{M} \times \frac{d\boldsymbol{M}}{dt}$$

$$B_x^i = B_x^0 - N_x M_x \qquad B_y^i = B_y^0 - N_y M_y \qquad B_z^i = B_z^0 - N_z M_z$$

$$\frac{dM_x}{dt} = \gamma\left(M_y B_z^i - M_z B_y^i\right) = \gamma[B_0 + \left(N_y - N_z\right)M]M_y$$

$$\frac{dM_y}{dt} = \gamma[M(-N_x M_x) - M_x(B_0 - N_z M)] = -\gamma[B_0 + (N_x - N_z)M]M_x$$

To first order $\qquad \dfrac{dM_z}{dt} = 0 \qquad M_z = M$

$$\begin{vmatrix} i\omega & \gamma[B_0 + \left(N_y - N_z\right)M] \\ -\gamma[B_0 + (N_x - N_z)M] & i\omega \end{vmatrix} = 0$$

$$\omega_0^2 = \gamma^2[B_0 + \left(N_y - N_z\right)M][B_0 + (N_x - N_z)M] \qquad \text{Uniform mode}$$

Uniform mode

Sphere   flat plate with perpendicular field   flat plate with in-plane field
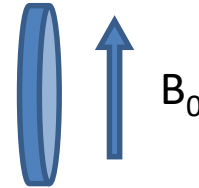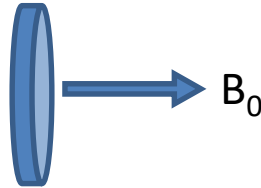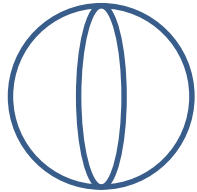
$$N_x = N_y = N_z$$

$$\omega_0 = \gamma\, B_0$$

$$N_x = N_y = 0 \qquad N_z = 4\pi$$

$$\omega_0 = \gamma\,(B_0 - 4\pi M)$$

$$N_x = N_z = 0 \qquad N_y = 4\pi$$

$$\omega_0 = \gamma\,[B_0(B_0 + 4\pi M)]^{1/2}$$

Spin wave resonance; Magnons

Consider a one-dimensional spin chain with only nearest-neighbor interactions.

$$U = -2J \sum \vec{S_i} \cdot \vec{S_j} \quad \text{We can derive} \quad \hbar\omega = 4JS(1 - \cos ka)$$

When $ka \ll 1$ $\hbar\omega \cong (2JSa^2)k^2$

flat plate with perpendicular field $\omega_0 = \gamma\,(B_0 - 4\pi M) + Dk^2$

Quantization of (uniform mode) spin waves, then consider the thermal excitation of Mannons, leads to Bloch $T^{3/2}$ law. $\Delta M / M(0) \propto T^{3/2}$

AFMR
Spin wave resonance; Antiferromagnetic Magnons

Consider a one-dimensional antiferromangetic spin chain with only nearest-neighbor interactions. Treat sublattice A with up spin S and sublattice B with down spin –S, J<0.

$$U = -2J \sum \vec{S_i} \cdot \vec{S_j}$$

We can derive $\hbar\omega = -4JS|\sin ka|$

When $ka << 1$ $\hbar\omega \cong (-4JS)|ka|$

AFMR

exchange plus anisotropy fields on the two sublattices

$$\boldsymbol{B}_1 = -\lambda \boldsymbol{M}_2 + B_A \hat{\boldsymbol{z}} \quad \text{on } \boldsymbol{M}_1 \qquad\qquad \boldsymbol{B}_2 = -\lambda \boldsymbol{M}_1 - B_A \hat{\boldsymbol{z}} \quad \text{on } \boldsymbol{M}_2$$

$$M_1^z \equiv M \qquad M_2^z \equiv -M \qquad M_1^+ \equiv M_1^x + iM_1^y \qquad M_2^+ \equiv M_2^x + iM_2^y \qquad B_E \equiv \lambda M$$

$$\frac{dM_1^+}{dt} = -i\gamma[M_1^+(B_A + B_E) + M_2^+ B_E]$$

$$\frac{dM_2^+}{dt} = -i\gamma[M_2^+(B_A + B_E) + M_1^+ B_E]$$

$$\begin{vmatrix} \gamma(B_A + B_E) - \omega & \gamma B_E \\ B_E & \gamma(B_A + B_E) + \omega \end{vmatrix} = 0$$

$$\omega_0^2 = \gamma^2 B_A(B_A + 2B_E) \qquad\qquad \text{Uniform mode}$$

Spintronics

Electronics with electron spin as an extra degree of freedom
Generate, inject, process, and detect spin currents

- Generation: ferromagnetic materials, spin Hall effect, spin pumping effect etc.

- Injection: interfaces, heterogeneous structures, tunnel junctions

- Process: spin transfer torque

- Detection: Giant Magnetoresistance, Tunneling MR

- Historically, from magnetic coupling to transport phenomena

  important materials: CoFe, CoFeB, Cu, Ru, IrMn, PtMn, MgO, Al2O3, Pt, Ta

- Magnetic coupling
- Magnetic transport properties

RKKY (*Ruderman-Kittel-Kasuya-Yosida*) interaction
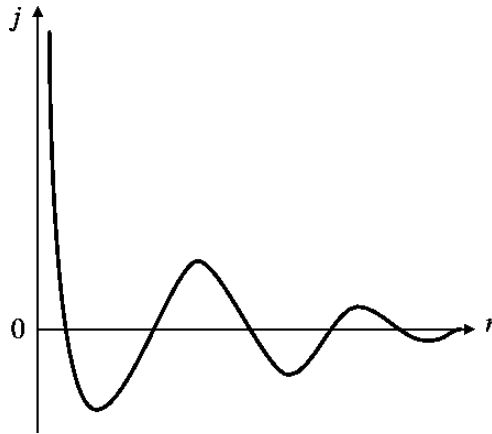
coupling coefficient

$$j\left(\boldsymbol{R_l} - \boldsymbol{R_{l'}}\right) = 9\pi \left(\frac{j^2}{\epsilon_F}\right) F\left(2k_F|\boldsymbol{R_l} - \boldsymbol{R_{l'}}|\right)$$

$$F(x) = \frac{x\cos x - \sin x}{x^4}$$

Magnetic coupling in superlattices

• Long-range incommensurate magnetic order in a Dy-Y multilayer

   M. B. Salamon, Shantanu Sinha, J. J. Rhyne, J. E. Cunningham, Ross W. Erwin, Julie Borchers, and C. P. Flynn, Phys. Rev. Lett. **56**, 259 - 262 (1986)

• Observation of a Magnetic Antiphase Domain Structure with Long- Range Order in a Synthetic Gd-Y Superlattice

   C. F. Majkrzak, J. W. Cable, J. Kwo, M. Hong, D. B. McWhan, Y. Yafet, and J. V. Waszczak,C. Vettier, Phys. Rev. Lett. **56**, 2700 - 2703 (1986)

• Layered Magnetic Structures: Evidence for Antiferromagnetic Coupling of Fe Layers across Cr Interlayers

   P. Grünberg, R. Schreiber, Y. Pang, M. B. Brodsky, and H. Sowers, Phys. Rev. Lett. **57**, 2442 - 2445 (1986)

Magnetic coupling in multilayers

- Long-range incommensurate magnetic order in a Dy-Y multilayer
 M. B. Salamon, Shantanu Sinha, J. J. Rhyne, J. E. Cunningham, Ross W. Erwin, Julie Borchers, and C. P. Flynn, Phys. Rev. Lett. 56, 259 - 262 (1986)

- Observation of a Magnetic Antiphase Domain Structure with Long-Range Order in a Synthetic Gd-Y Superlattice
 C. F. Majkrzak, J. W. Cable, J. Kwo, M. Hong, D. B. McWhan, Y. Yafet, and J. V. Waszczak,C. Vettier, Phys. Rev. Lett. 56, 2700 - 2703 (1986)

- Layered Magnetic Structures: Evidence for Antiferromagnetic Coupling of Fe Layers across Cr Interlayers
 P. Grünberg, R. Schreiber, Y. Pang, M. B. Brodsky, and H. Sowers, Phys. Rev. Lett. 57, 2442 - 2445 (1986)
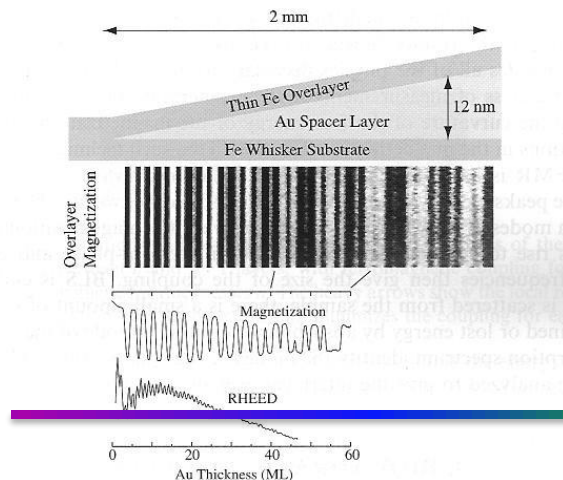
Coupling in wedge-shaped
Fe/Cr/Fe
Fe/Au/Fe
Fe/Ag/Fe
J. Unguris, R. J. Celotta, and D. T. Pierce
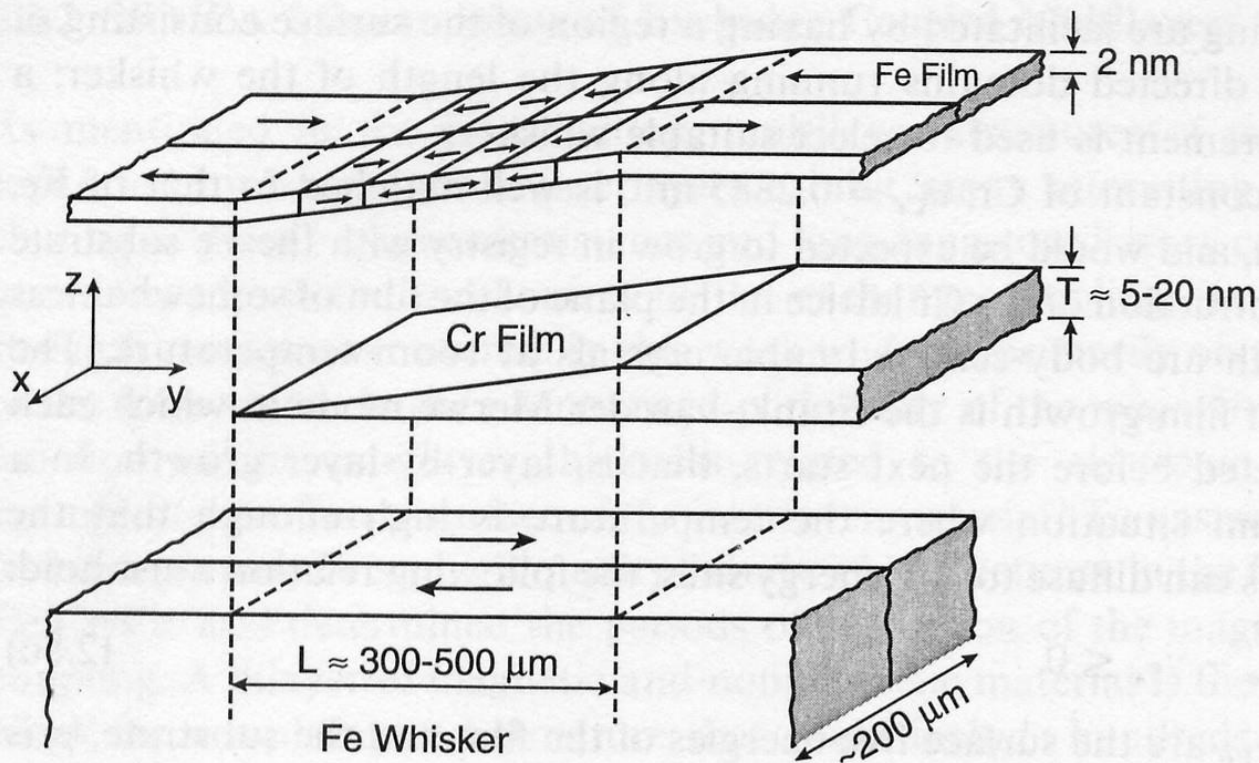
Fig. 2.41. A schematic expanded view of the sample structure showing the Fe(0 0 1) single-crystal whisker substrate, the evaporated Cr wedge, and the Fe overlayer. The arrows in the Fe show the magnetization direction in each domain. The z-scale is expanded approximately 5000 times. (From [2.206])
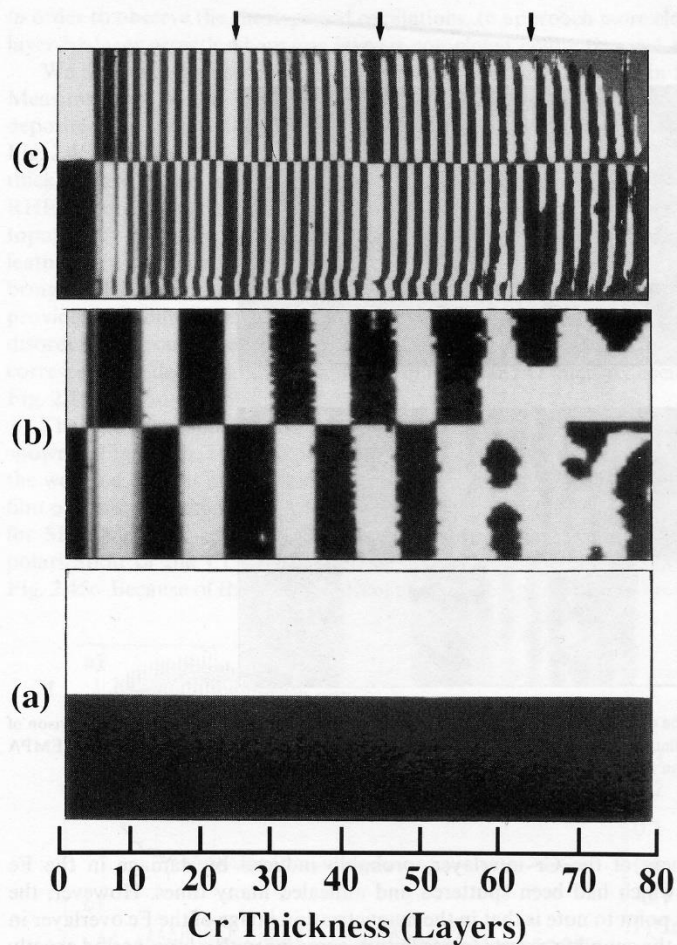
Fig. 2.43. SEMPA image of the magnetization M_y (axes as in Fig. 2.41) showing domains in (**a**) the clean Fe whisker, (**b**) the Fe layer covering the Cr spacer layer evaporated at 30 °C, and (**c**) the Fe layer covering a Cr spacer evaporated on the Fe whisker held at 350 °C. The scale at the bottom shows the increase in the thickness of the Cr wedge in (**b**) and (**c**). The arrows at the top of (**c**) indicate the Cr thicknesses where there are phase slips. The region of the whisker imaged is about 0.5 mm long
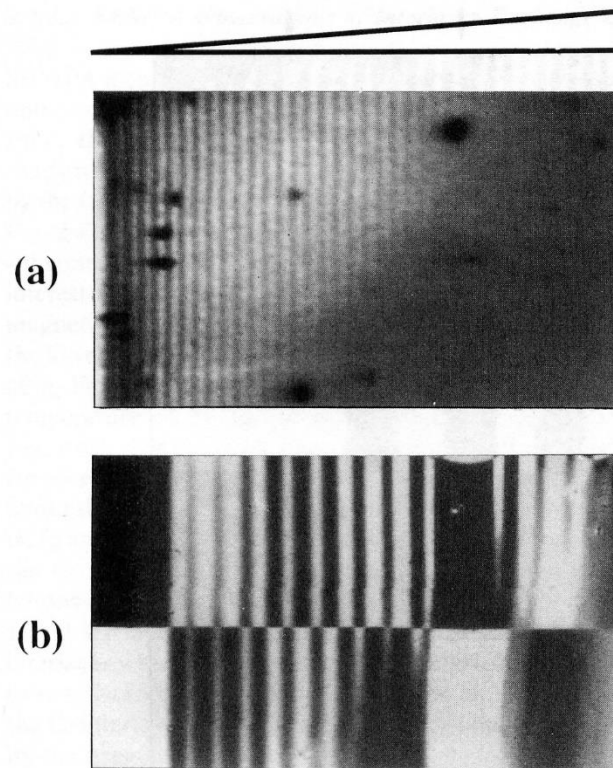
Fig. 2.44. The effect of roughness on the inertlayer exchange coupling is shown by a comparison of (**a**) the oscillations of the RHEED intensity along the bare Cr wedge with (**b**) the SEMPA magnetization image over the same part of the wedge

43
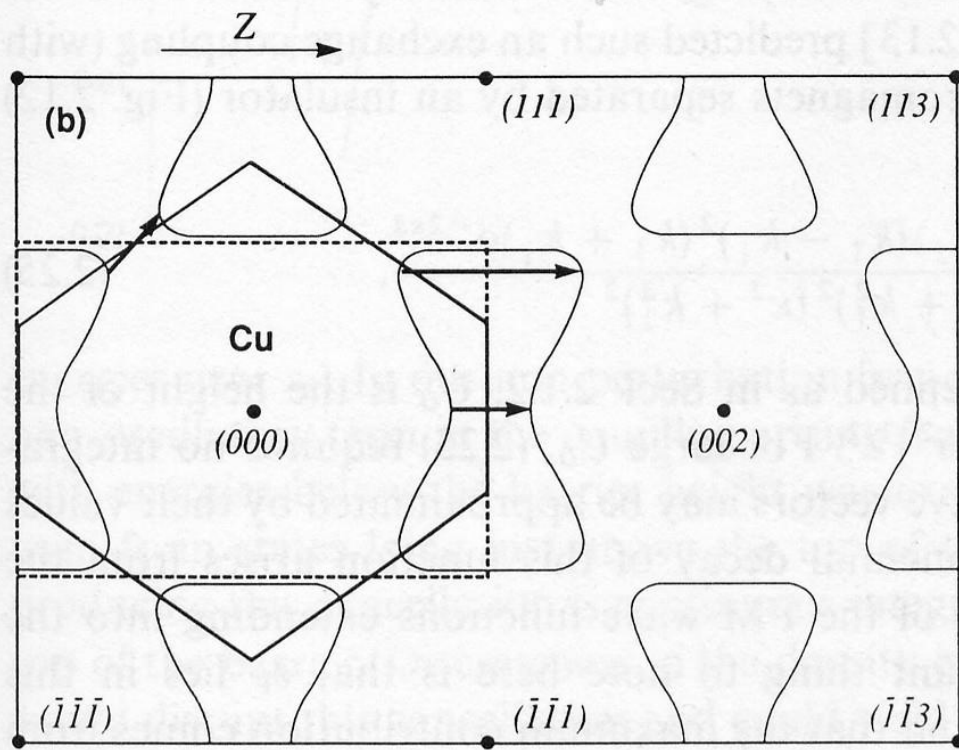
Fig. 2.11. Fermi surface of Cu in the (100) plane in the extended zone scheme. Arrows indicate values of $2(k_F - G)$ for reciprocal lattice vectors G which can give rise to oscillations with periods greater than π/k_F

Oscillatory magnetic coupling in multilayers

Ru interlayer has the largest coupling strength

Fig. 2.58. Dependence of saturation field on Ru spacer layer thickness for several series of $Ni_{81}Fe_{19}/Ru$ multilayers with structure, 100 Å $Ru/[30$ Å $Ni_{81}Fe_{19}/Ru(t_{Ru})]_{20}$, where the topmost Ru layer thickness is adjusted to be $\simeq 25$ Å for all samples
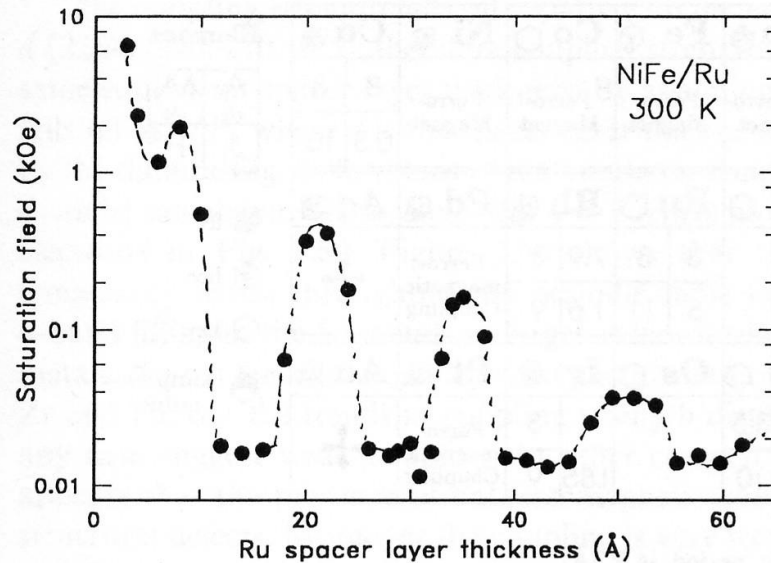
	$|J_1|$ at 1st peak (erg/cm²)	Period (nm)
Cu	0.3	1
V	0.1	0.9
Cr	0.24	1.8
Ir	0.81	0.9
Ru	5.0	1.2

S. S. P. Parkin

- Magnetic coupling
- Magnetic transport properties

Spin-dependent conduction in Ferromagnetic metals (Two-current model)

First suggested by Mott (1936)
Experimentally confirmed by I. A. Campbell and A. Fert (~1970)

At low temperature

$$\rho = \frac{\rho_\uparrow \rho_\downarrow}{\rho_\uparrow + \rho_\downarrow}$$

At high temperature

$$\rho = \frac{\rho_\uparrow \rho_\downarrow + \rho_{\uparrow\downarrow}(\rho_\uparrow + \rho_\downarrow)}{\rho_\uparrow + \rho_\downarrow + 4\rho_{\uparrow\downarrow}}$$
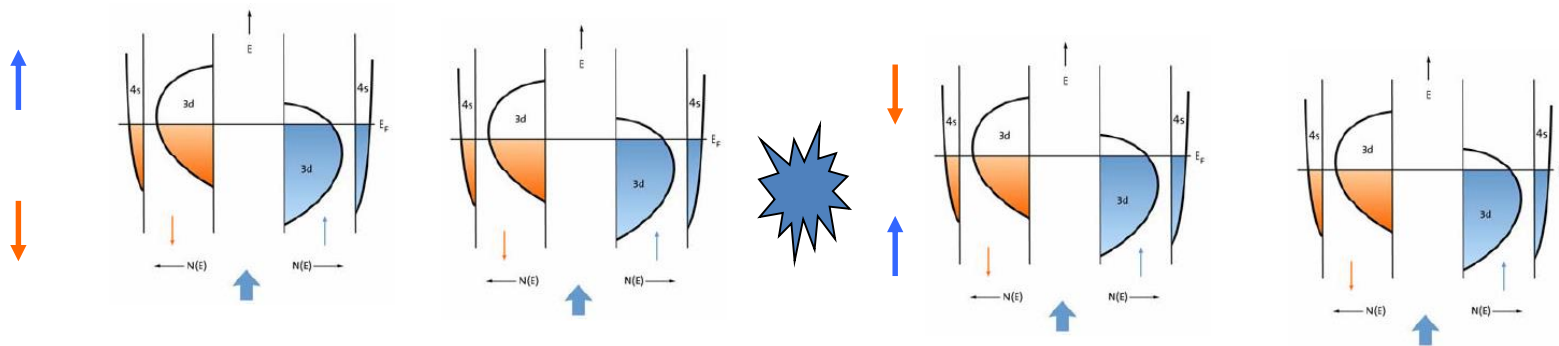
Spin mixing effect equalizes two currents

Two Current Model

s electrons carry the electric current

resistivity (spin-dependent $s \to d$ scattering)

$$R^S = \text{const.} \; N_d^S$$

number of empty d states

Spin excitations in the "two current model"
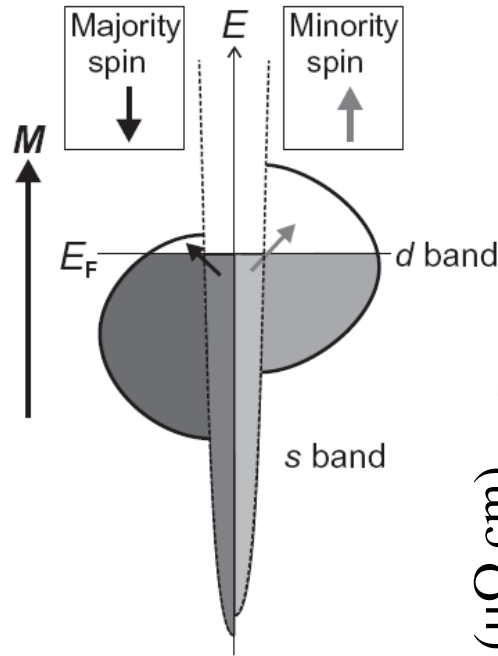
spin selective scattering

$\alpha \approx 0.3$

$\alpha = \rho_\downarrow \, / \, \rho_\uparrow$

$\alpha \approx 20$

$\rho_\downarrow$

$\rho_\uparrow$

Ti V Cr Mn Fe Co Ni

element	N_h^{d} [a]	$|m|$ [μ_B]	R [b] [Ω m]
Fe (bcc)	3.90	2.216	9.71×10^{-8}
Co (hcp)	2.80	1.715	6.25×10^{-8}
Ni (fcc)	1.75	0.616	6.84×10^{-8}
Cu (fcc)	0.50	–	1.68×10^{-8}

A. Fert, I.A. Campbell, PRL **21**, 1190 (1968)

48

Anisotropic magnetoresistance (AMR)

Polar

Transverse

I

H

Longitudinal

e^-
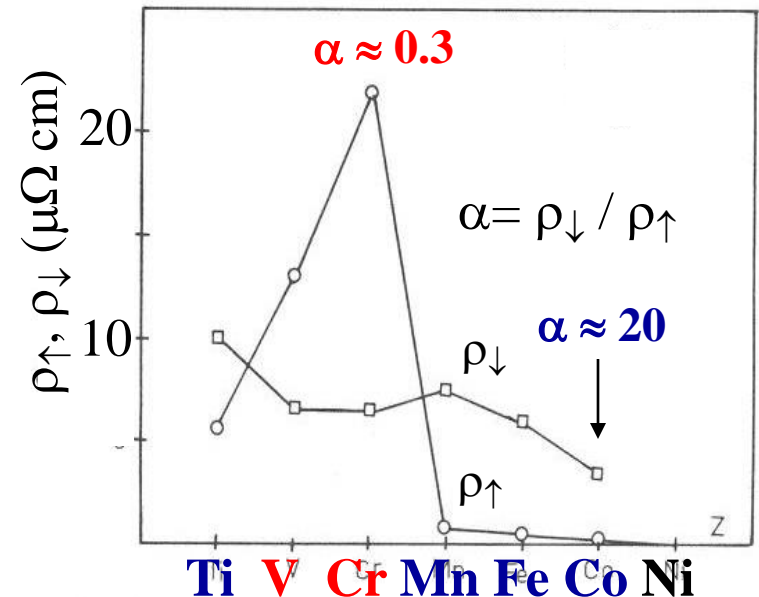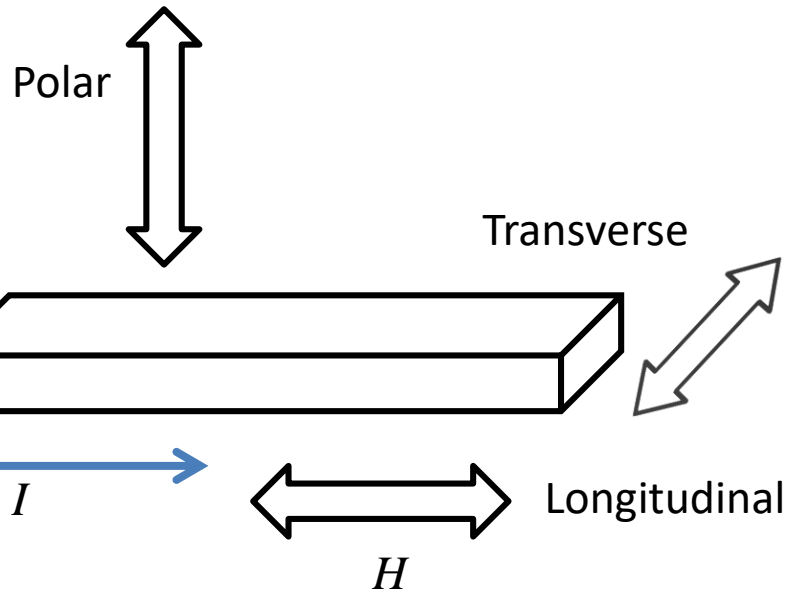
$$R_{Long.} > R_{Trans.}, R_{Pol.}$$

Geometrical size effect

Fe 100nm   10K
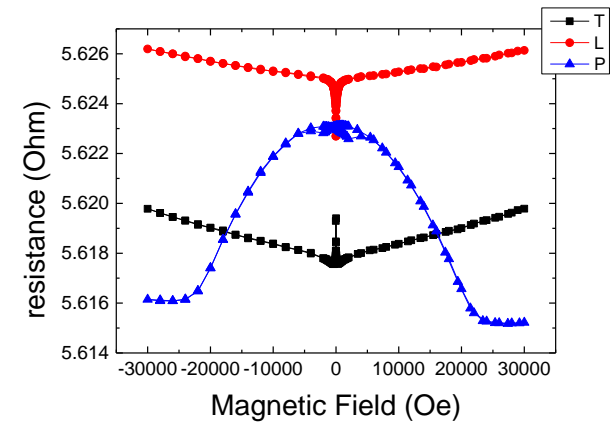
Ni 100nm   10K
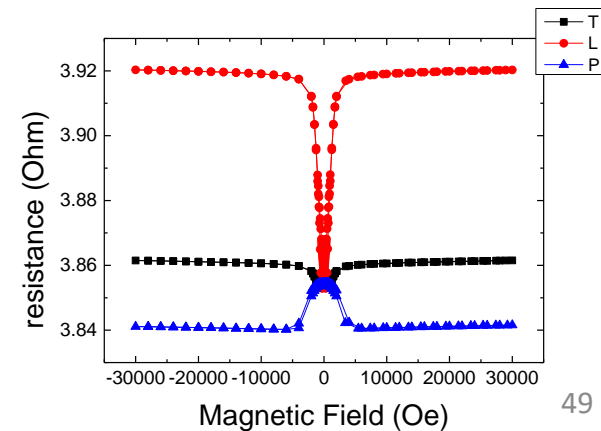
outline

- Giant Magnetoresistance, Tunneling Magnetoresistance
- Spin Transfer Torque (STT)
- Pure Spin current (no net charge current)
  - Spin Hall, Inverse Spin Hall effects
  - Spin Pumping effect
  - Spin Seebeck effect
- Spin Orbit torque (SOT)
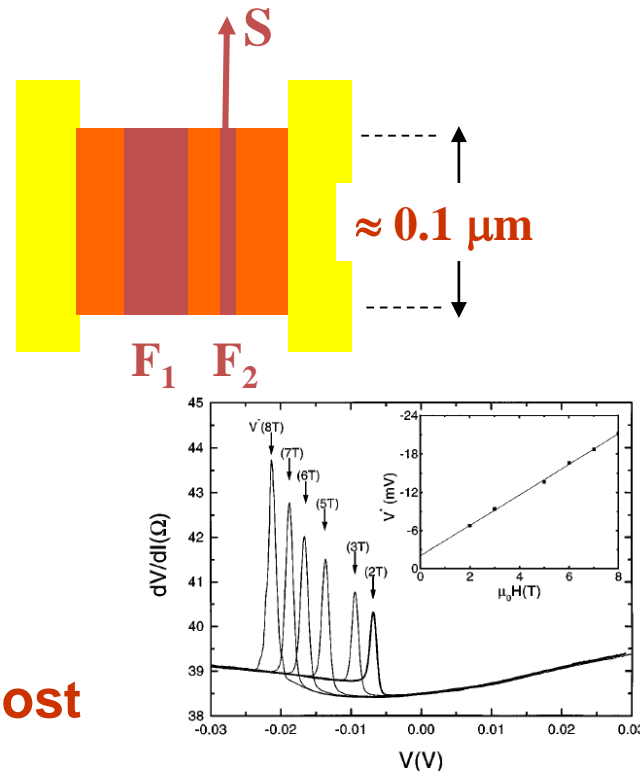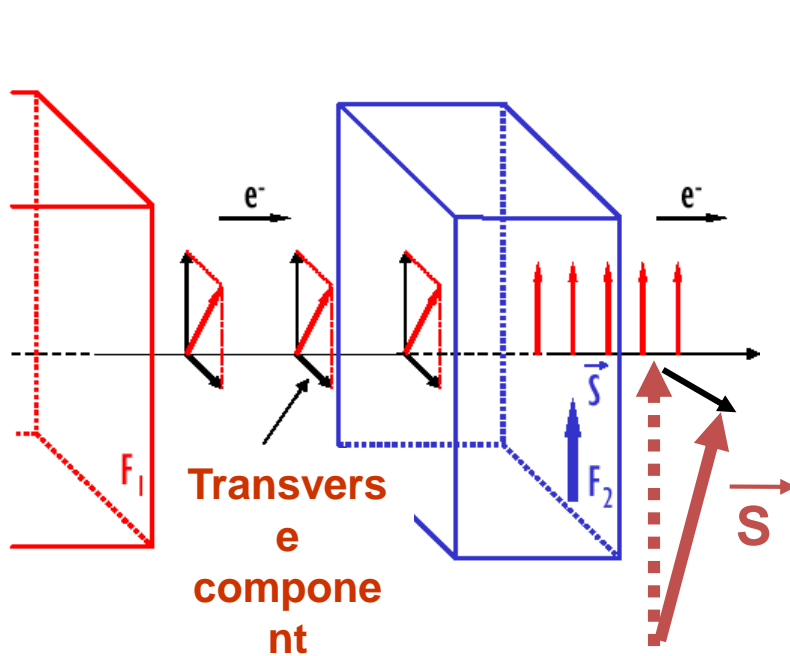- Spin wave in micro and nano magnetic structures

2007 Nobel prize in Physics

2007年諾貝爾物理獎得主 左 亞伯·費爾(Albert Fert) 與 右彼得·葛倫貝格(Peter Grünberg)

(圖片資料來源：Copyright © Nobel Web AB 2007/ Photo: Hans Mehlin)

Giant Magnetoresistance
Tunneling Magnetoresistance
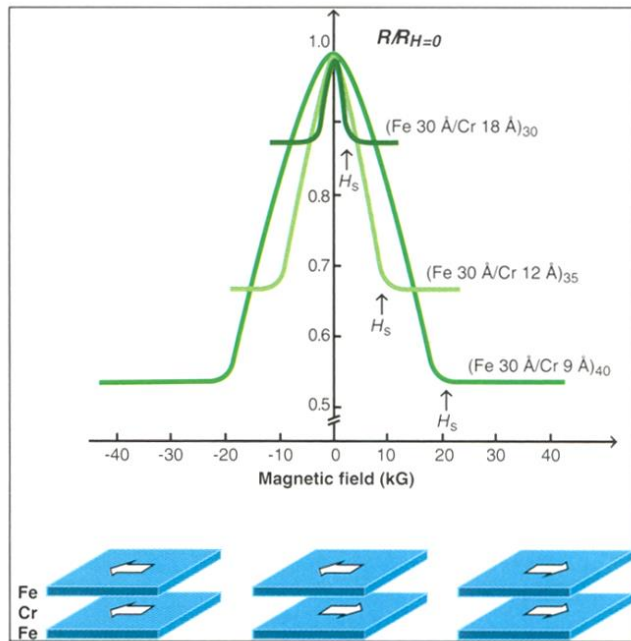
Discovery of Giant MR -- Two-current model combines with magnetic coupling in multilayers
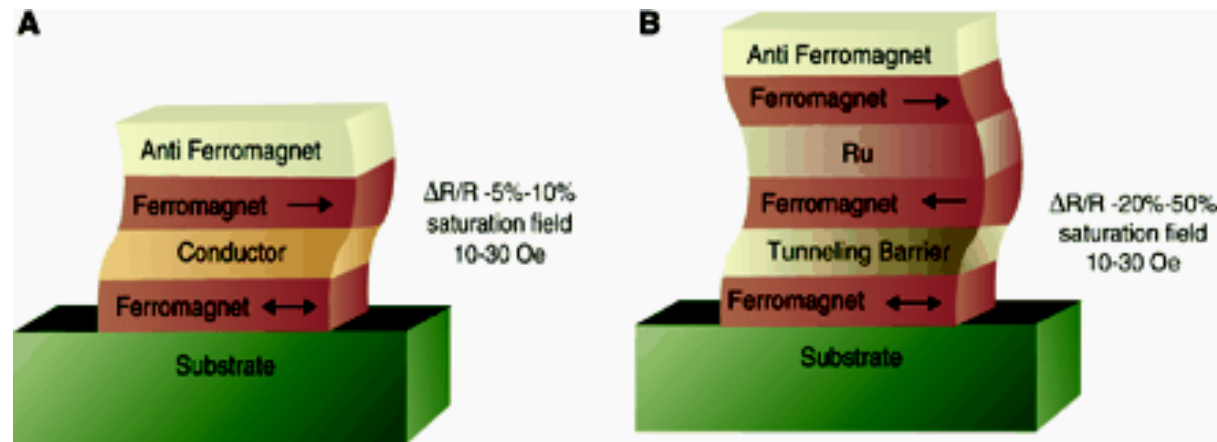
Spin-dependent transport structures. (A) Spin valve. (B) Magnetic tunnel junction. (from Science)

Moodera's group, PRL **74**, 3273 (1995)

Fert's group, PRL **61**, 2472 (1988)

Miyazaki's group, JMMM **139**, L231 (1995)

Spin valve –
a sandwich structure
with a free ferromagnetic layer (F) and a fixed F layer
pinned by an antiferromagnetic (AF) layer

F (free)

N

F (fixed)

AF

Negatively biased
Positively biased?

When $T_N < T < T_C$

When $T < T_N < T_C$
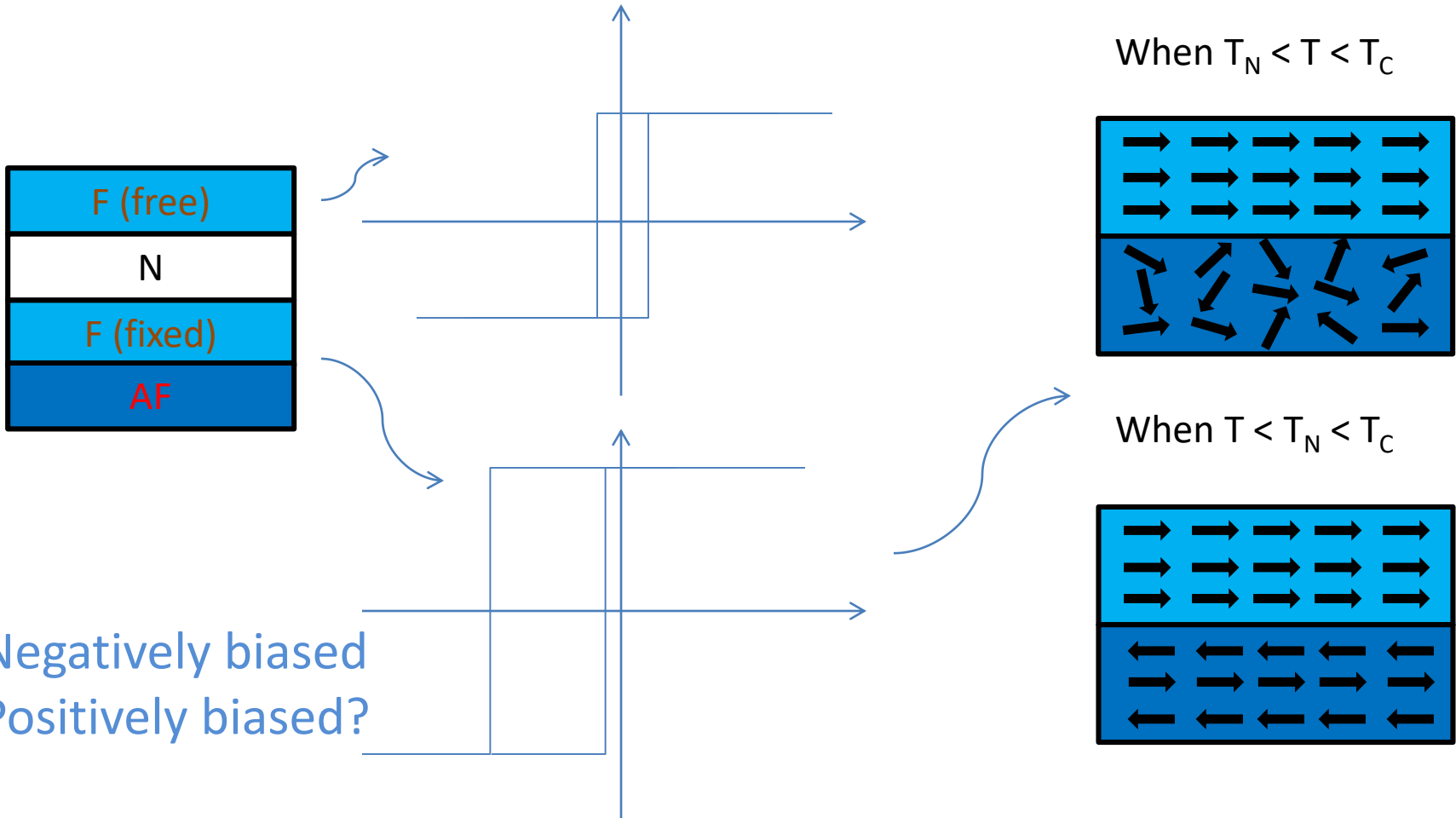
Transport geometry
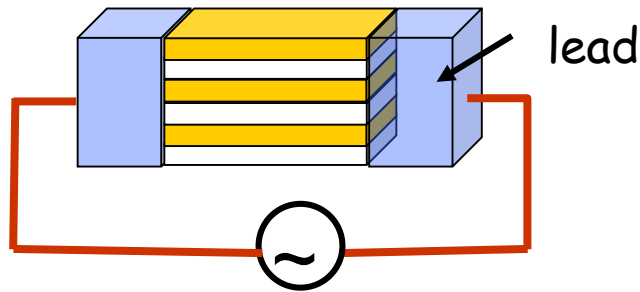
CIP geometry
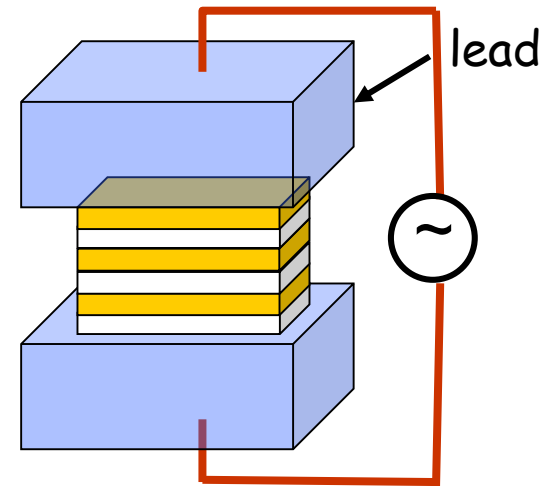
CPP geometry

- In metallic multilayers, CIP resistance can be measured easily, CPP resistance needs special techniques.
- From CPP resistance in metallic multilayers, one can measure interface resistances, spin diffusion lengths, and polarization in ferromagnetic materials, etc.
- CPP magnetoresistance of magnetic multilayers: A critical review
    Jack Bass
    Journal of Magnetism and Magnetic Materials 408 (2016) 244–320

Valet and Fert model of (CPP-)GMR

Based on the Boltzmann equation

A semi-classical model with spin taken into consideration

$$j_{+(-)} = \frac{1}{e\rho_{+(-)}} \frac{\partial \mu_{+(-)}}{\partial x}$$

$$j_+ + j_- = j_e$$

$$\frac{\partial(j_+ - j_-)}{\partial x} = \frac{2eN(E_F)\Delta\mu}{\tau_{sf}}$$

$$\frac{\partial^2 \mu_{+(-)}}{\partial z^2} = \frac{\mu_{+(-)}}{l_{sf}^2} \qquad l_{sf}^F = \left[\lambda_{sf}^F / 3(\lambda_\uparrow^{-1} + \lambda_\downarrow^{-1})\right]^{1/2}, \quad l_{sf}^N = \left[\lambda_{sf}^N \lambda / 6\right]^{1/2}$$

FM   Interface   **NM**
z=0

potential drop at the interface

$\bar{\mu}_{\uparrow,\downarrow}^0$ $\delta\bar{\mu}_\uparrow$

$\delta\bar{\mu}_\downarrow$
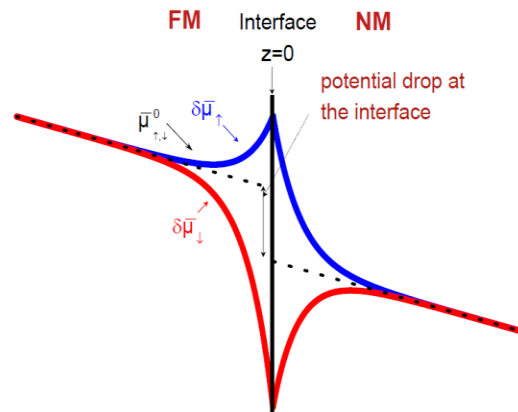
$\Delta\mu$ for antiparallel aligned multilayers

(a)   (A)   (B)   (C)
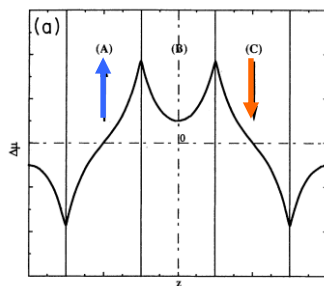
$\Delta\mu$ for parallel aligned multilayers

(d)   (A)   (B)   (C)
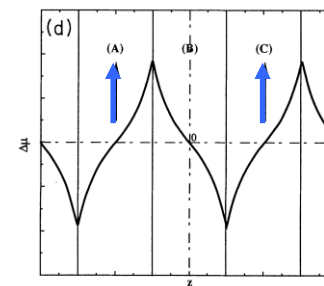
Spin imbalance induced charge accumulation at the interface is important
Spin diffusion length, instead of mean free path, is the dominant physical length scale

55

Spin Diffusion: The Johnson Transistor
non-local measurement

N

e-

F_1 L F_2

M. Johnson and R. H. Silsbee,
Phys. Rev. Lett. **55**, 1790 (1985)

M. Johnson,
Science **260**, 320 (1993)
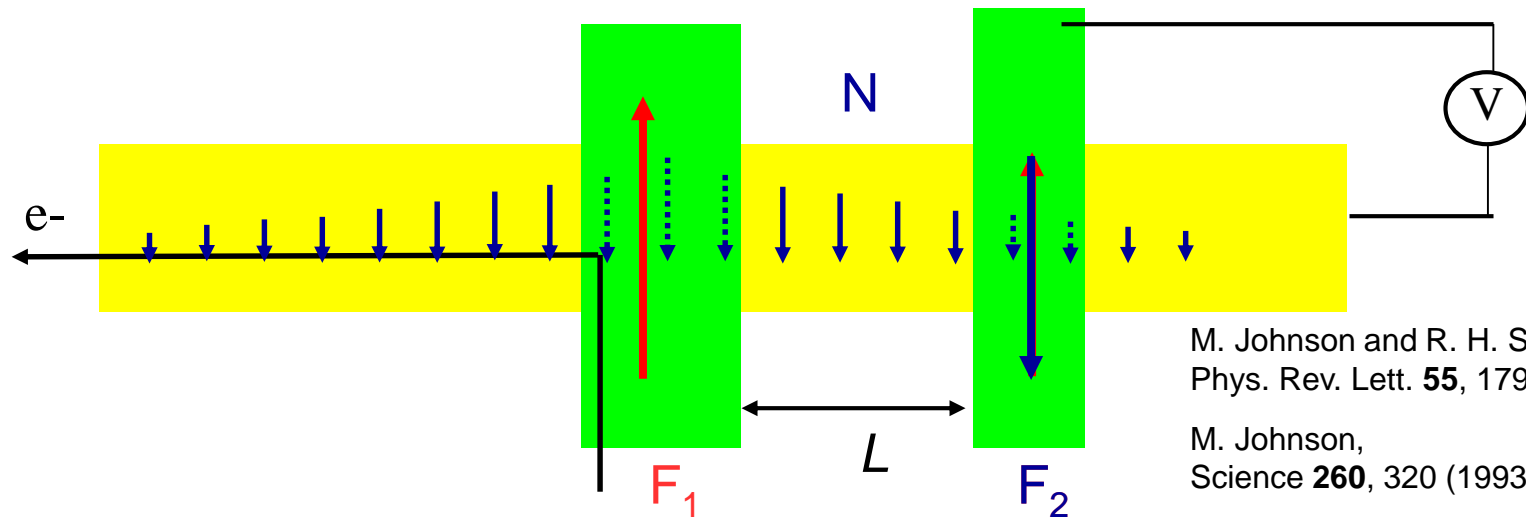
First Experimental Demonstrations

$T = 4.2$ K

R (mΩ)
B (mT)

ΔR (mΩ)
L (nm)

- $T = 4.2$ K
- $T = 293$ K

$\lambda_N = 1{,}000$ nm

$\lambda_N = 350$ nm

I_+

I_-

500 nm
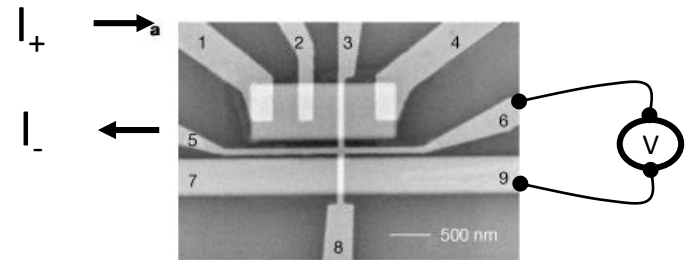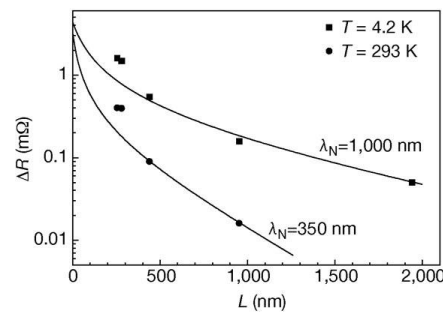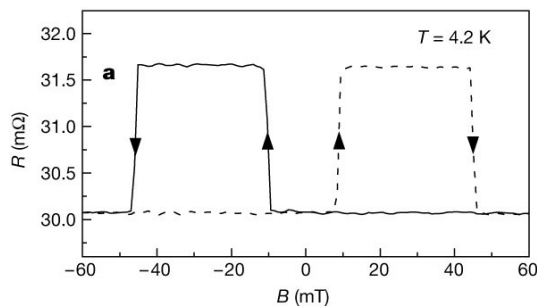
Cu film: $\lambda_s = 1$ μm   (4.2 K)

Jedema *et al.*, Nature **410**, 345 (2001)

outline

- Giant Magnetoresistance, Tunneling Magnetoresistance
- Spin Transfer Torque (STT)
- Pure Spin current (no net charge current)
  - Spin Hall, Inverse Spin Hall effects
  - Spin Pumping effect
  - Spin Seebeck effect
- Spin Orbit torque (SOT)
- Spin wave in micro and nano magnetic structures

Spin Transfer Torque

S

≈ 0.1 μm

F₁ F₂

Transverse component

The transverse spin component is lost by the conduction electrons, transferred to the global spin of the $\vec{S}$

$$\dot{\boldsymbol{S}}_{1,2} = (I_e\, g/e)\, \hat{\boldsymbol{s}}_{1,2} \times (\hat{\boldsymbol{s}}_1 \times \hat{\boldsymbol{s}}_2)$$

Slonczewski JMMM **159**, L1 (1996)

FIG. 1. The point contact $dV/dI(V)$ spectra for a series of magnetic fields (2, 3, 5, 6, 7, and 8 T) revealing an upward step and a corresponding peak in dV/dI at a certain negative bias voltage $V^*(H)$. The inset shows that $V^*(H)$ increases linearly with the applied magnetic field H.

Tsoi et al. PRL **61**, 2472 (1998)

Modified Landau-Lifshitz-Gilbert (LLG) equation

$$\frac{dm}{dt} = -\gamma m \times H_{eff} + \alpha m \times \frac{dm}{dt} + \frac{\gamma \hbar P I}{2e\mu_0 M_S V}(m \times \sigma \times m)$$

Experimantally determined current density ~10^{10}-10^{12} A/m²

Spin Transfer Torque
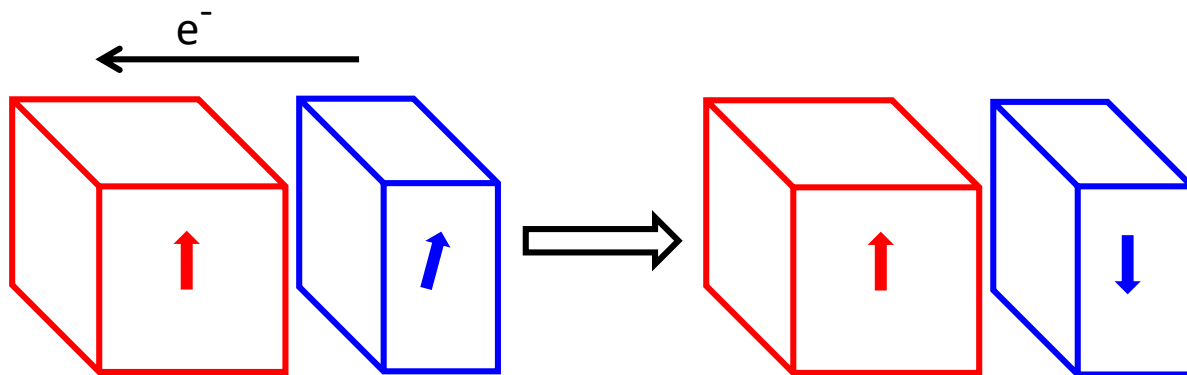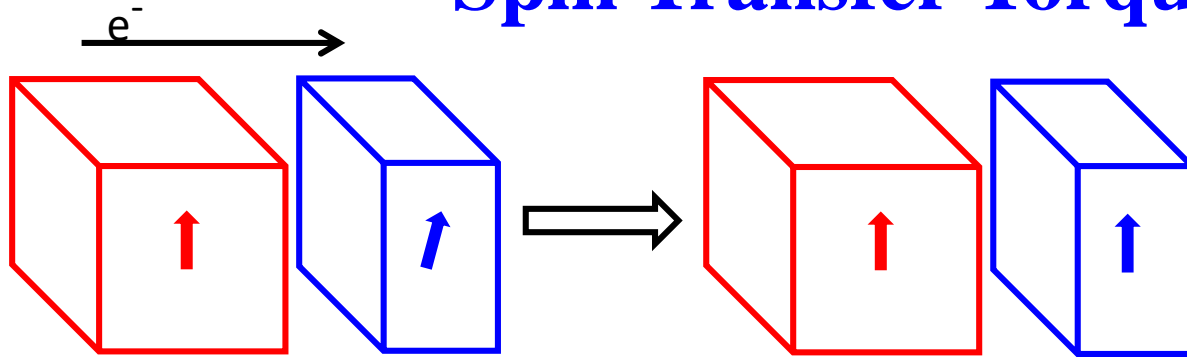
when there is a saturation field, magnetization precession radiates microwave.

In a trilayer, current direction determines the relative orientation of F_1 and F_2 when $H = 0$

Spin Transfer Torque

Point contact device

Nanopillar device

Cu
← free layer →
← fixed layer →
Cu
~10 nm

Cu
Cu
~100 nm
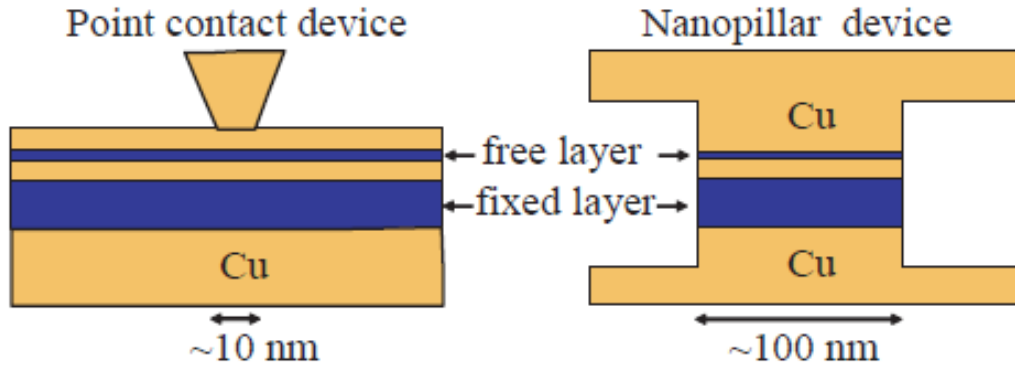
Ralph and Stiles "Spin transfer torques". *JMMM* **320,** 1190–1216 (2008).

(a) 40 nm
120 nm

(b) +I   Cu   Py

(c) dV/dI (Ω)
8.2
8.1
8.0
0   200   400   600
H (Oe)

(d) dV/dI (Ω)
8.2
8.1
8.0
-0.4 -0.2 0.0 0.2 0.4
I (mA)
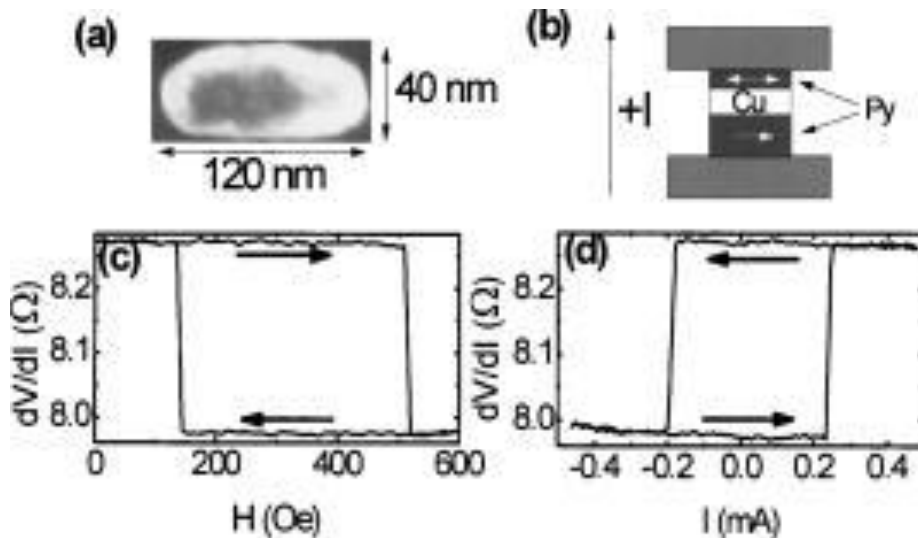
(c) Minor loop of free layer and (d) spin transfer curve at 293*K* 120 Cu∕20 Py∕12 Cu∕X Py∕2 Cu∕30 Au

Ralph and Buhrman's group, APL **87**, 112507 (2005)

Spin Transfer Torque

Landau-Lifshitz-Gilbert equation with Spin Transfer Torque terms

Current induced domain wall motion

Passing spin polarized current from Domain A to Domain B⇒B switches
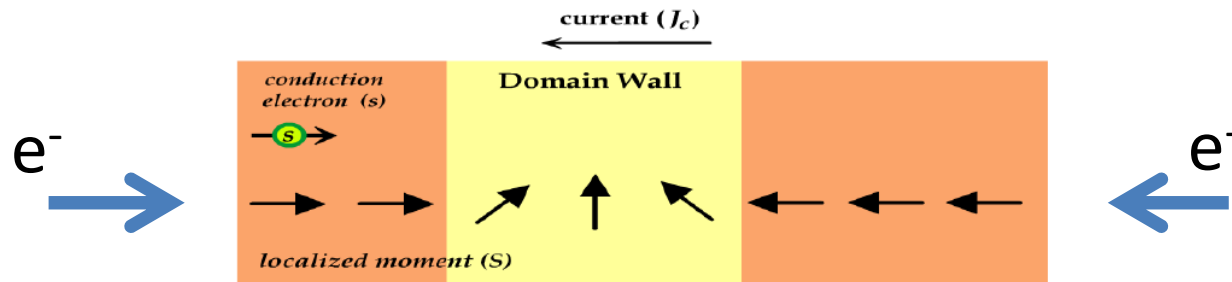
$$\frac{\partial \vec{M}}{\partial t} = -\gamma \vec{M} \times \vec{H}_{eff} + \frac{\alpha}{M_s} \vec{M} \times \frac{\partial \vec{M}}{\partial t} + \vec{T}_{STT}$$

Berger, *JAP* **55**, 1954 (1984)
Tatara *et. al.*, *PRL* **92**, 086601 (2004)
Zhang *et. al.*, *PRL* **93**, 127204 (2004)
Thiaville *et. al.*, *Europhys. Lett.* **69**, 990 (2005)
Stiles *et. al.*, *PRB* **75**, 214423 (2007)

Spin Transfer Torque

Landau-Lifshitz-Gilbert equation with Spin Transfer Torque terms

$$\frac{\partial \vec{M}}{\partial t} = \boxed{-\gamma \vec{M} \times \vec{H}_{\text{eff}}} + \boxed{\frac{\alpha}{M_s} \vec{M} \times \frac{\partial \vec{M}}{\partial t}} \boxed{-\frac{b_j}{M_s^2} \vec{M} \times (\vec{M} \times \frac{\partial \vec{M}}{\partial x})} \boxed{-\frac{c_j}{M_s} \vec{M} \times \frac{\partial \vec{M}}{\partial x}} \qquad b_j, c_j \sim JP/t$$

precession term due to an effective field.

$-\gamma \vec{M} \times \vec{H}_{eff}$

Damping term

$\frac{\alpha}{M_s} \vec{M} \times \frac{\partial \vec{M}}{\partial t}$

$\vec{M}$ localized spin

$-\frac{c_j}{M_s} \vec{M} \times \frac{\partial \vec{M}}{\partial x}$

$-\frac{b_j}{M_s^2} \vec{M} \times \left(\vec{M} \times \frac{\partial \vec{M}}{\partial x} \right)$

Non-adiabatic Spin Transfer Torque (Field-like torque)

Adiabatic Spin Transfer Torque

$\boldsymbol{m_0} = n_0 \frac{\vec{M}}{M_s}$

$\vec{m}$ conduction spin

$\vec{j}$

$\delta \vec{m}$ nonequlibrium spin

T_{IP}
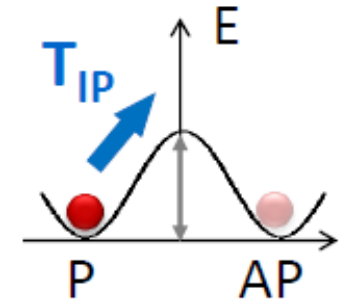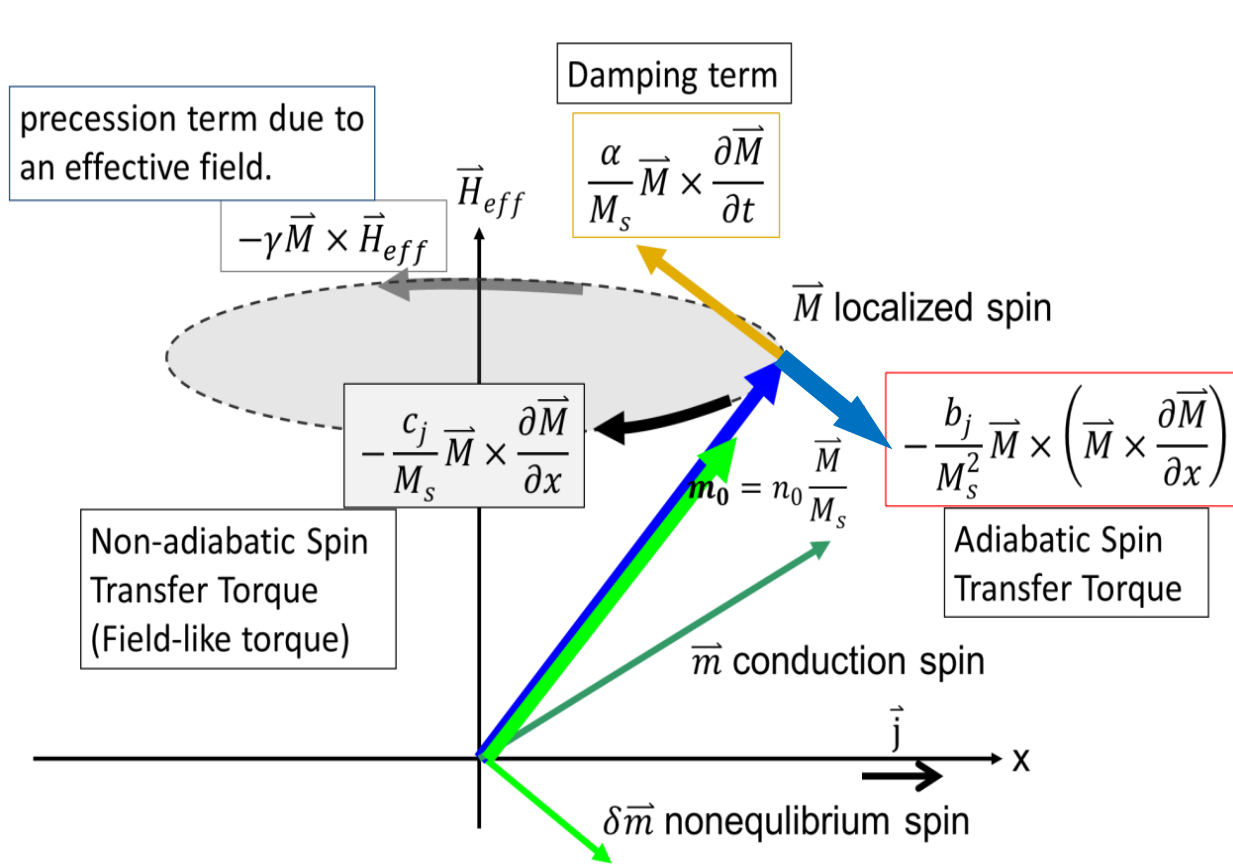
In-plane torque
Anti-damping
Destabilizes M

H_{oop}
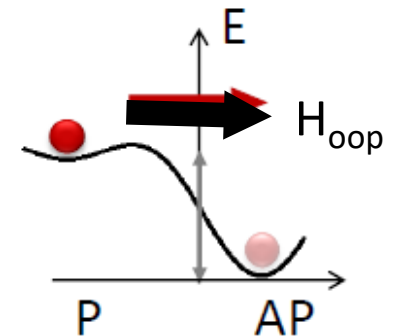
Out-of-plane torque
Field-like torque
Modifies energy barrier

Onsager reciprocity relations

Conjugate variables
$\begin{cases} X_i \\ J_i \end{cases}$

X_i generalized forces

J_i generalized currents

$J_i = \sum_j L_{ij} X_j$ linear response

$i = \{mass, charge, spin, energy, \ldots\}$

$\dot{S} = \sum_i X_i J_i$ entropy creation rate

$L_{ij}(\mathbf{m}, \mathbf{H}_{ext}) = \varepsilon_i \varepsilon_j L_{ji}(-\mathbf{m}, -\mathbf{H}_{ext})$

$L_{ij} = L_{ji}$

LARS ONSAGER

1903 - 1976
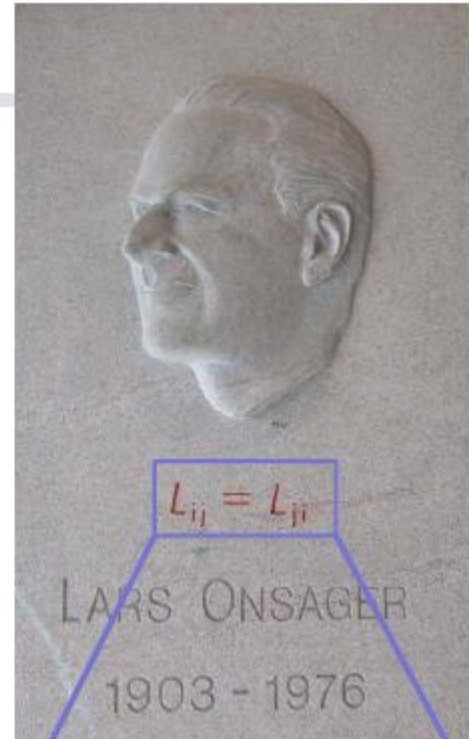
$L_{ij} = L_{ji}$

Equality between certain relations between flows and forces out of equilibrium

Currents can induce magnetization excitations

A time-dependent magnetization can induce (charge and spin) currents

Industrial applications

Read head in hard drives

Anatomy of a Hard Disk Drive

GMR
⬇
Large TMR + Low R
Large CPP-GMR

MRAM

Reading a bit

Word Line   Bit Line

Writing "1"
Writing "0"

Word Line   Bit Line   Bit Line

Bit Line

Magnetic Free Layer
Tunnel barrier
Magnetic Pinned Layer
Antiferromagnetic

Write Word Line

Vdd   Read Word Line

N   P   N

64
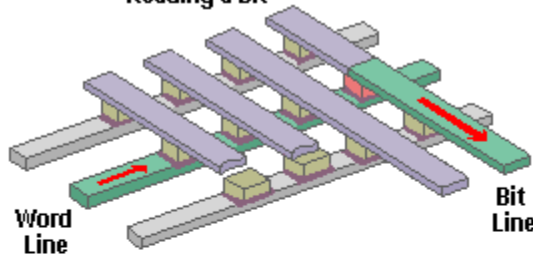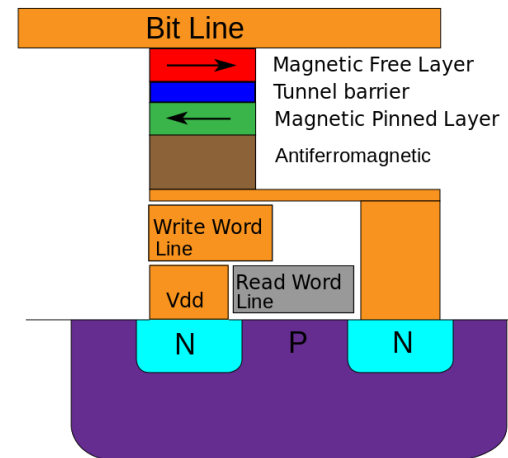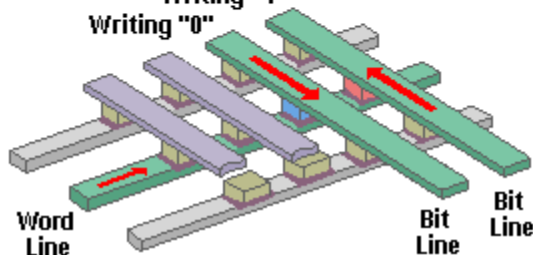
Application of Spin Transfer Torque

Magnetic Domain-Wall Racetrack Memory

Dr. Stuart S. P. Parkin Science **320**, 190 (2008)

A novel three-dimensional spintronic storage class memory

Magnetic nanowires: information stored in the domain walls

- Immense storage capacity of a hard disk drive

- High reliability and performance of solid state memory (DRAM, FLASH, SRAM...)

Reading

Writing

Racetrack storage array
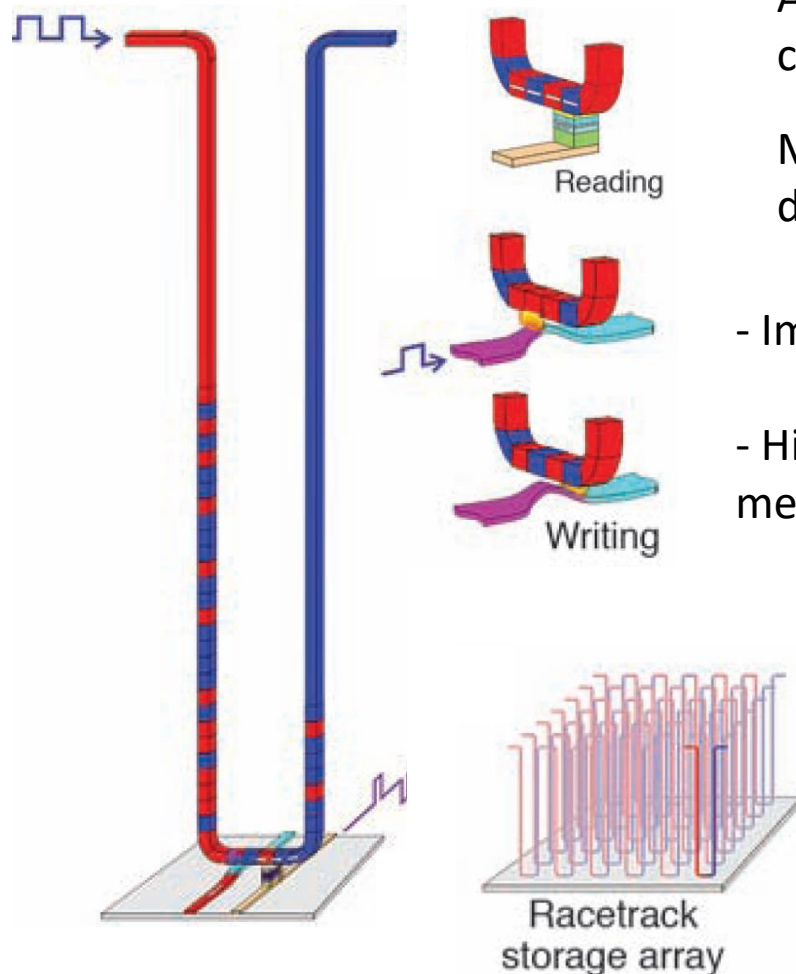
⟶ **Understanding of current induced domain wall (DW) motion**

Application of Spin Transfer Torque

Domain Wall Structures in Permalloy Nanowires

(a)

Transvers DW

(b)

Vortex DW

Vortex Wall

$61.3*\Lambda^2/w$

Asymmetric Transverse Wall

Symmetric Transverse Wall

strip thickness h (nm)

strip width w (nm)
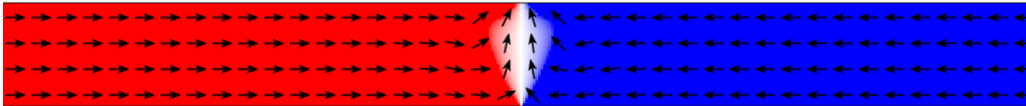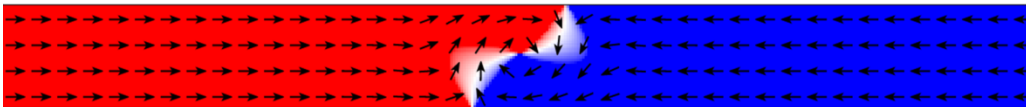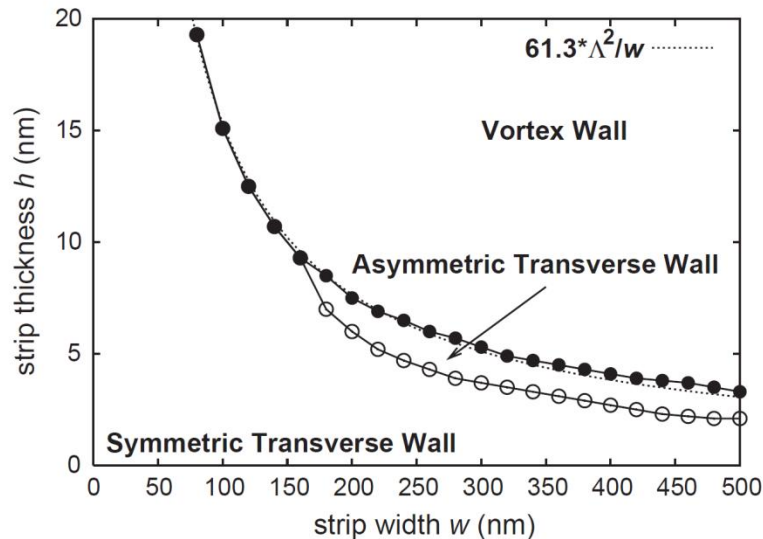
DW traps

protrusion   notch

J. Magn. Magn. Mater. **290**, 750 (2005)
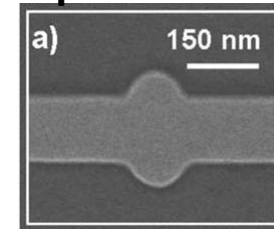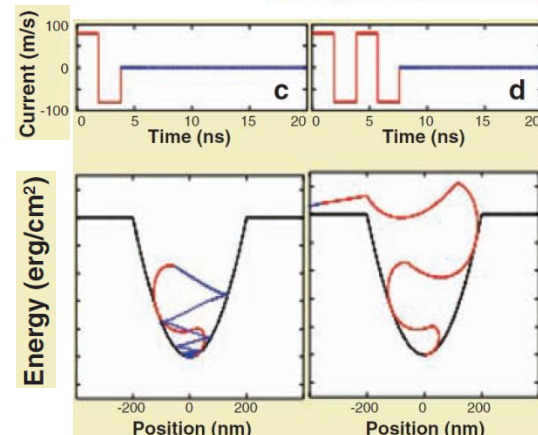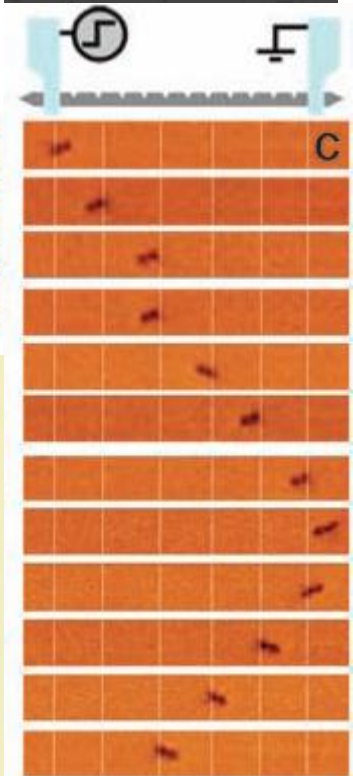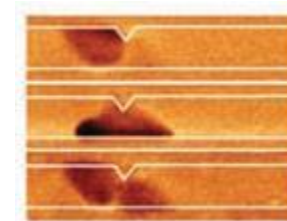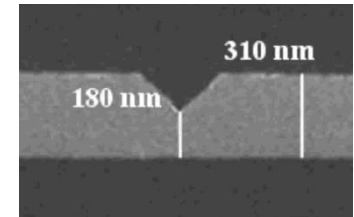
Application of Spin Transfer Torque

DW Oscillators

$j_W < j_a < j_{dep}$

Walker breackdown
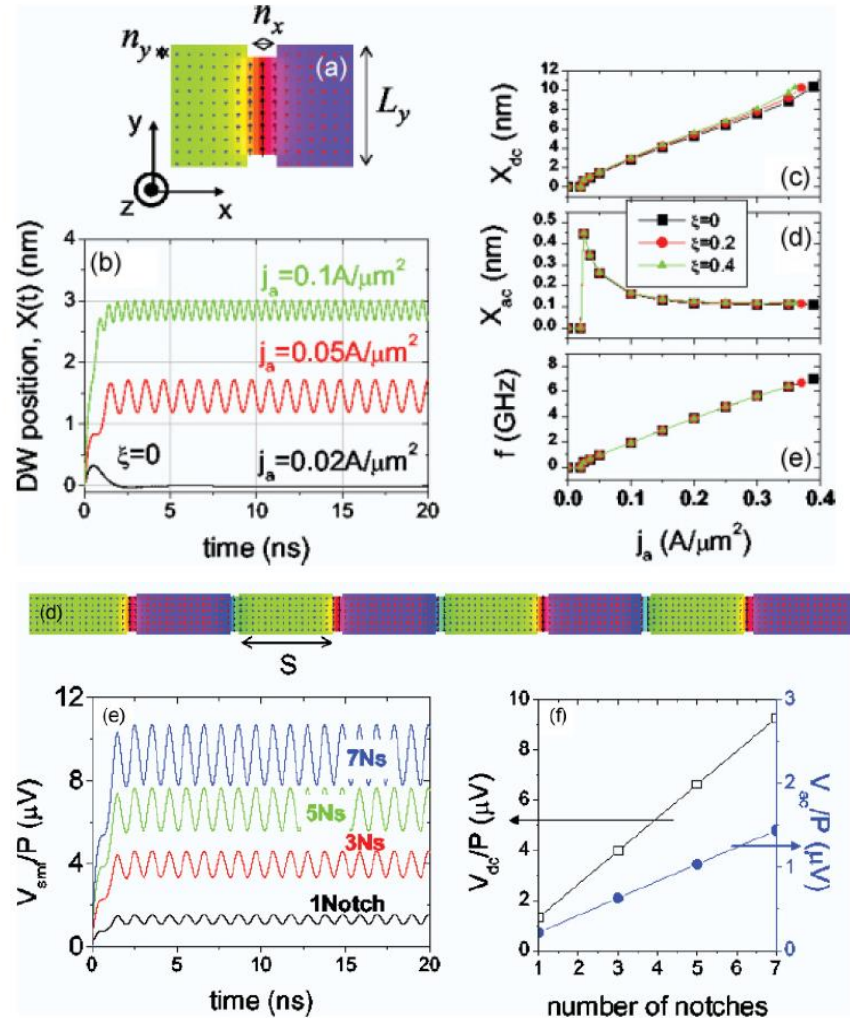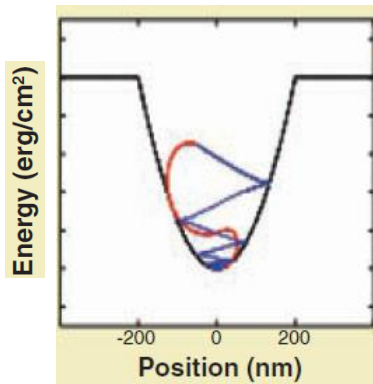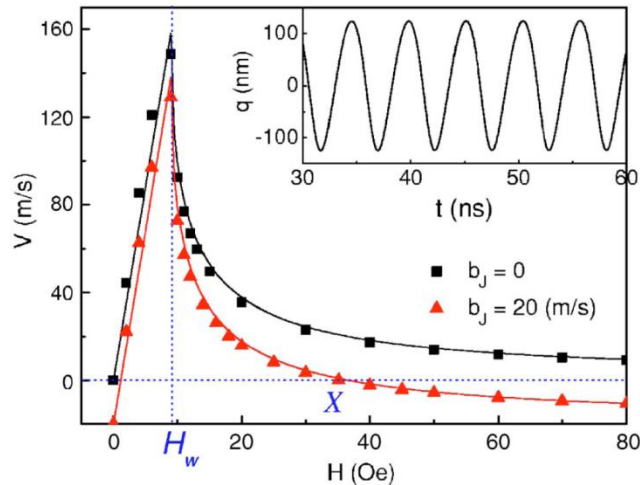
AC Current-Induced DW Resonance
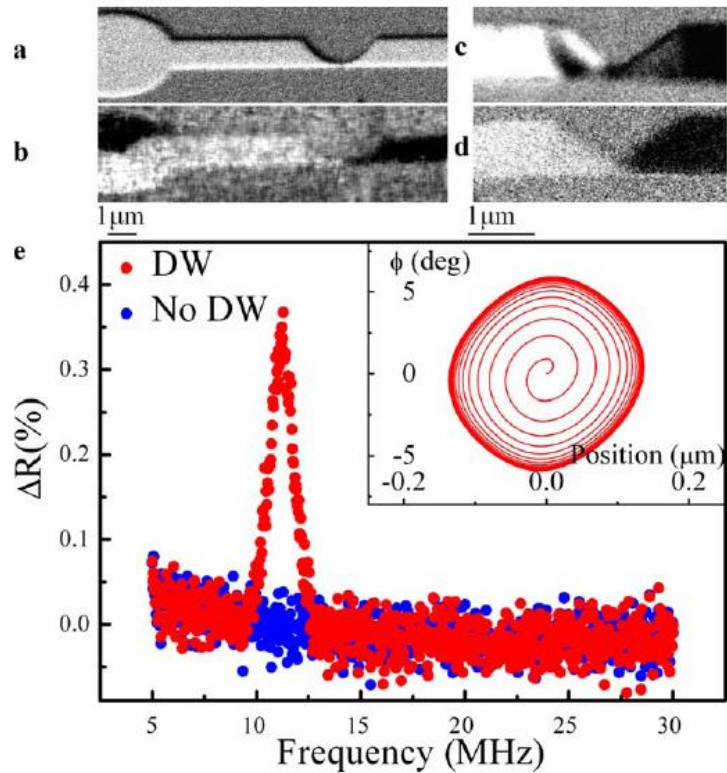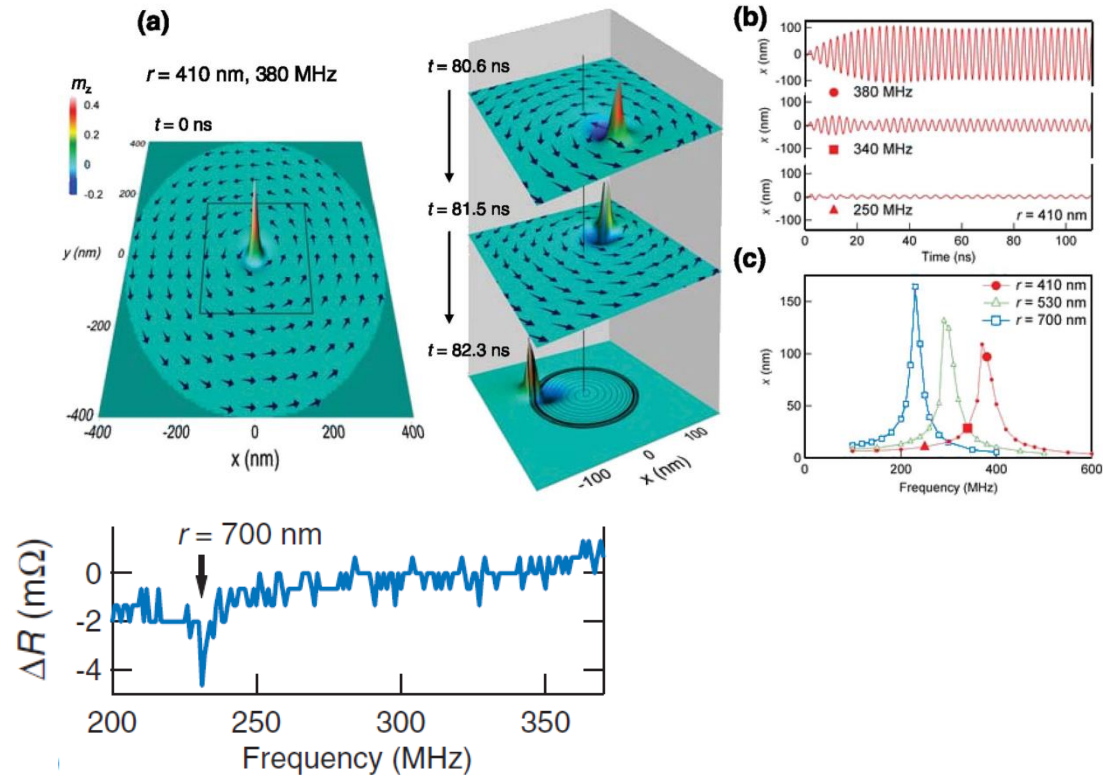
PRB **81**, 060402 (2010),   PRL **97**, 107204 (2006)

Application of Spin Transfer Torque

Radio-Frequency DW Oscillators

✖ CPP-nanopillar

AC

DC
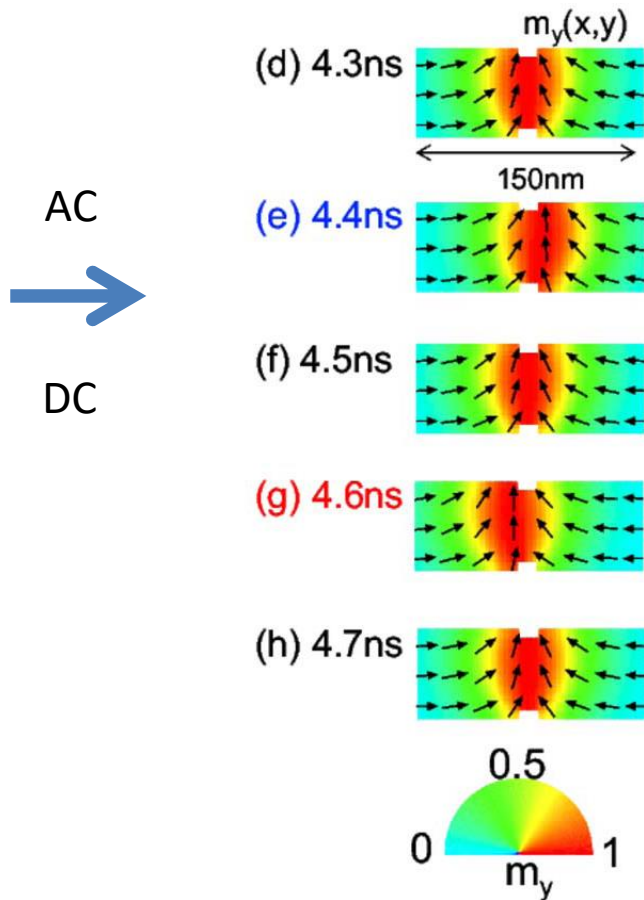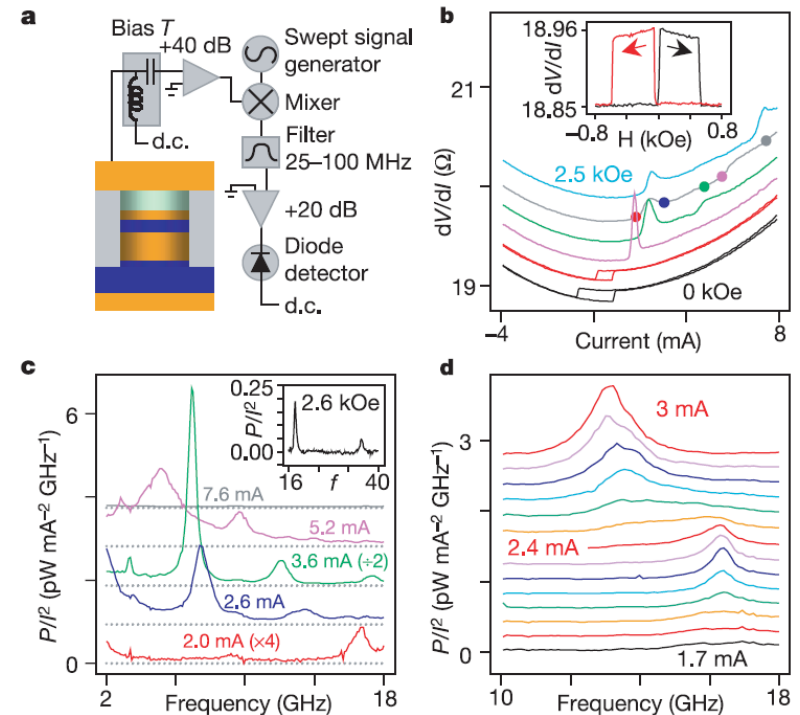
Nature **425**, 380 (2003)

outline

- Giant Magnetoresistance, Tunneling Magnetoresistance
- Spin Transfer Torque (STT)
- Pure Spin current (no net charge current)
    - Spin Hall, Inverse Spin Hall effects
    - Spin Pumping effect
    - Spin Seebeck effect
- Spin Orbit torque (SOT)
- Spin wave in micro and nano magnetic structures

Spin polarized current vs pure spin current

Pure Spin Current

-- with no accompanying net charge current

- Theoretically

$$J_S = \hat{s} \cdot \vec{v} \qquad \rightarrow \qquad J_S = \frac{d}{dt}(\hat{s} \cdot \vec{r}) = \hat{s} \cdot \vec{v} + \frac{d}{dt}\hat{s} \cdot \vec{r}$$

- Experimentally
  - Spin Hall, Inverse Spin Hall effects
  - Spin Pumping effect
  - Spin Seebeck effect
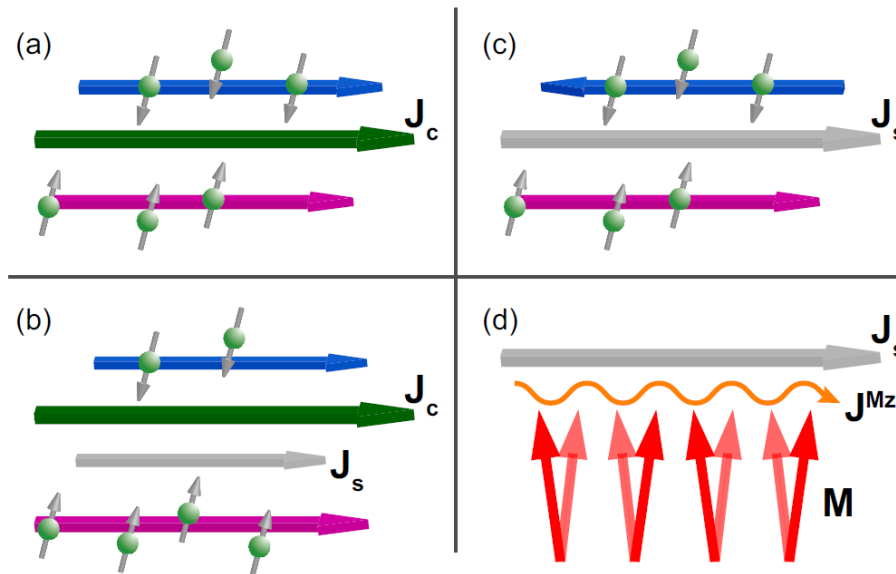
Spin Current

Proper Definition of Spin Current in Spin-Orbit Coupled Systems

Junren Shi,[1,2] Ping Zhang,[2,3] Di Xiao,[2] and Qian Niu[2]

[1]Institute of Physics and ICQS, Chinese Academy of Sciences, Beijing 100080, People's Republic of China
[2]Department of Physics, The University of Texas at Austin, Austin, Texas 78712, USA
[3]Institute of Applied Physics and Computational Mathematics, Beijing 100088, People's Republic of China

The conventional definition of spin current is incomplete and unphysical in describing spin transport in systems with spin-orbit coupling. A proper and measurable spin current is established in this study, which fits well into the standard framework of near-equilibrium transport theory and has the desirable property to vanish in insulators with localized orbitals. Experimental implications of our theory are discussed.

$$J_S = \hat{s} \cdot \vec{v} \qquad \rightarrow \qquad J_S = \frac{d}{dt}(\hat{s} \cdot \vec{r}) = \hat{s} \cdot \vec{v} + \frac{d}{dt}\hat{s} \cdot \vec{r}$$

torque dipole term

1. spin current is not conserved
2. can even be finite in insulators with localized eigenstates only
3. not in conjugation with any mechanical or thermodynamic force, not fitted into the standard near-equilibrium transport theory

1. spin current conserved
2. vanishes identically in insulators with localized orbitals
3. in conjugation with a force given by the gradient of the Zeeman field or spin-dependent chemical potential

Spin Current

Spin currents and spin superfluidity

E.B. Sonin*

*Racah Institute of Physics, Hebrew University of Jerusalem, Jerusalem 91904, Israel*

The present review analyses and compares various types of dissipationless spin transport: (1) Superfluid transport, when the spin-current state is a metastable state (a local but not the absolute minimum in the parameter space). (2) Ballistic spin transport, when spin is transported without losses simply because the sources of dissipation are very weak. (3) Equilibrium spin currents, i.e. genuine persistent currents. (4) Spin currents in the spin Hall effect. Since superfluidity is frequently connected with Bose condensation, recent debates about magnon Bose condensation are also reviewed. For any type of spin currents simplest models were chosen for discussion in order to concentrate on concepts rather than the details of numerous models. The various hurdles on the way of using the concept of spin current (absence of the spin-conservation law, ambiguity of spin current definition, etc.) were analysed. The final conclusion is that the spin-current concept can be developed in a fully consistent manner, and is a useful language for the description of various phenomena in spin dynamics.

4. Conclusions

The present review focused on four types of dissipationless spin transport: (1) superfluid transport, when the spin-current state is a metastable state (a local but not the absolute minimum in the parameter space); (2) Ballistic spin transport, when spin is transported without losses simply because the sources of dissipation are very weak; (3) equilibrium spin currents, i.e. genuine persistent currents and (4) spin currents in the spin Hall effect. The dissipationless spin transport was a matter of debate for decades, though sometimes they were to some extent semantic. Therefore, it was important to analyse what physical phenomenon was hidden under this or that name remembering that any choice of terminology is inevitably subjective and is a matter of taste and convention. The various hurdles on the way of using the concept of spin current (absence of the spin-conservation law, ambiguity of spin current definition, etc.) were analysed. The final conclusion is that the spin-current concept can be developed in a fully consistent manner, though this is not an obligatory language of description: spin currents are equivalent to deformations of the spin structure, and one may describe the spin transport also in terms of deformations and spin stiffness.

The recent revival of interest to spin transport is motivated by the emerging of spintronics and high expectations of new applications based on spin manipulation. This is far beyond the scope of the present review, but hopefully the review could justify using of the spin-current language in numerous investigations of spin-dynamics problems, an important example of which is the spin Hall effect.

Spin Hall effect

Spin Hall Effect: Electron flow generates transverse spin current

n-type GaAs

Electron flow

Spin up

Spin down
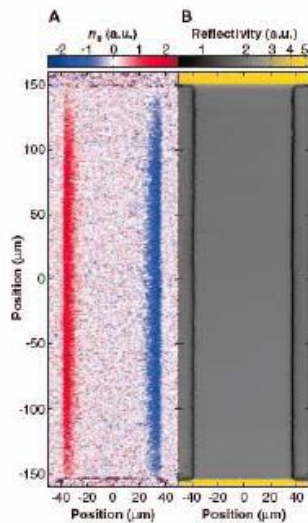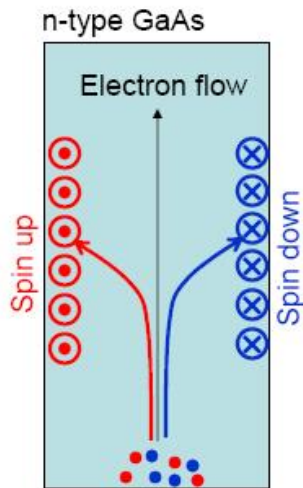
SHE observed
in GaAs
using Kerr effect
to measure spin

Kato et.al. (Awschalom),
Science 306, 1910 (2004)

Now observed at room temperature in ZnSe

M. I. Dyakonov and V. I. Perel, *JETP* **13** 467 (1971)

J. E. Hirsch, *Phys. Rev. Lett.* **83** 1834 (1999)

Guo *et al*, PRL **100** 096401 (2008)

The Intrinsic SHE is due to topological band structures

Berry curvature

$$\dot{\vec{r}} = \frac{1}{\hbar}\frac{\partial \varepsilon_n(\vec{k})}{\partial \vec{k}} + \frac{e}{\hbar}\vec{E}\times\vec{\Omega}(\vec{k})$$

The extrinsic SHE is due to asymmetry in electron scattering for up and down spins. – spin dependent probability difference in the electron trajectories
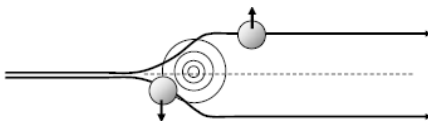
Side jump
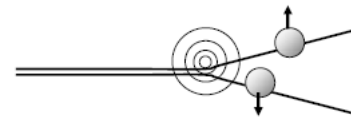
Skew scattering

Inverse Spin Hall effect
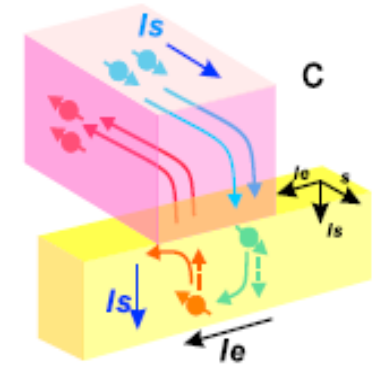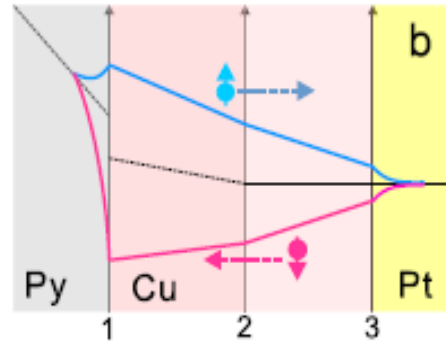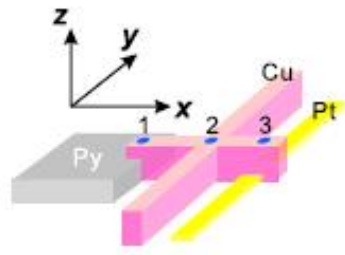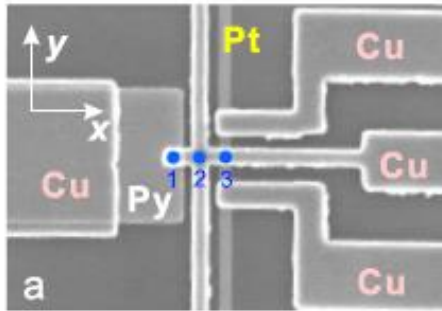
FIG. 1 (color online). (a) Scanning electron microscope (SEM) image of the fabricated spin Hall device together with a schematic illustration of the fabricated device. (b) Schematic spin dependent electrochemical potential map indicating spin accumulation in Cu and Pt induced by the spin injection from the Py pad. Dashed line represents the equilibrium position. (c) Schematic illustration of the charge accumulation process in the Pt wire, where I_S and I_e denote injected pure spin current and induced charge current, respectively. (d) Spin dependent electrochemical potential map for the charge to spin-current conversion and (e) corresponding schematic illustration.
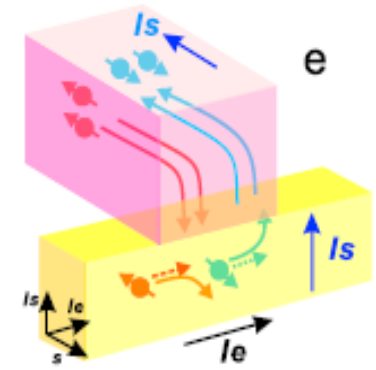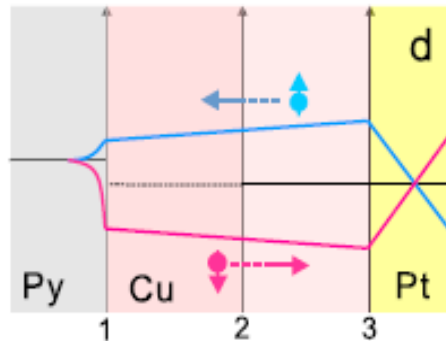
Kimura *et al*, PRL **98**, 156601 (2007)

Guo *et al*, PRL **100** 096401 (2008)

Inverse Spin Hall effect : ISHE

Spin Hall Effect

J. E. Hirsch

Department of Physics, University of California, San Diego, La Jolla, California 92093-0319
(Received 24 February 1999)

It is proposed that when a charge current circulates in a paramagnetic metal a transverse spin imbalance will be generated, giving rise to a "spin Hall voltage." Similarly, it is proposed that when a spin current circulates a transverse charge imbalance will be generated, giving rise to a Hall voltage, in the absence of charge current and magnetic field. Based on these principles we propose an experiment to generate and detect a spin current in a paramagnetic metal.

ISHE: converts a spin current into an electric voltage

SO-coupling bends the two electrons in the same direction → charge accumulation → E_{ISHE}.

$$\mathbf{E}_{ISHE} \propto \mathbf{J}_s \times \boldsymbol{\sigma}$$

Js : spin current density

σ : direction of the spin-polarization vector of a spin current.

ISHE: Governed by spin-orbit coupling
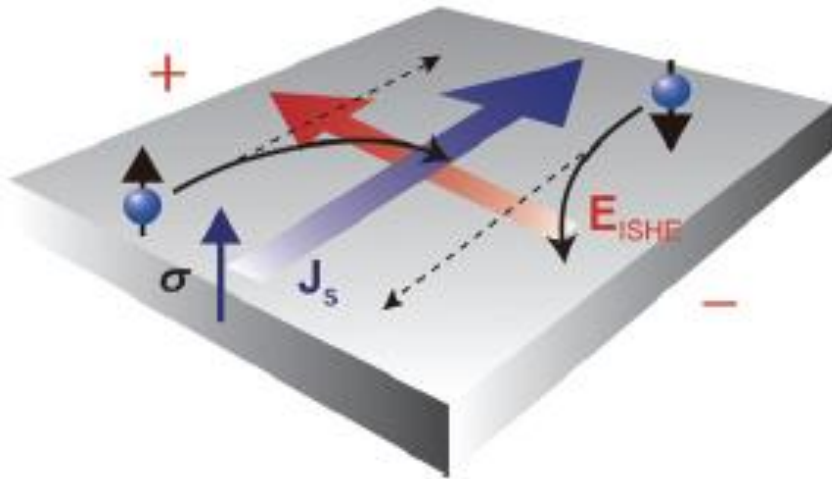
J. Appl. Phys. **109**, 103913 (2011)

SHE vs. ISHE

Spin Hall

Charge Current

⇓

Transverse

Spin Imbalance
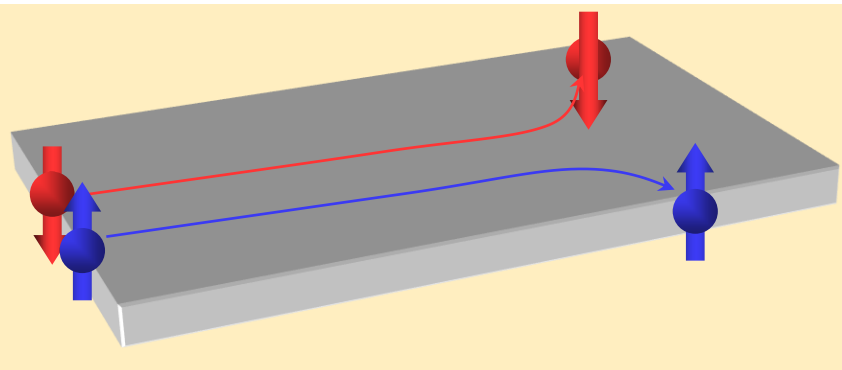
Inverse Spin Hall

Spin Current

⇓

Transverse

Charge Imbalance
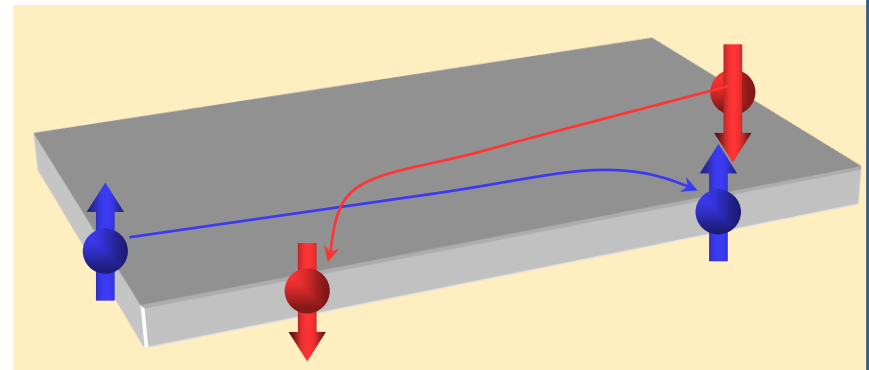
ISHE : direct & sensitive detection of a spin current !

Spin Hall Angle

$$\gamma = \frac{\sigma_{SH}}{\sigma_c}$$

⟵ spin Hall conductivity

⟵ charge conductivity

stronger spin orbit interaction ⟶ larger γ

Spin Pumping

F   N

I_S
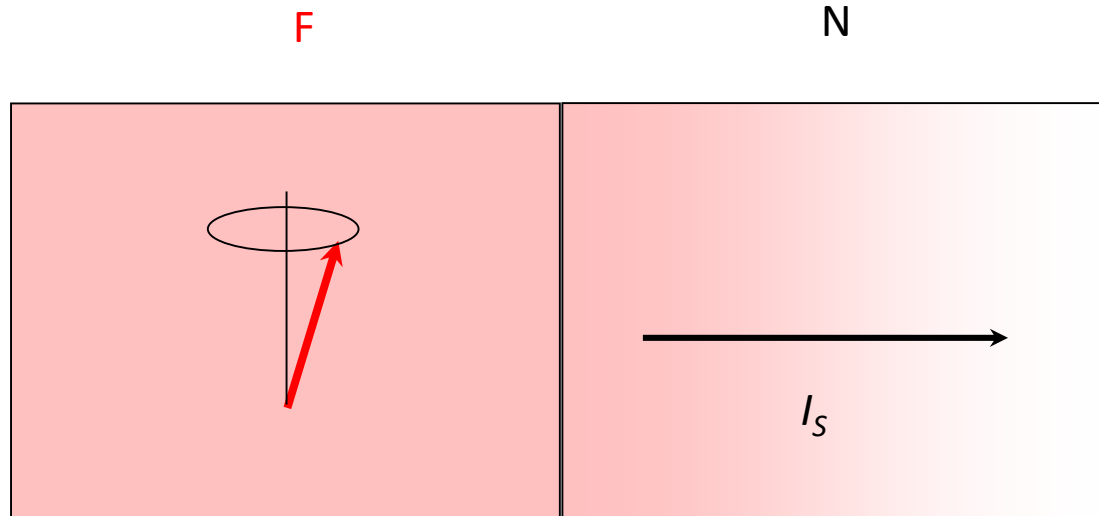
Landau-Lifshitz-Gilbert

$$\dot{\mathbf{m}} = -\gamma \mathbf{m} \times \mathbf{H}_{\text{eff}} + \mathbf{m} \times (\tilde{\alpha}\dot{\mathbf{m}})$$

$$I_S^{pump} = \frac{\hbar}{4\pi} g_r^{\downarrow\uparrow} m \times \frac{\partial m}{\partial t}$$

$g_r^{\downarrow\uparrow}$: spin mixing conductance

Spin accumulation gives rise to spin current
in neighboring normal metal
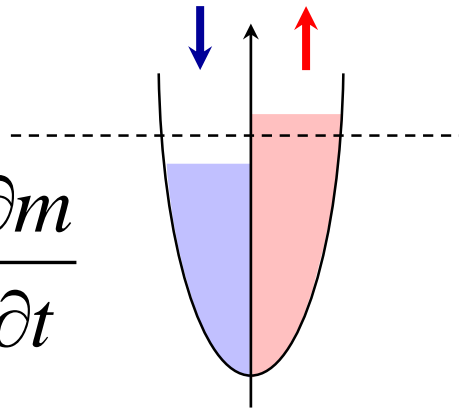
In the FMR condition, the steady
magnetization precession in a F is
maintained
by balancing the absorption of the
applied microwave
and the dissipation of the spin
angular momentum --the transfer
of angular momentum from the
local spins to conduction electrons,
which polarizes the conduction-
electron spins.

80

Spin Pumping
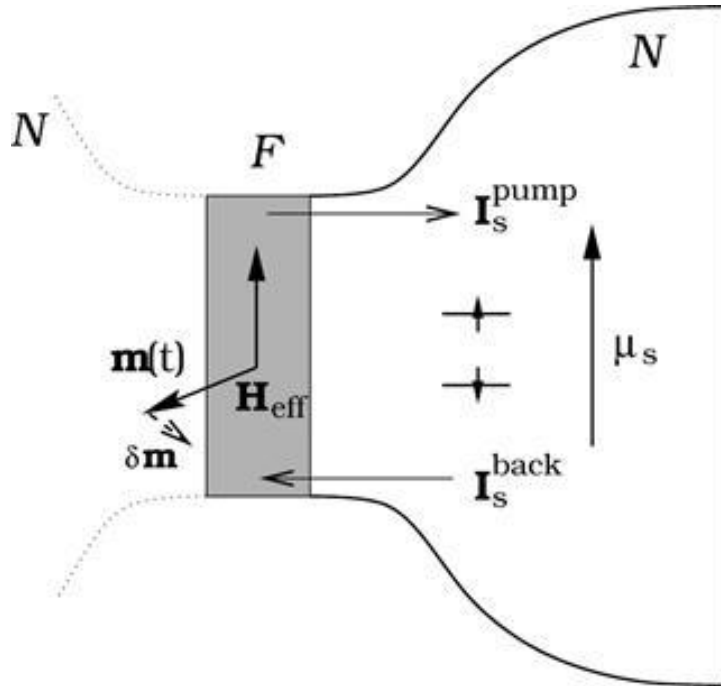
A ferromagnetic film F sandwiched between two nonmagnetic reservoirs N. For simplicity of the discussion in this section, we mainly focus on the dynamics in one (right) reservoir while suppressing the other (left), e.g., assuming it is insulating. The spin-pumping current I_s and the spin accumulation μ_s in the right reservoir can be found by conservation of energy, angular momentum, and by applying circuit theory to the steady state $I_s^{pump} = I_s^{back}$.

$$I_s^{pump} = \frac{\hbar}{4\pi}\left(A_r \mathbf{m} \times \frac{d\mathbf{m}}{dt} - A_i \frac{d\mathbf{m}}{dt}\right).$$

Tserkovnyak *et al*, PRL **88**, 117601 (2002), Enhanced Gilbert Damping in Thin Ferromagnetic Films
Brataas *et al*, PRB **66**, 060404(R) (2002), Spin battery operated by ferromagnetic resonance
Tserkovnyak *et al*, PRB **66**, 224403 (2002), Spin pumping and magnetization dynamics in metallic multilayers
Rev Mod Phys **77**, 1375 (2005) Nonlocal magnetization dynamics in ferromagnetic heterostructures

Spin Backflow and ac Voltage Generation by Spin Pumping and the Inverse Spin Hall Effect

HuJun Jiao1 and Gerrit E.W. Bauer2,1

1Kavli Institute of NanoScience, Delft University of Technology, 2628 CJ Delft, The Netherlands
2Institute for Materials Research and WPI-AIMR, Tohoku University, Sendai 980-8577, Japan

The spin current pumped by a precessing ferromagnet into an adjacent normal metal has a constant polarization component parallel to the precession axis and a rotating one normal to the magnetization. The former is now routinely detected as a dc voltage induced by the inverse spin Hall effect (ISHE). Here we compute ac ISHE voltages much larger than the dc signals for various material combinations and discuss optimal conditions to observe the effect. The backflow of spin is shown to be essential to distill parameters from measured ISHE voltages for both dc and ac configurations.
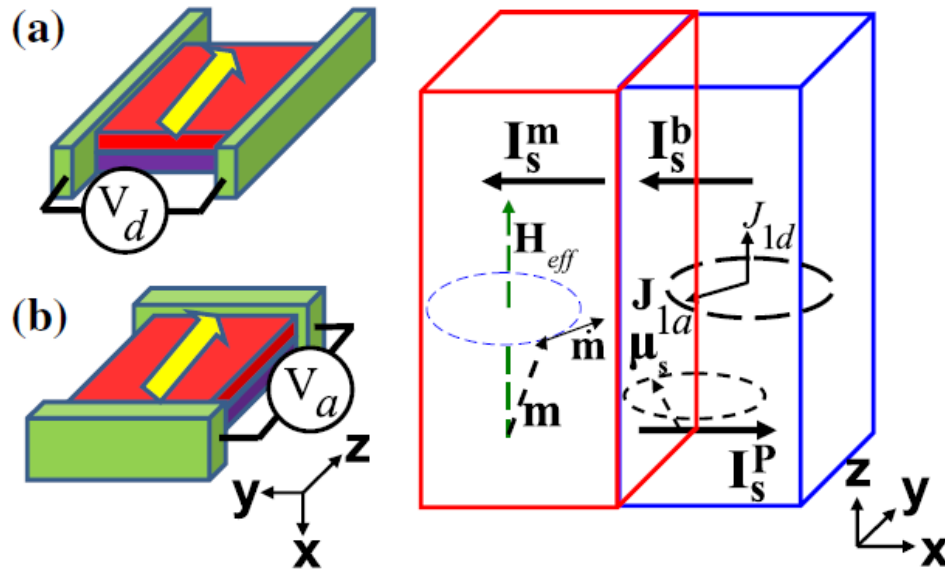
FIG. 1 (color online). Schematic spin battery operated by FMR, for the measurement configurations (a) and (b). The ac (dc) voltage drops along the z (y) direction. The right panel introduces the parameters of the model. The effective field $\mathbf{H}_{eff}$ is the sum of the external field $\mathbf{H}_{ex}$ and the uniaxial field $\mathbf{H}_{un}$, $\mathbf{H}_{ex}$, and $\mathbf{H}_{un}$ point along the z axis. The dc component $J_{1d}(j_{1s}^z)\mathbf{e}_z$ and ac component $\mathbf{J}_{1a}(\mathbf{j}_{1s}^a)$ constitute the spin current $\mathbf{j}_{1s}$.

Combining Spin Pumping and Inverse Spin Hall Effect
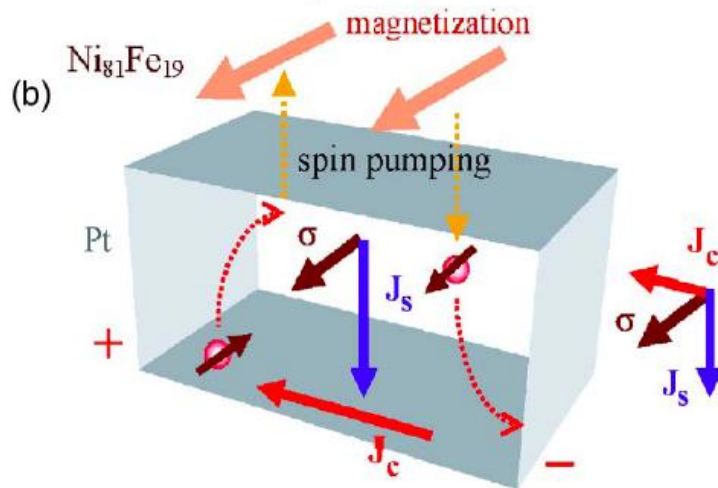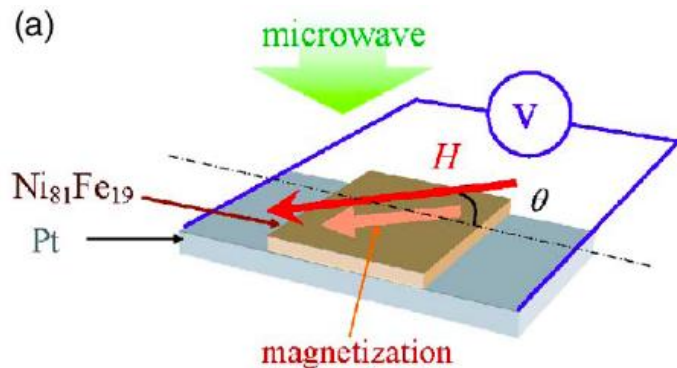
FMR

⇓

Spin Current

in adjacent

normal metal

⇓

Transverse

Charge Current

The spin-orbit interaction bends these two electrons in the same direction and induces a charge current transverse to Js,

$$\mathbf{J_c} = D_{ISHE}\mathbf{J_s} \times \sigma.$$

The surface of the Py layer is of a 1×1 mm^2 square shape. Two electrodes are attached to both ends of the Pt layer.

Saitoh *et al*, APL **88**, 182509 (2006)

Kimura *et al*, PRL **98**, 156601 (2007)

Spin Seebeck effect

a Thermocouple

Metal A
E
E
Metal B
∇T
T_1
T_2
V

$$\delta V = S \delta T$$

b Spin Seebeck effect

Metallic magnet
$\mu_\uparrow - \mu_\downarrow$
∇T
T_1
T_2
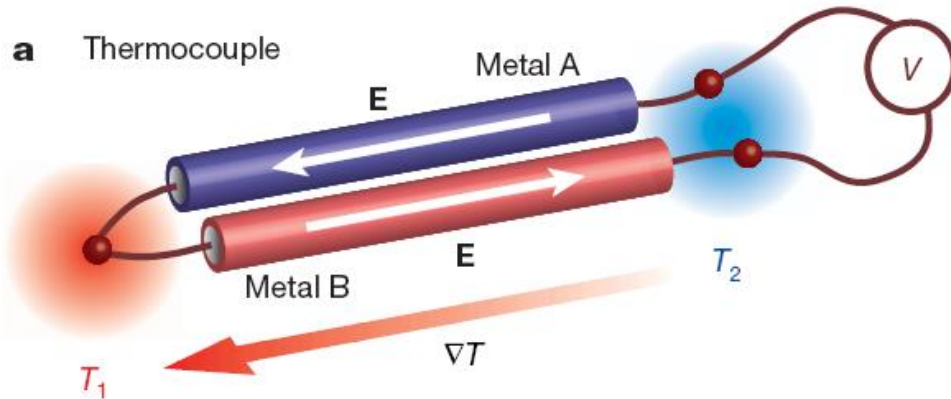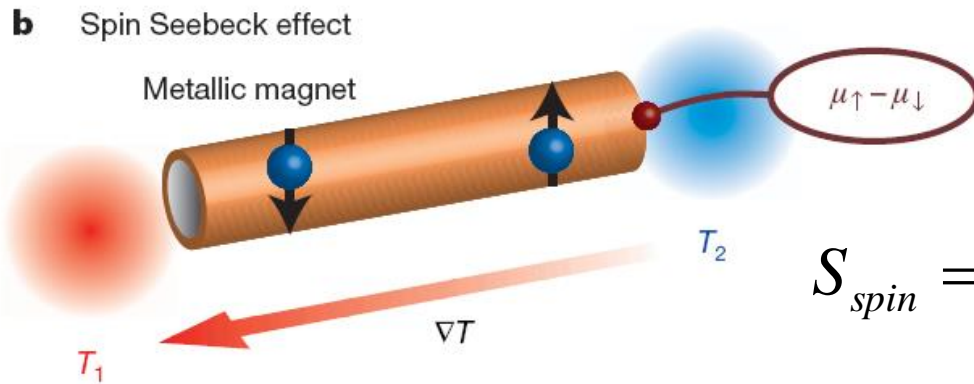
$$\delta V_{spin} = S_{spin} \delta T$$

$$S_{spin} = (1/e)[\partial \mu^c_\uparrow / \partial T - \partial \mu^c_\downarrow / \partial T]$$

Spin Seebeck effect

In a ferromagnetic metal, **up- spin and down-spin conduction** electrons have **different scattering rates and densities**, and thus have different Seebeck coefficients.

$$j_s = j_\uparrow - j_\downarrow = (\sigma_\uparrow S_\uparrow - \sigma_\downarrow S_\downarrow)(-\nabla T)$$

This **spin current** flows **without accompanying charge currents** in the open-circuit condition, and the up-spin and down-spin currents flow **in opposite directions** along the temperature gradient
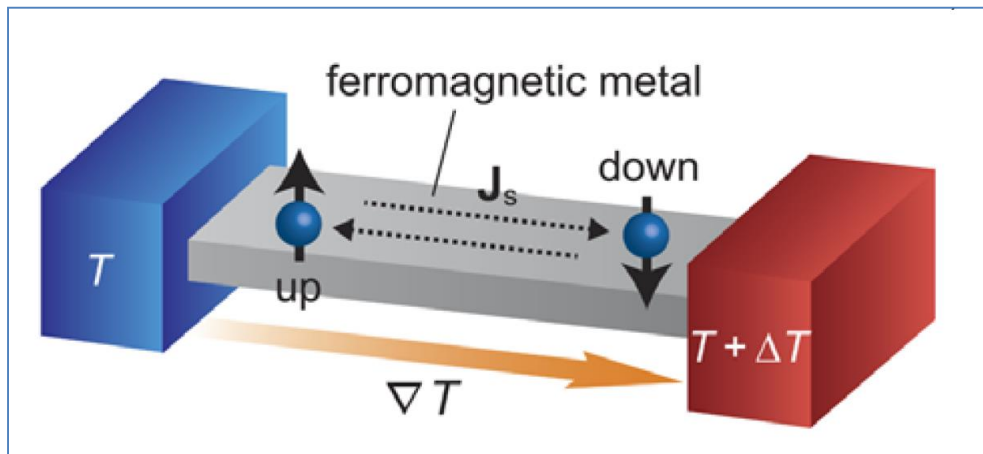
How to detect j_S ?

Inverse Spin Hall Effect coverts j_S into j_C

Detection of Spin Current by Inverse Spin Hall Effect

The ISHE converts a spin current into an **electromotive force** E_{SHE} by means of spin–orbit scattering.
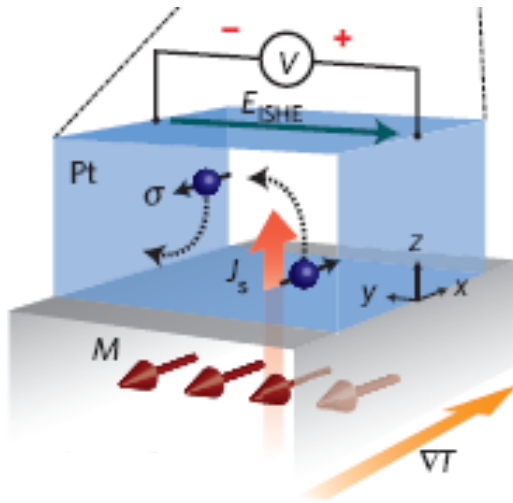
$$E_y = E_{SHE} = D_{ISHE} J_S \times \sigma$$

A spin current carries a spin-polarization vector σ along a spatial direction J_S.

(a) Conventional SSE setup

(b) Longitudinal SSE setup
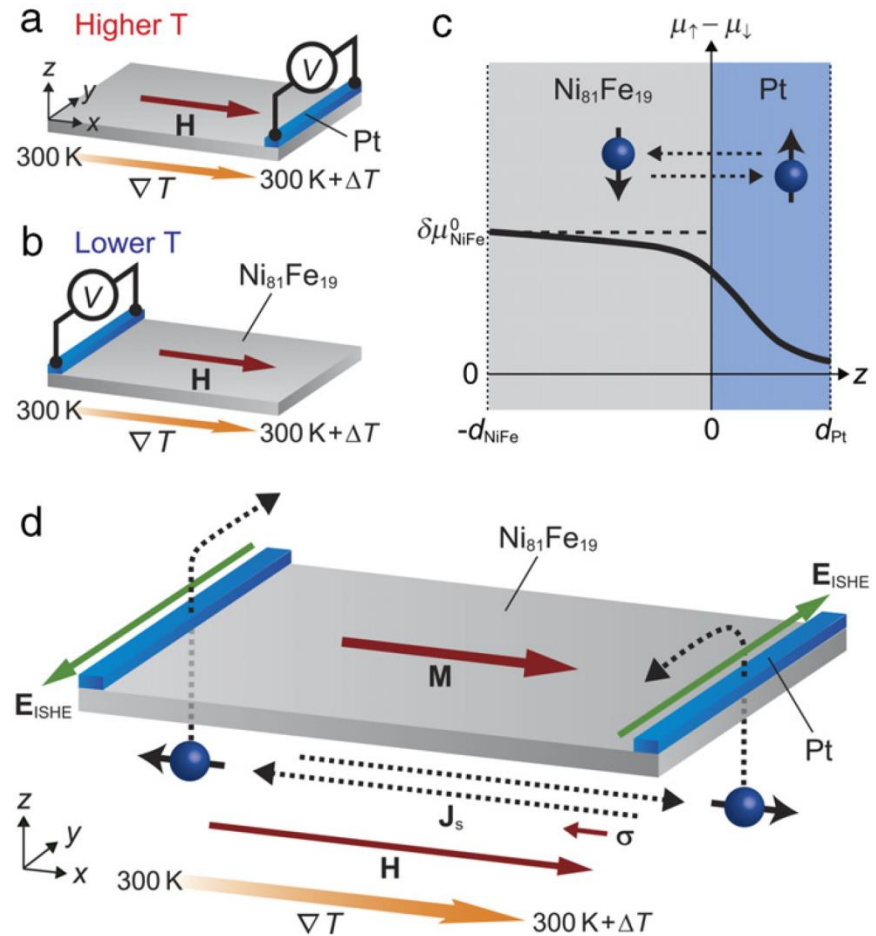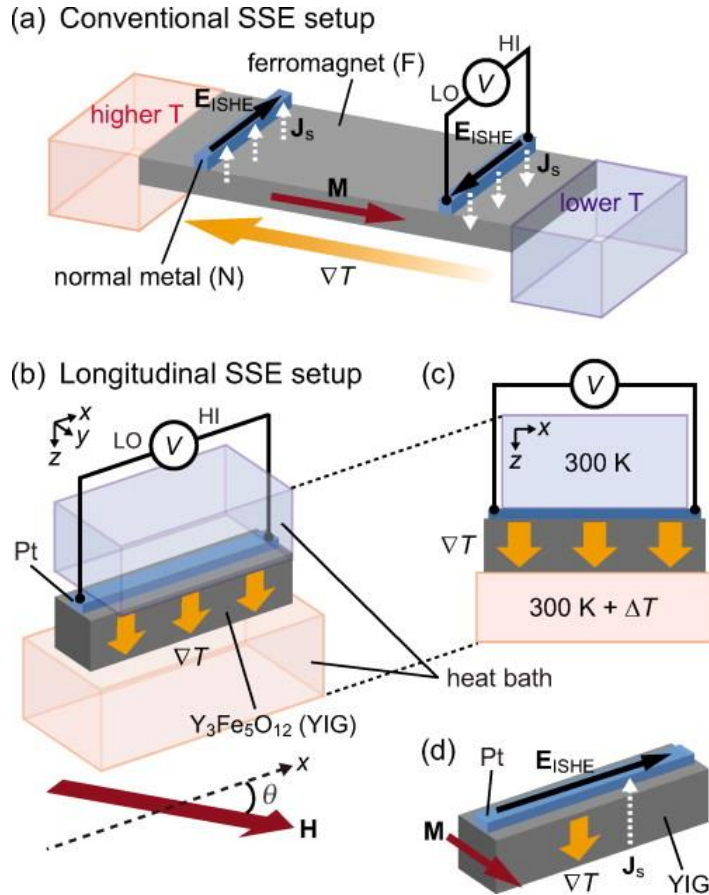
(a) A schematic of the conventional setup for measuring the ISHE induced by the SSE. Here, ∇T, M, Js, and EISHE denote a temperature gradient, the magnetization vector of a ferromagnet (F), the spatial direction of the spin current flowing across the F/no...
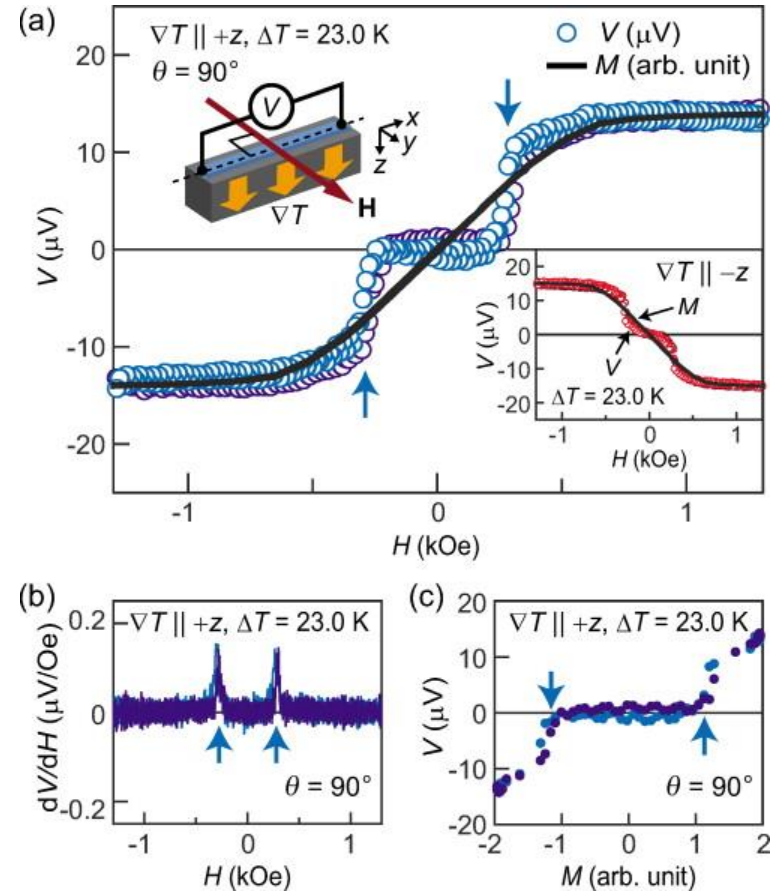
(a) Comparison between the H dependence of V at ΔT = 23.0 K in the YIG/Pt system and the magnetization M curve of the YIG. During the V measurements, ∇T was applied along the +z direction [the −z direction for the inset to (a)] and H was applied along the...

Uchida et al, APL 97, 172505 (2010)

Thermoelectric effect:

The thermoelectric effect is the direct conversion of temperature differences to electric voltage and vice-versa.

Seebeck effect (1821):
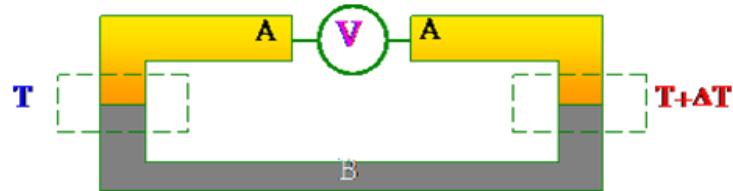
$\Delta T \rightarrow V$

Peltier effect (1823):
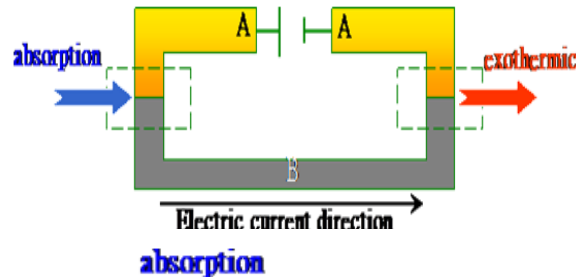
$I \rightarrow Q$

Thomson effect (1851):
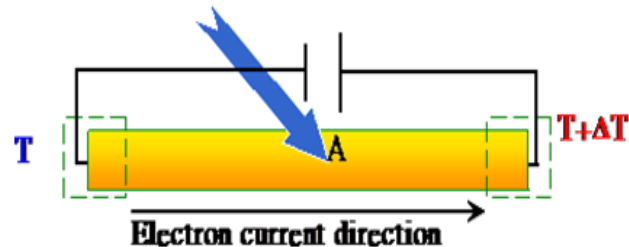
$I + \Delta T \rightarrow Q$

Nernst effect :
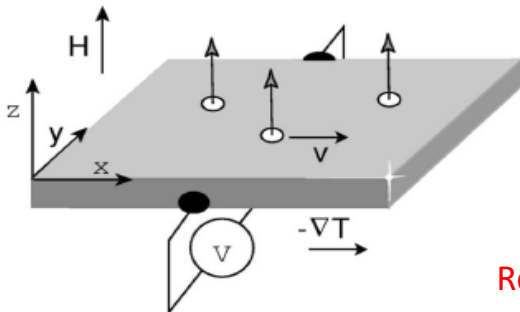
When a sample is subjected to a magnetic field and a temperature gradient normal (perpendicular) to each other, an electric field will be induced normal to both.

Ref: http://web.nchu.edu.tw/~lschang/Thermoelectric.htm

88

outline

- Giant Magnetoresistance, Tunneling Magnetoresistance
- Spin Transfer Torque (STT)
- Pure Spin current (no net charge current)
  - Spin Hall, Inverse Spin Hall effects
  - Spin Pumping effect
  - Spin Seebeck effect
- Spin Orbit torque (SOT)
- Spin wave in micro and nano magnetic structures

Spin Orbit Torque in a dilute magnetic semiconductor

Evidence for reversible control of magnetization in a ferromagnetic material by means of spin–orbit magnetic field

Alexandr Chernyshov, Mason Overby, Xinyu Liu, Jacek K. Furdyna, Yuli Lyanda-Geller & Leonid P. Rokhinson

Nature Physics **5**, 656 (2009)

magnetization can be reversibly manipulated by the spin–orbit-induced polarization of carrier spins generated by the injection of unpolarized currents. Specifically, we demonstrate domain rotation and hysteretic switching of magnetization between two orthogonal easy axes in a model ferromagnetic semiconductor.
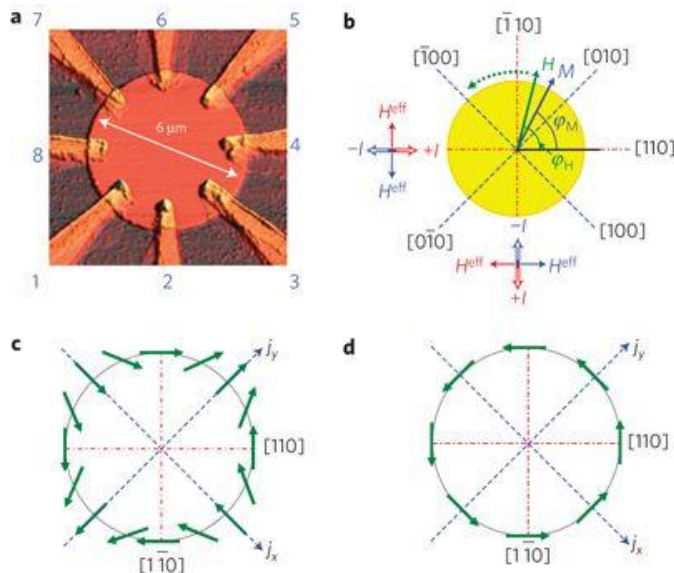
a, Atomic force micrograph of sample A with eight non-magnetic metal contacts. **b**, Diagram of device orientation with respect to crystallographic axes, with easy and hard magnetization axes marked with blue dashed and red dot–dash lines, respectively. Measured directions of H^{eff} field are shown for different current directions. **c,d**, Orientation of effective magnetic field with respect to current direction for strain-induced (**c**) and Rashba (**d**) spin–orbit interactions. The current-induced Oersted field under the contacts has the same symmetry as the Rashba field.
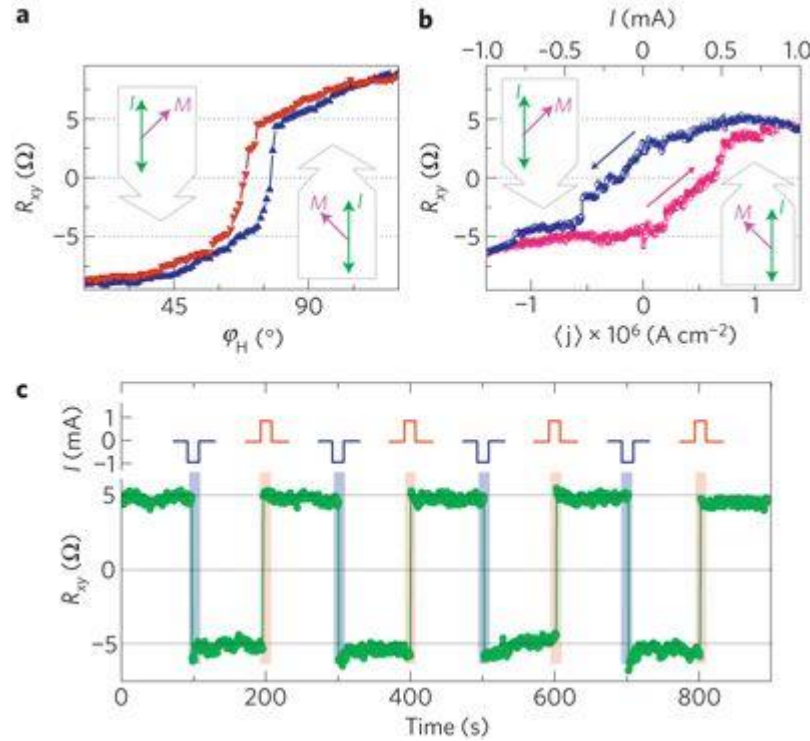
a, ϕ_H dependence of R_{xy} near the $[010] \rightarrow [\bar{1}00]$ magnetization switching for $I=\pm0.7$ mA in sample A for $I \| [1\bar{1}0]$. **b**, R_{xy} shows hysteresis as a function of current for a fixed field $H=6$ mT applied at $\phi_H=72°$. **c**, Magnetization switches between the $[0\bar{1}0]$ and $[\bar{1}00]$ directions when alternating ±1.0 mA current pulses are applied. The pulses have 100 ms duration and are shown schematically above the data curve. R_{xy} is measured with $I=10$ μA.

Spin Orbit Torque in ferromagnetic heterostructures

Symmetry and magnitude of spin–orbit torques in ferromagnetic heterostructures

Kevin Garello[1]*, Ioan Mihai Miron[2], Can Onur Avci[1], Frank Freimuth[3], Yuriy Mokrousov[3], Stefan Blügel[3], Stéphane Auffret[2], Olivier Boulle[2], Gilles Gaudin[2] and Pietro Gambardella[1,4,5]*

Recent demonstrations of magnetization switching induced by in-plane current injection in heavy metal/ferromagnetic heterostructures have drawn increasing attention to spin torques based on orbital-to-spin momentum transfer. The symmetry, magnitude and origin of spin–orbit torques (SOTs), however, remain a matter of debate. Here we report on the three-dimensional vector measurement of SOTs in AlO_x/Co/Pt and MgO/CoFeB/Ta trilayers using harmonic analysis of the anomalous and planar Hall effects. We provide a general scheme to measure the amplitude and direction of SOTs as a function of the magnetization direction. Based on space and time inversion symmetry arguments, we demonstrate that heavy metal/ferromagnetic layers allow for two different SOTs having odd and even behaviour with respect to magnetization reversal. Such torques include strongly anisotropic field-like and spin transfer-like components, which depend on the type of heavy metal layer and annealing treatment. These results call for SOT models that go beyond the spin Hall and Rashba effects investigated thus far.

Spin Orbit Torque

Landau-Lifshitz-Gilbert equation with Spin Orbit Torque term

$$\frac{\partial \vec{M}}{\partial t} = -\gamma \vec{M} \times \vec{H}_{\text{eff}} + \frac{\alpha}{M_s} \vec{M} \times \frac{\partial \vec{M}}{\partial t} - \frac{b_j}{M_s^2} \vec{M} \times (\vec{M} \times \frac{\partial \vec{M}}{\partial x}) - \frac{c_j}{M_s} \vec{M} \times \frac{\partial \vec{M}}{\partial x} \qquad b_j, c_j \sim JP/t$$

$$\frac{\partial \mathbf{M}}{\partial t} = -\gamma \mathbf{M} \times \mathbf{H} + \frac{a}{M_s} \mathbf{M} \times \frac{\partial \mathbf{M}}{\partial t} - (\mathbf{u} \cdot \nabla)\mathbf{M} + \frac{\beta}{M_s} \mathbf{M} \times (\mathbf{u} \cdot \nabla)\mathbf{M} + \frac{\alpha_{\text{SHE}}}{M_s} \mathbf{M} \times (\boldsymbol{\sigma} \times \mathbf{M})$$

dissipative and reactive torques
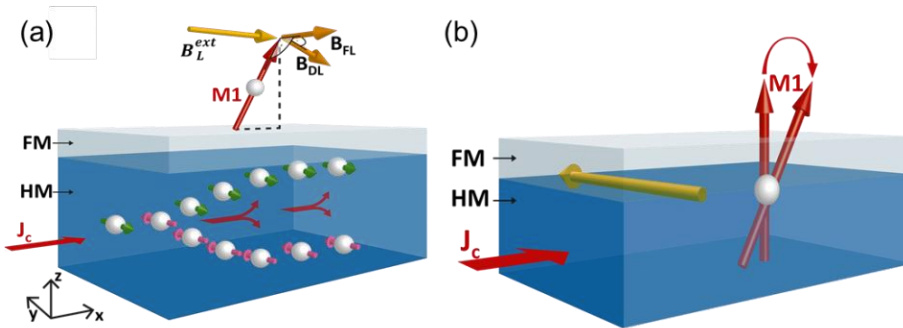
(a) schematics of spin Hall effect. A longitudinal electron current, Jc, in heavy metal (HM) is converted into a transverse spin current by spin-orbit scattering. The spin current leads to a spin accumulation at the HM/FM interface that diffuses across the interface into the FM and exerts torques. (b) The effective field generated by the inverse spin galvanic effect at the interface, which can lead to a switching of the magnetization.
Webpage of **Prof. Dr. Mathias Kläui,** University of Mainz
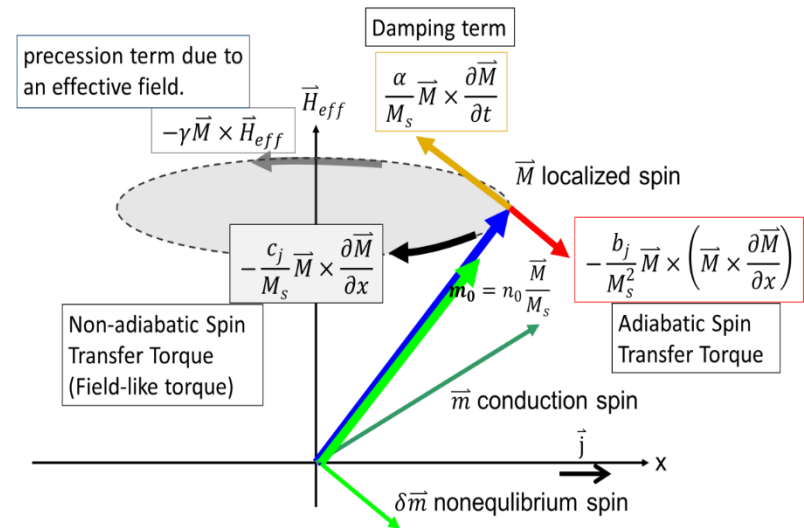
outline

- Giant Magnetoresistance, Tunneling Magnetoresistance
- Spin Transfer Torque (STT)
- Pure Spin current (no net charge current)
  - Spin Hall, Inverse Spin Hall effects
  - Spin Pumping effect
  - Spin Seebeck effect
- Spin Orbit torque (SOT)
- Spin wave in micro and nano magnetic structures

Nano Magnetism

Vortex induced by dc current in a circular magnetic spin valve nanopillar
L. J. Chang and S. F. Lee
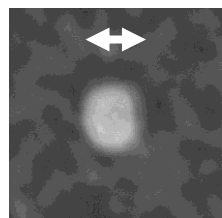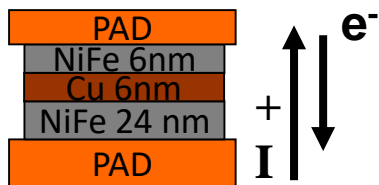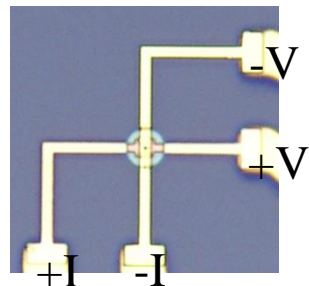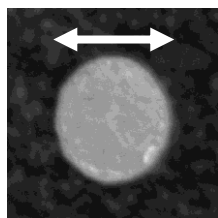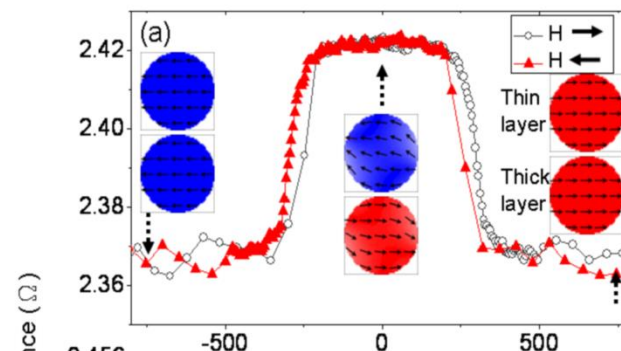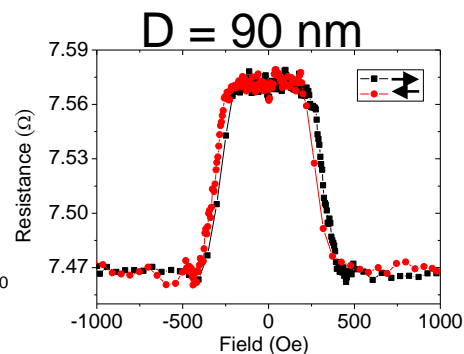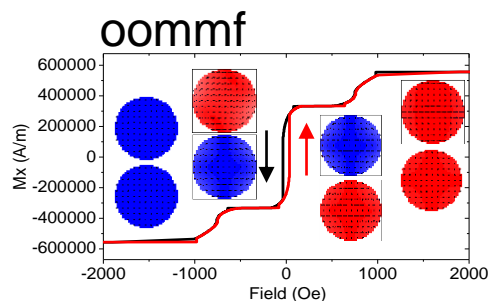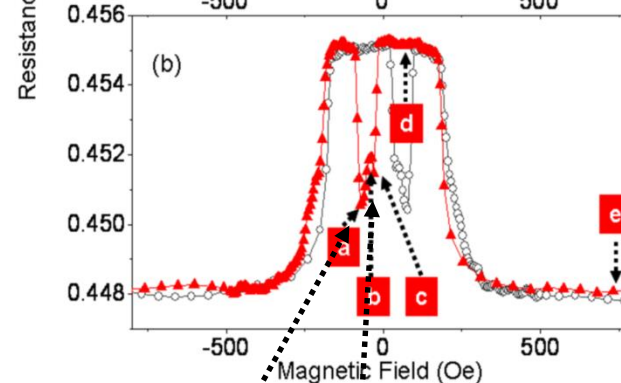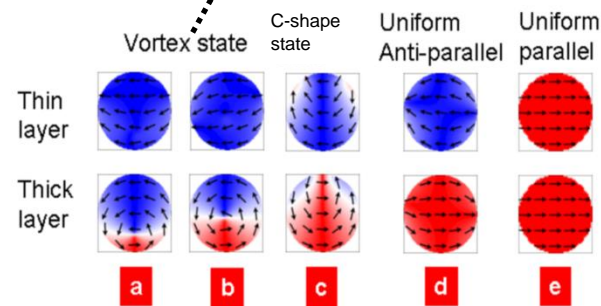
Current driven vortex nucleation

D = 160 nm   H = 0 Oe
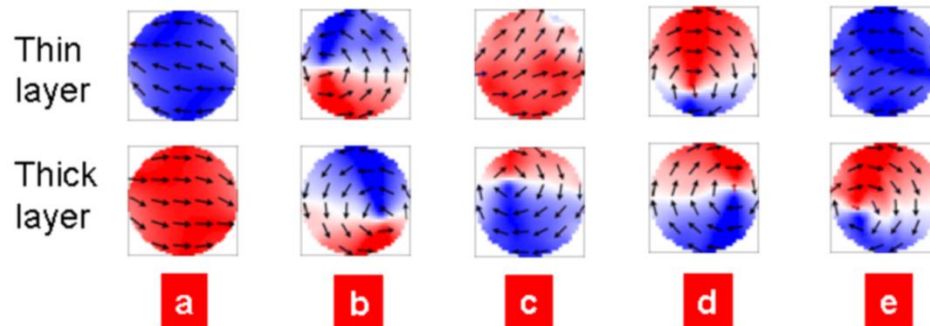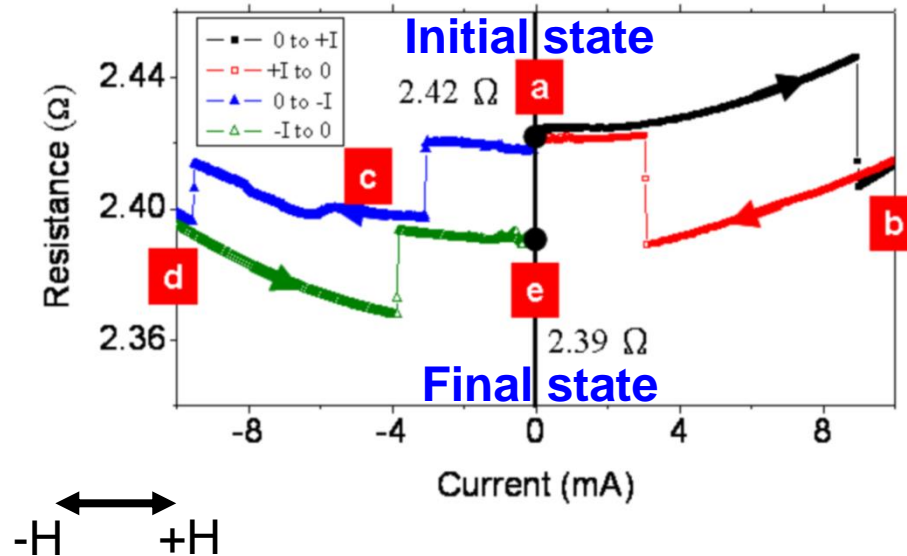
Other research interest include superconductor-magnetic material proximity effect, Ferromagnetic Resonance etc.

Domain wall oscillation in a trapping potential

Theoretical Backgrounds

Resonant DW induced by AC spin-polarized current in Ferromagnetic strips

DW dynamics equation

$$(1 + \alpha^2)m\frac{d^2x}{dt^2} = F_p(x) + F_f + F_s + F_d$$

where $m = \frac{2(\mu_0 L_y L_z)}{\gamma_0^2(N_z - N_y)\Delta_0}$ is the effective DW

mass (kg), and the other variables are listed

below.

L_y : width of wire (m)

L_z : thickness of wire (m)

μ_0 : permeability ($4\pi \times 10^{-7}$ VsA^{-1}m^{-1})

γ_0 : electron gyromagnetic ratio (2.2×10^5 Vs^{2}m^{-1}kg^{-1})

N_z, N_y : transverse demagnetizing factors

Δ_0 : DW width (m)

x : DW position (m)

Experiment Methods

four point probe measurement circuit

high frequency measurements circuit

AC current induced localized domain wall oscillators in NiFe/Cu/NiFe submicron wires

Nucleation of Pinned anti-parallel transverse DW

DW resonators for frequency-selective operation
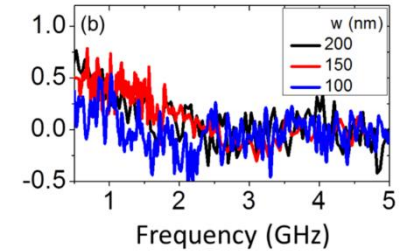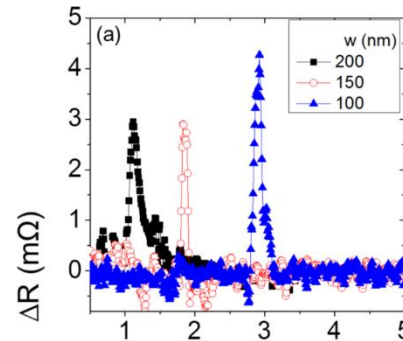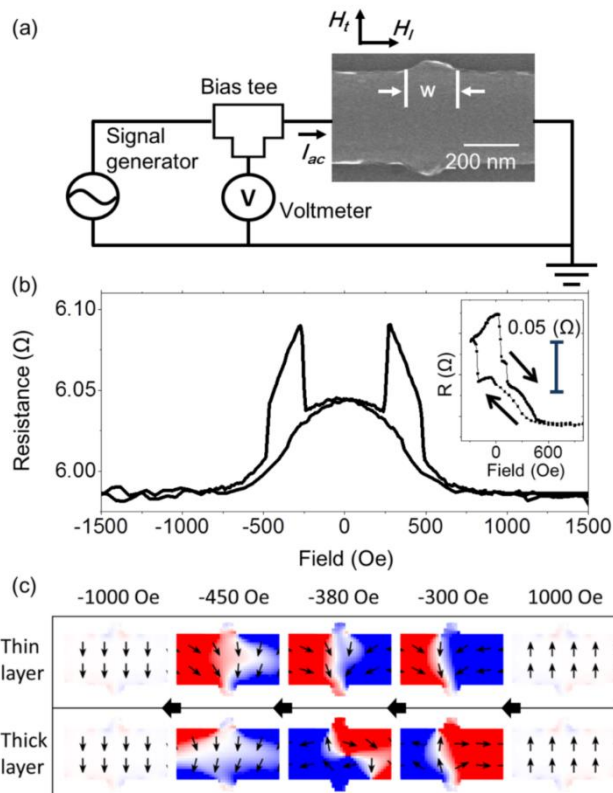
(a) Experimental measurement of the ac current induces resonance excitation of pinned DW trapped at the protrusion. Resistance change as a function of ac excitation current frequency for the submicron wires containing artificial symmetric protrusions with three different widths of protrusion w = 200, 150, and 100 nm. (b) The response curve measured at the saturation field with a uniform state of submicron wires (without DW). The ΔR is observed unchanged with frequency for each of the samples.

AC current induced localized domain wall oscillators in NiFe/Cu/NiFe submicron wires

Resonance frequency of pinned DW dependence on the width of trap w, the solid circles and the open triangles indicate the experiment and simulation results respectively. The inset shows the simulated time evolutions of the DW motion with w = 150 nm. (b)-(d) Potential landscape of pinned DW from micromagnetic simulation with three different width of protrusion w = 200, 150, 100 nm.

Measurement and simulation results

Reversible domain wall motion induced by dc current in NiFe/Cu/NiFe submicron wires
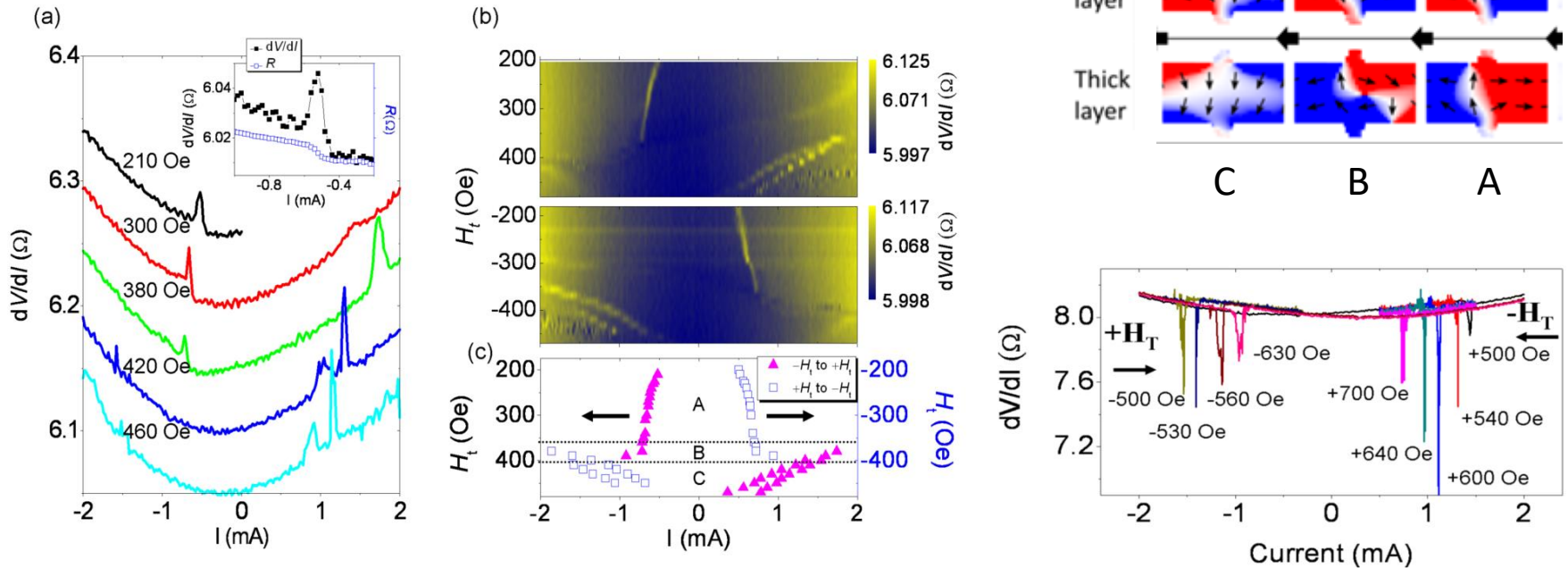
Differential resistance vs. current density at different external transverse fields H_t, enlarged in the inset for V/I vs. j at $H_t = 210$ Oe. (b) Map of dV/dI versus transverse field and dc current. (c) Critical current I_c vs. H_t.

Strong angular dependent transmission ratio due to interplay between spin waves and the domain wall in perpendicular magnetic anisotropy materials

Simulation on magnetic nanowires
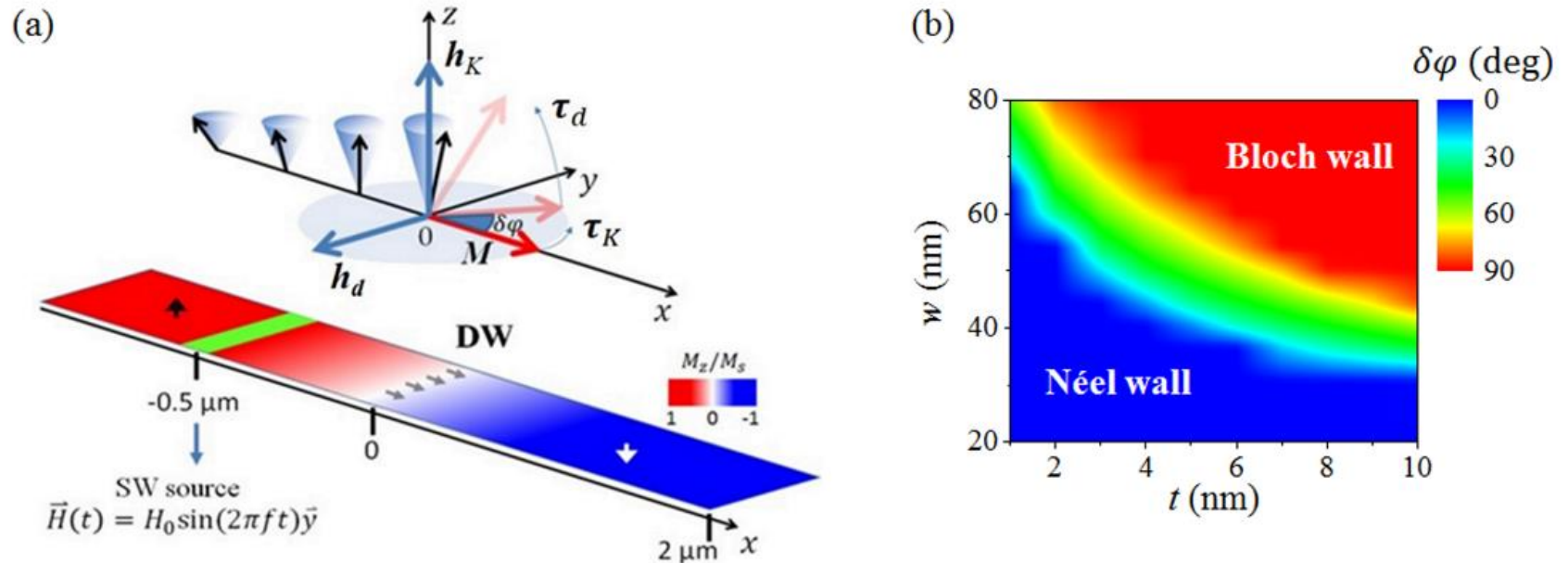
Domain wall motion induced by the magnonic spin current

Xi-guang Wang, Guang-hua Guo,* Yao-zhuang Nie, Guang-fu Zhang, and Zhi-xiong Li

School of Physics Science and Technology, Central South University, Changsha, 410083, China

The spin-wave induced domain wall motion in a nanostrip with perpendicular magnetic anisotropy is studied. It is found that the domain wall can move either in the same direction or in the opposite direction to that of spin-wave propagation depending on whether the spin wave is reflected by the wall or transmitted through the wall. A magnonic momentum transfer mechanism is proposed and, together with the magnonic spin-transfer torque, a one-dimensional phenomenal model is constructed. The wall motion calculated based on this model is in qualitative agreement with micromagnetic simulations, showing that the model can describe the characteristics of spin-wave-induced wall motion and, especially, the wall motion direction.

FIG. 1. (Color online) Illustration of the Model PMA nanostrip with the geometry and dimensions. A 180° Bloch domain wall is positioned at the center $X = 0$. The magnetization direction is represented by arrows. The gray area with $H(t)$ represents the region where spin waves are excited. The Cartesian coordinate system is shown on the higher left. The lower right inset shows the magnetization components of the wall profiles.
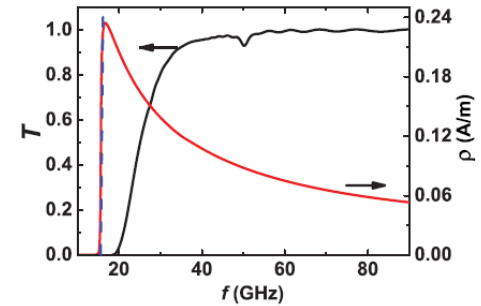

FIG. 2. (Color online) The wall displacement X as a function of time t, induced by propagating spin waves of frequency (a) 22 GHz and (b) 70 GHz. The black squares are the micromagnetic simulation results. The red solid line and green dashed line represent the model calculation with $\alpha = 0.01$ and 0, respectively. The blue circle is the simulation results of wall motion driven by the equivalent spin-polarized electrical current.

FIG. 4. (Color online) Transmission coefficient T of spin wave passing through the domain wall (black solid line) and amplitude of spin wave ρ (red/dark gray solid line) as a function of the frequency.

saturation magnetization $M_s = 8.6 \times 10^5 \, A/m$

(b)

$\delta\varphi$ (deg)

Bloch wall

Néel wall

w (nm)

t (nm)
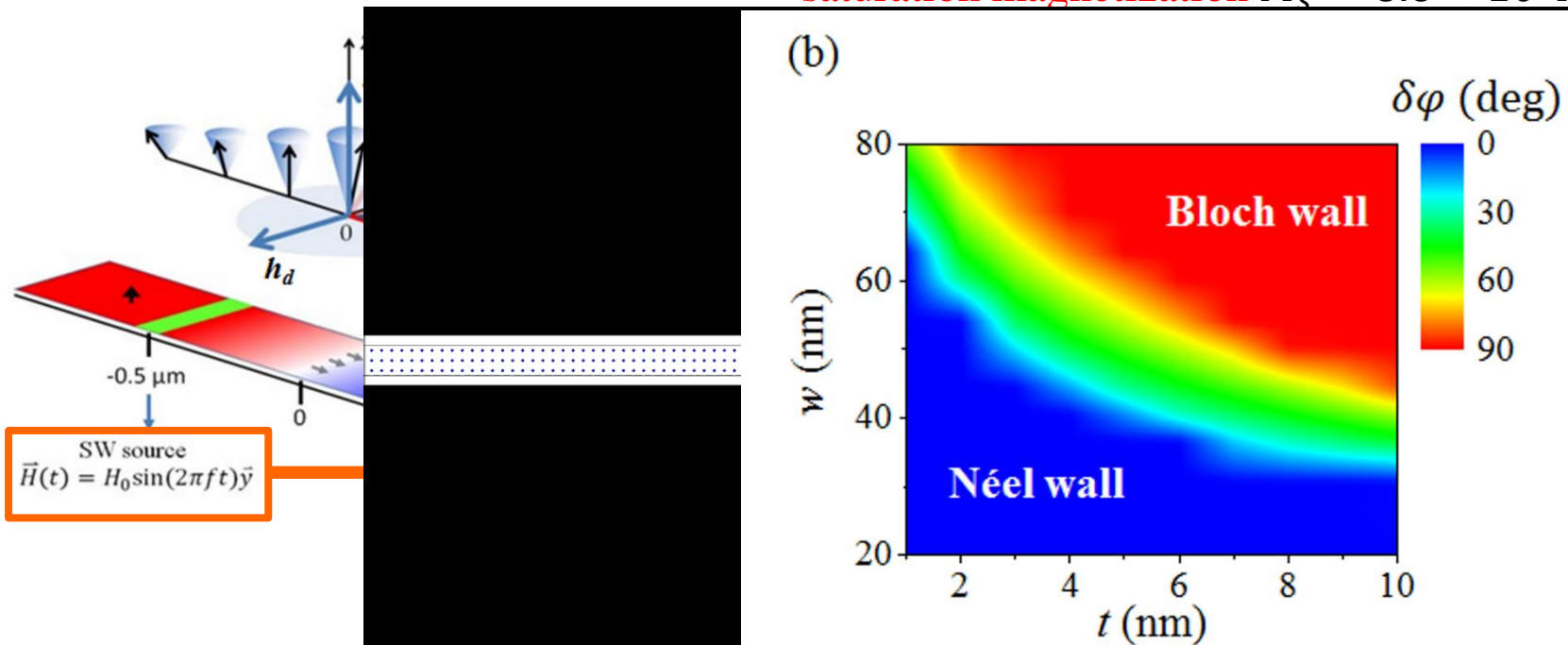
The sample geometry [...] nanostrip 4 µm long, with a Néel domain wall located at the center, and a spin wave source 0.5 µm to the left. The cones indicate the precession of the magnetizations. $\delta\varphi$ is the rotation of the magnetization at the center of the domain wall. $\boldsymbol{\tau}_d$, $\boldsymbol{h}_d$, $\boldsymbol{\tau}_K$, and $\boldsymbol{h}_K$ are the torques and effective fields due to demagnetization and anisotropy, respectively. Drawing not to scale.

SW source
$\vec{H}(t) = H_0 \sin(2\pi f t)\vec{y}$

h_d

-0.5 µm

0

$\vec{m}(t)$

$e^{-\frac{|x-x_0|}{\Lambda}}$

x_0

0

SW source
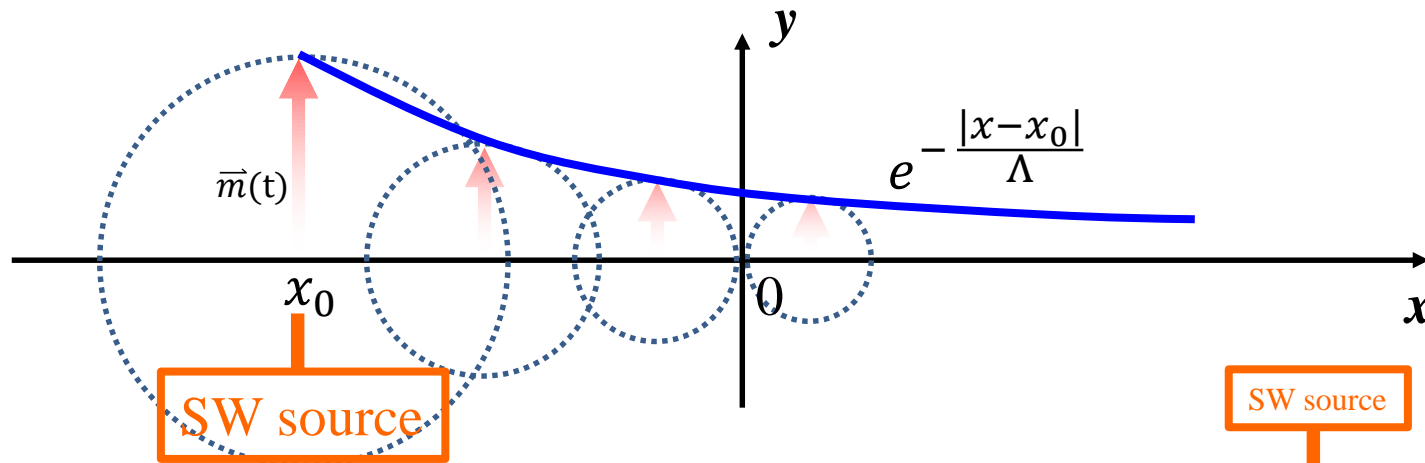
Total instantaneous magnetization

$$\vec{M} = \vec{M}_0 + \vec{m}(t)e^{-\frac{|x-x_0|}{\Lambda}}$$

large equilibrium component

small time-varying component
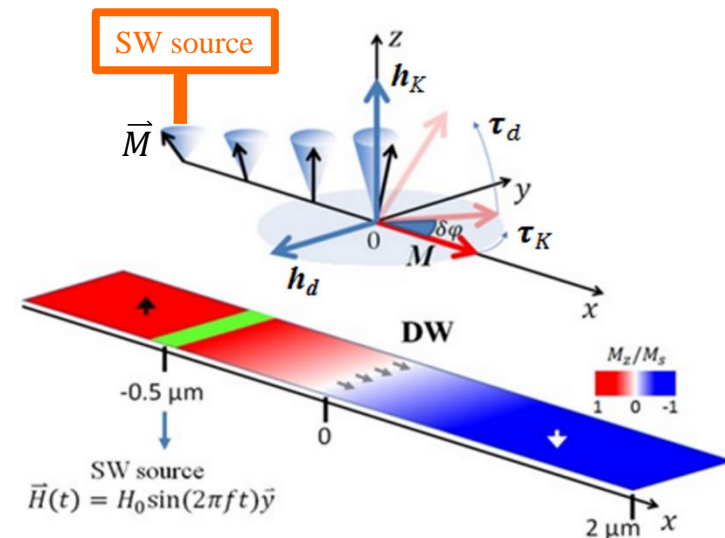
Λ : attenuation length

SW source

$\vec{M}$ h_K τ_d

τ_K

h_d M

DW

M_z/M_s

$-0.5\ \mu m$ 0 $2\ \mu m$

SW source
$\vec{H}(t) = H_0 \sin(2\pi f t)\vec{y}$

$$\partial \vec{M} \qquad \vec{M} \quad \vec{H} \qquad \frac{\alpha}{} \quad \vec{M} \qquad \partial \vec{M} \qquad \partial \vec{J}_m$$

Effectiv

$\hat{Z}$

0

Doma

d

δφ=0°

$$\frac{\partial \vec{M}}{\partial t} = -\gamma \vec{M} \times \vec{H}_{eff} + \frac{\alpha}{M_s} \vec{M} \times \frac{\partial \vec{M}}{\partial t} - \frac{\partial \vec{J}_m}{\partial x}$$
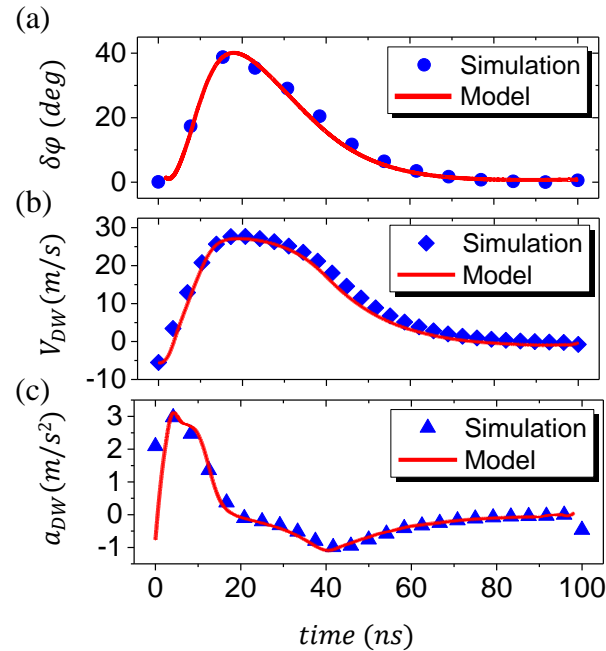
Effective anisotropy field   Demagnetization field

$$\vec{h}_K(x) = \frac{2K_\perp m_z e^{-\frac{x}{\Lambda}}}{\mu_0 M_S^2} \hat{z}$$

$$\vec{T}_K = -\gamma \vec{M} \times \vec{h}_K$$

Domain wall
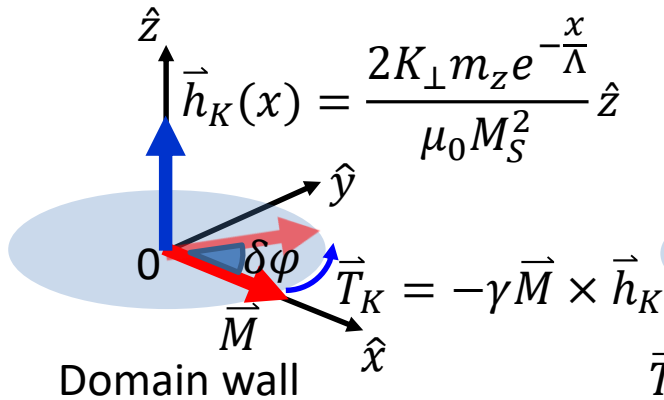
$$\vec{T}_d = -\gamma \vec{M} \times \vec{h}_d$$
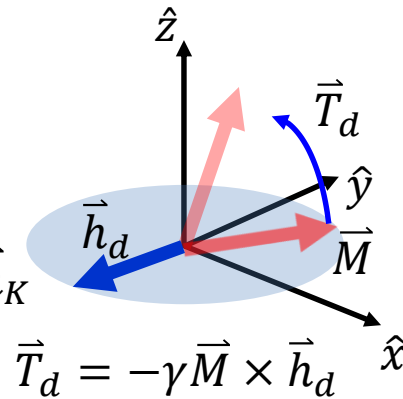
Effective demagnetization field

$$h_d = -N_y M_y e_y$$

where N_y is the demagnetization factor related to the DW itself

Demagnetization torque

$$\tau_d = -\gamma M \times h_d$$

$$V_d = -\frac{\Delta \gamma}{2(1+\alpha^2)M_S} \vec{M} \times \vec{h}_d$$

Magnonic spin transfer torque

$$\frac{\partial \vec{M}}{\partial t} = -\frac{\partial \vec{J}_m}{\partial x}$$

$\vec{J}_m$: magnonic spin current

$$\vec{V}_{DW-magnon} = -\frac{(e^{-\frac{x}{\Lambda}})^2}{2}\frac{\partial \omega}{\partial k}\hat{x}$$

All-Magnonic Spin-Transfer Torque and Domain Wall Propagation

P. Yan,[1] X. S. Wang,[1] and X. R. Wang[1,2,*]

[1]*Physics Department, The Hong Kong University of Science and Technology, Clear Water Bay, Hong Kong SAR, China*
[2]*School of Physics, Wuhan University, Wuhan, China*
(Received 22 June 2011; published 20 October 2011)
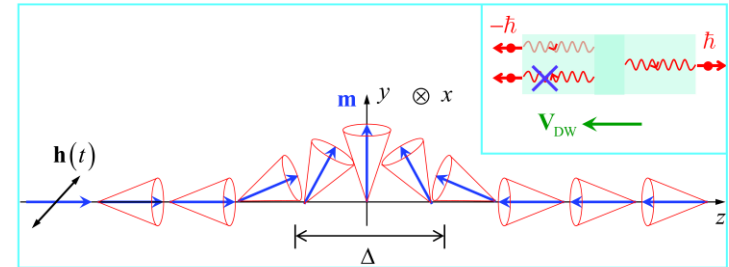
$$\mathbf{V}_{DW} = -\frac{\rho^2}{2}V_g\hat{z},$$

$V_g = \partial\omega/\partial k = 2Ak$ is the group velocity.

($\omega = 0$) [20,21]. Equation (6) describes propagating spin waves without reflection, and takes an asymptotic form of $\varphi(\xi \to -\infty) = \rho e^{iq\xi}$ and $\varphi(\xi \to +\infty) = -\rho\frac{1-iq}{1+iq}e^{iq\xi}$.

$$\varphi(\xi) = \rho\frac{\tanh\xi - iq}{-iq - 1}e^{iq\xi}, \tag{6}$$

$$\frac{\partial \vec{M}}{\partial t} = -\gamma \vec{M} \times \vec{H}_{eff} + \frac{\alpha}{M_s} \vec{M} \times \frac{\partial \vec{M}}{\partial t} - \frac{\partial \vec{J}_m}{\partial x}$$

Total instantaneous velocity of DW

To estimate the total instantaneous velocity

$\boldsymbol{V}_{DW} = \boldsymbol{V}_d + \boldsymbol{V}_m$, we obtain

$$\boldsymbol{V}_{DW} = \left(\frac{\Delta \gamma M_S (N_y - N_x)}{2(1+\alpha^2)} sin2\delta\varphi - \frac{\left(e^{-\frac{x}{\Lambda}}\right)^2}{2} \frac{\partial \omega}{\partial k}\right)\hat{x}$$

where $\frac{\partial \omega}{\partial k} = 2Ak$ is the SW group velocity

(a)

(b)

(c)

$h_K = 5.1557 \, Oe$

$\Lambda = 138 \, nm$

$h_{DW} = 0.63383 \, Oe$

Néel wall   20GHz

Neel 20GHz / 288.8mT

$H_0 = 320$ mT (e)

$H_0 = 288.8$ mT (d)

$H_0 = 280$ mT (c)

$H_0 = 200$ mT (b)

Time (ns)

Time (ns)
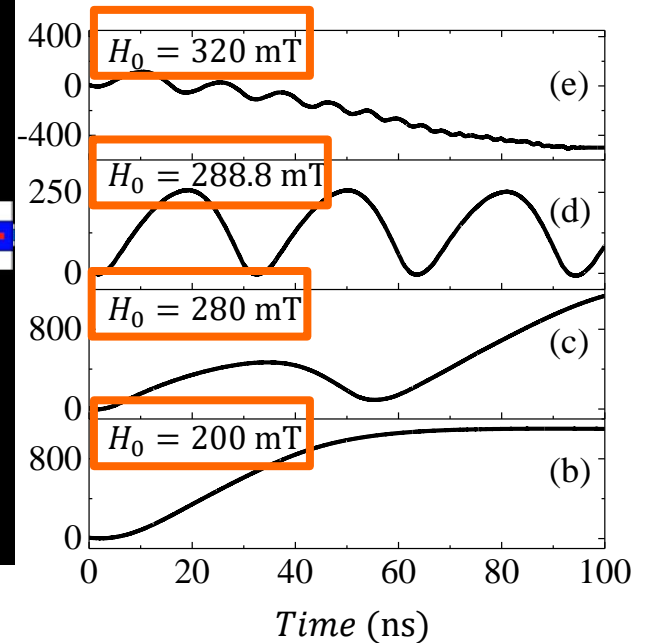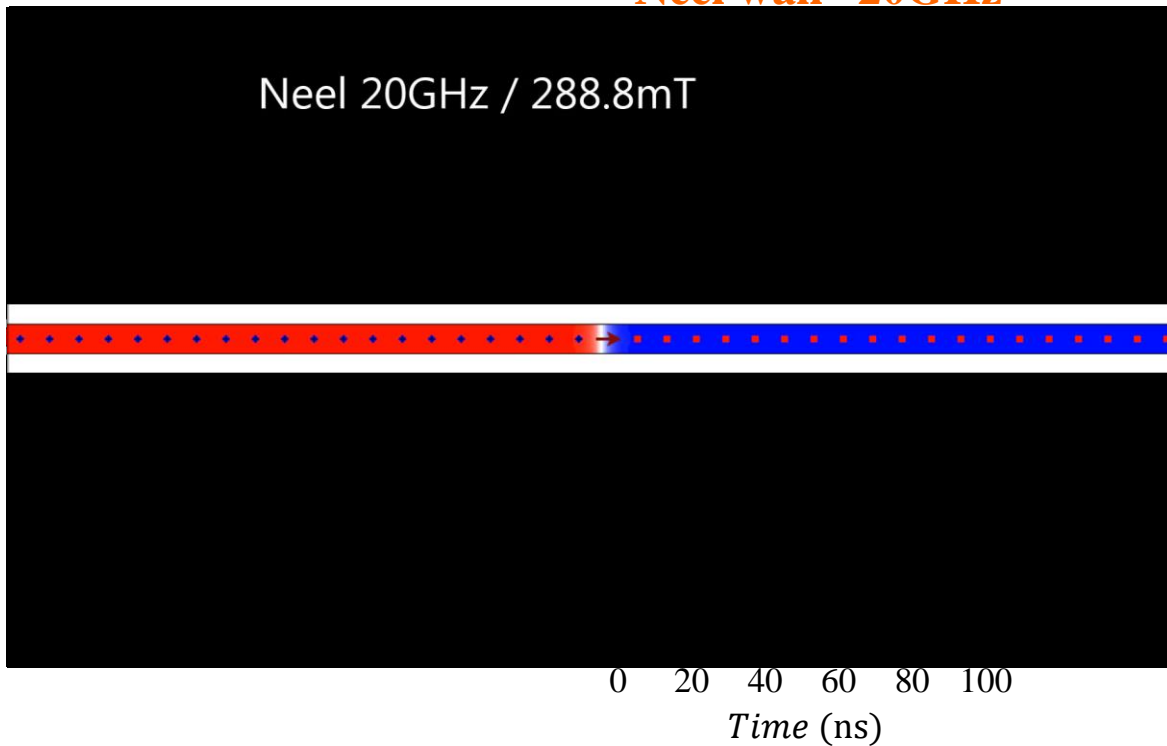
Domain wall displacement as functions of simulation time and magnetic field amplitude of the spin wave with frequency 20 GHz.

Neel 20GHz / 288.8mT

$\delta\varphi\ (deg)$
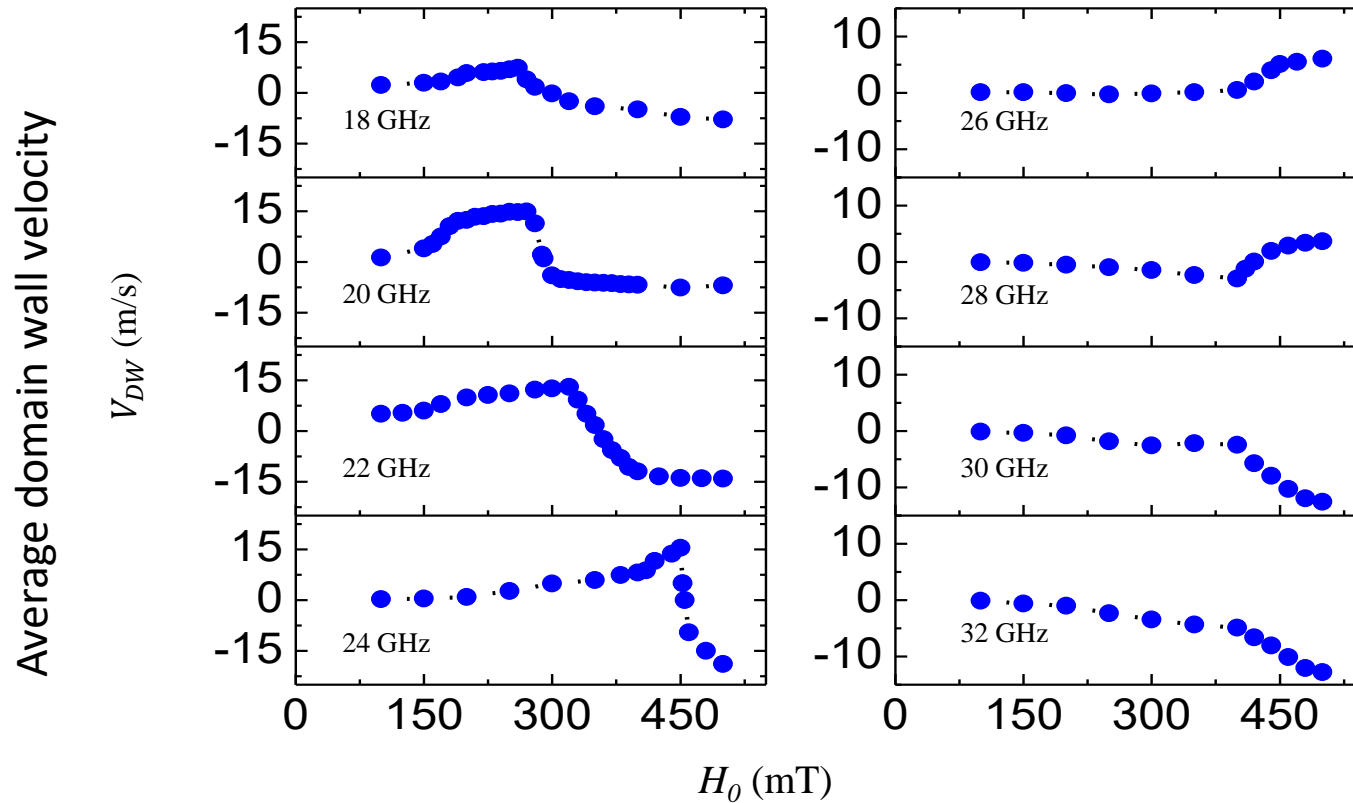
Phase shift for a propagating SW with f = 20 GHz and H_0 = 288.8 mT. There are π phase jumps at the minima of transmission.
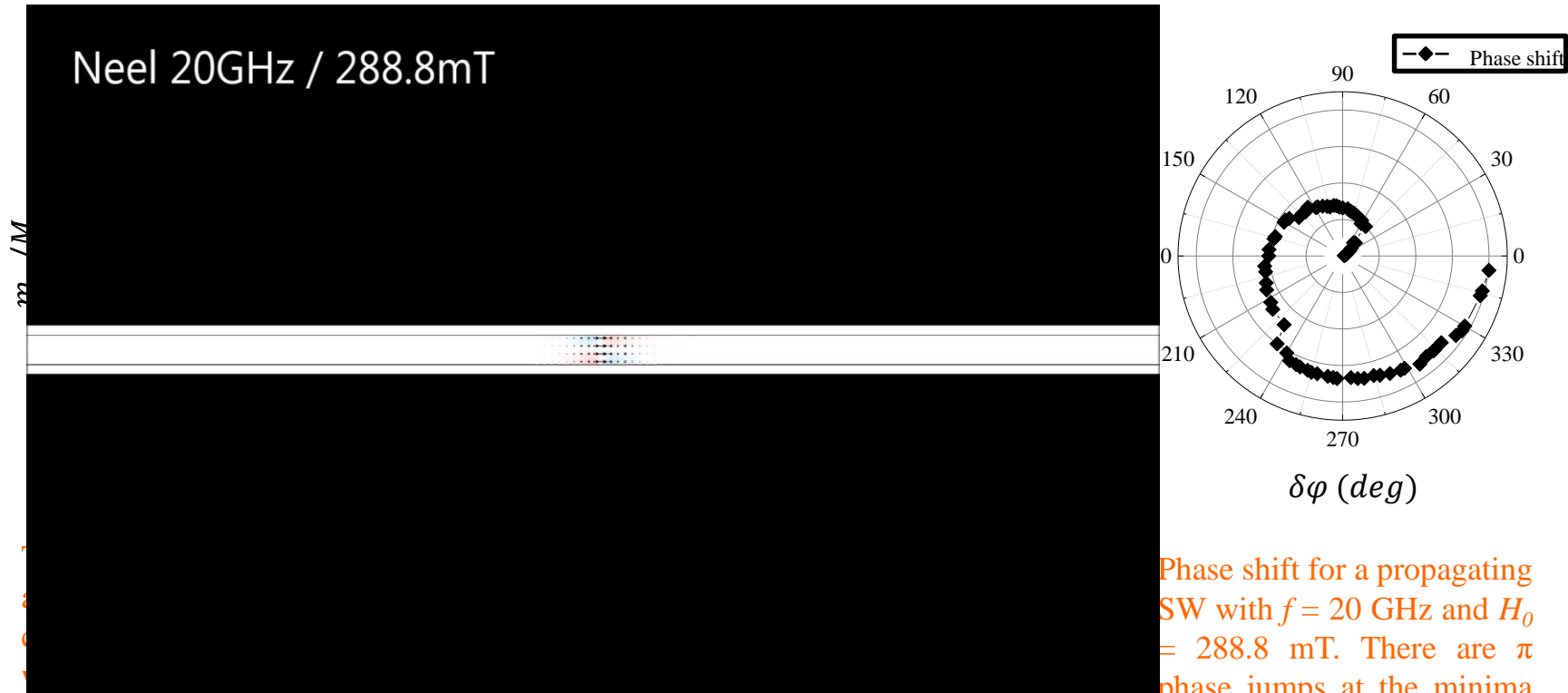
selected values of $\delta\varphi$, 45° and 140°.

Analytical self-consistence check

modified Landau-Lifshitz-Gilbert (LLG) equation

$$\frac{\partial M}{\partial t} = -\gamma M \times H_{eff} + \frac{\alpha}{M_s} M \times \frac{\partial M}{\partial t} - \frac{\partial J_m}{\partial x}$$

Spinwave $\qquad \boldsymbol{M} = \boldsymbol{M_0} + m(t)e^{-x/\Lambda} \qquad\qquad \Lambda \sim 370 \text{ nm}$

$$\delta\varphi(t) = \frac{\gamma}{V} \int_0^{x(t)} (h_K - h_{DW})dx = -\frac{\gamma}{V}(\Lambda h_K + h_{DW}x(t))$$

$$V_d = -\frac{\Delta\gamma}{2(1+\alpha^2)M_S} |\vec{M} \times \vec{h}_d|$$

$$V_{DW} = (\frac{\Delta\gamma M_S(N_y - N_x)}{2(1+\alpha^2)} \sin 2\delta\varphi - \frac{\left(e^{-\frac{x}{\Lambda}}\right)^2}{2} \frac{\partial\omega}{\partial k})\hat{x}$$

γ_0 : electron gyromagnetic ratio (2.2×10^5 Vs^{2}m^{-1}kg^{-1})

N_z, N_y : transverse demagnetizing factors, Δ_0 : DW width (m), x : DW position (m)

Analytical self-consistence check

$$\vec{H}_{eff} = \vec{H}_d + \vec{h}(x)e^{i\omega t} = (H_{dx} + h_x e^{i\omega t}, H_{dy} + h_y e^{i\omega t}, h_z e^{i\omega t}),$$

$$H_{dx} = -M_S N_x cos\delta\varphi$$

$$H_{dy} = -M_S N_y sin\delta\varphi$$

$$\vec{M} = (M_x + m_x e^{i\omega t}, M_y + m_y e^{i\omega t}, m_z e^{i\omega t})$$

$$M_x = -M_S cos\delta\varphi$$

$$M_y = -M_S sin\delta\varphi \ .$$

$$\begin{bmatrix} i\omega & 0 & -\omega_y \\ 0 & i\omega & \omega_x \\ \omega_y & -\omega_x & i\omega \end{bmatrix} \begin{bmatrix} m_x \\ m_y \\ m_z \end{bmatrix} = -\gamma M_s \begin{bmatrix} -sin\delta\varphi h_z \\ cos\delta\varphi h_z \\ sin\delta\varphi h_x - cos\delta\varphi h_y \end{bmatrix}$$

$$\begin{bmatrix} m_x \\ m_y \\ m_z \end{bmatrix} = \frac{-i\gamma M_s}{\omega_x^2 + \omega_y^2 - \omega^2} \begin{bmatrix} \dfrac{-\omega^2 + \omega_x^2}{\omega} & \dfrac{\omega_x\omega_y}{\omega} & i\omega_y \\ \dfrac{\omega_x\omega_y}{\omega} & \dfrac{-\omega^2 + \omega_y^2}{\omega} & -i\omega_x \\ -i\omega_y & i\omega_x & -\omega \end{bmatrix} \begin{bmatrix} -sin\delta\varphi h_z \\ cos\delta\varphi h_z \\ sin\delta\varphi h_x - cos\delta\varphi h_y \end{bmatrix}$$

$$\omega_x = \left(\gamma H_{dx} + \frac{\alpha}{M_S} i\omega M_x\right) \qquad \omega_y = \left(\gamma H_{dy} + \frac{\alpha}{M_S} i\omega M_y\right)$$

The dispersion relation

$$\omega^2 = \omega_H(\omega_H + \omega_M) + \frac{\omega_M^2}{2\big(1 + \coth(kd)\big)}$$

$$\text{with } \omega_H = \frac{\omega_x \omega_y}{\omega} \text{ and } \omega_M = \gamma M_s.$$

Using $k = k_r - i\kappa$

$$\frac{1}{\big(1 + \coth(kd)\big)} = \frac{1}{2}\big(1 - e^{-2k_r d}\big) + i\frac{d}{\Lambda}e^{-2k_r d} \qquad \Lambda = 1/\kappa$$

$$\frac{1}{\Lambda_D} = \frac{1}{de^{-2kd}}\left[\frac{\alpha\gamma M_s}{\omega}\big(N_x + N_y\big)N_x N_y \sin^2 2\delta\varphi + \alpha\big(N_x + N_y\big)\sin 2\delta\varphi\right]$$

Λ_D is the attenuation length inside the DW

$$T_{DW} = e^{-2\Delta\left|\frac{1}{\Lambda_D} - \frac{1}{\Lambda_0}\right|},$$

Strong angular dependent transmission ratio due to interplay between spin waves and the domain wall in perpendicular magnetic anisotropy materials

Results
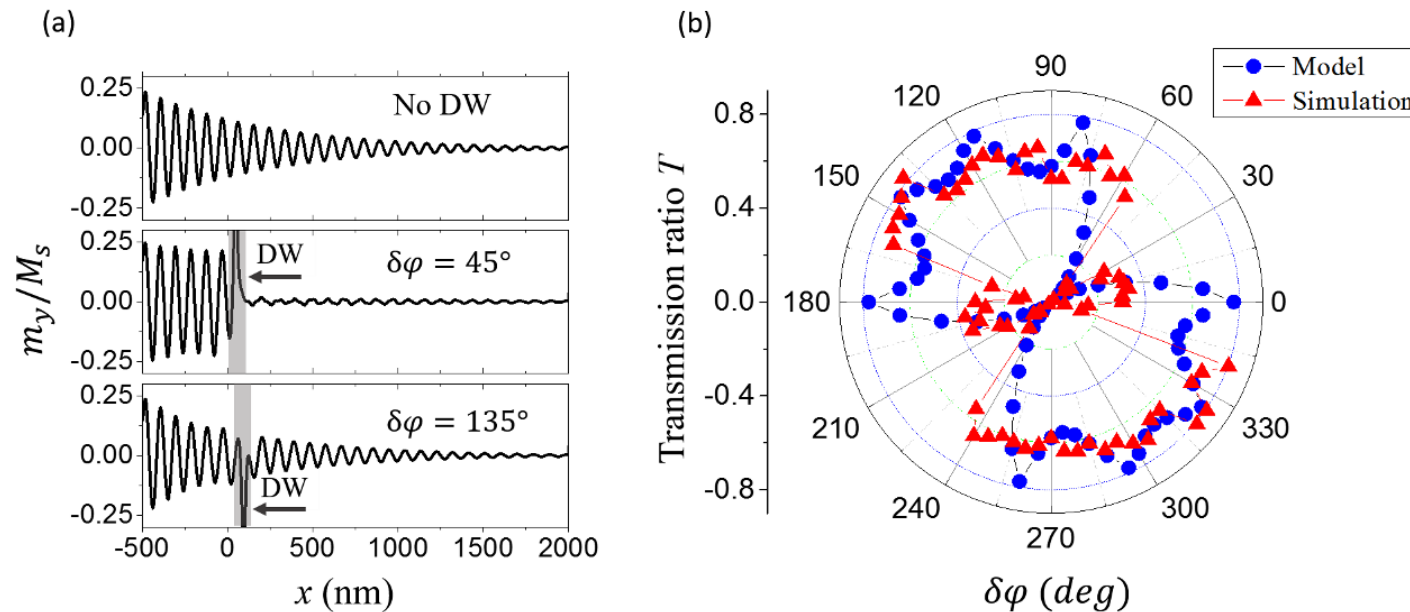
Transmission of SW in the case of (d). (a) Spatial variation of the normalized m_y component without and with DW for $\delta\varphi = 45°$ and 140°. Shaded areas indicate the domain wall region. (b) Polar plot of the transmission ratio versus $\delta\varphi$. Blue circles are calculated results and the red triangles are from simulations.

Spin wave driven domain wall motion

simple model

$$\delta\dot\varphi = \gamma\left(h_K - h_W\right)$$

$$\dot{x} = \frac{\Delta\gamma M_s\left(N_y - N_x\right)}{2\left(1+\alpha^2\right)}\sin\left(2\delta\varphi\right) - \frac{1}{2}T\left(\delta\varphi\right)e^{-2(x-x_0)/\Lambda}\frac{\partial\omega}{\partial k}$$

$h_K = 2K_\wedge m_{z0}e^{-x/\mathsf{L}}/m_0 M_S^2$ ⟵ spin wave effective field

$h_W = h_{W0}\sin\left(2dj\right)$ ⟵ Walker break down field

$T\left(dj\right) = e^{-2\mathsf{D}\left|1/\mathsf{L}_D - 1/\mathsf{L}\right|}$

$1/\mathsf{L}_D = \dfrac{1}{de^{-2kd}}\left[\dfrac{agM_S}{W}\left(N_X + N_Y\right)N_X N_Y \sin^2\left(2dj\right) + a\left(N_X + N_Y\right)\sin\left(2dj\right)\right]$

dispersion relation: $W^2 = W_H\left(W_H + W_M\right) + \dfrac{W_M^2}{2\left(1+\coth\left(kd\right)\right)}$

Experiments on spin wave sources

- **Spin-wave wavelength imposed by the size of the antenna**

Excitation of short-wavelength spin waves in magnonic waveguides

V. E. Demidov,[1,a)] M. P. Kostylev,[2] K. Rott,[3] J. Münchenberger,[3] G. Reiss,[3] and S. O. Demokritov[1]

[1]Institute for Applied Physics and Center for Nonlinear Science, University of Muenster, Corrensstrasse 2-4, Muenster 48149, Germany
[2]School of Physics, University of Western Australia, Crawley, Western Australia 6009, Australia
[3]Department of Physics, Bielefeld University, P. O. Box 100131, Bielefeld 33501, Germany

We emphasize that a microstrip antenna can only efficiently excite spin waves with the wavelengths $\lambda > w_a$ where w_a is the width of the antenna

Spin-wave antenna — Microwave current — Permalloy waveguide — Propagating spin wave
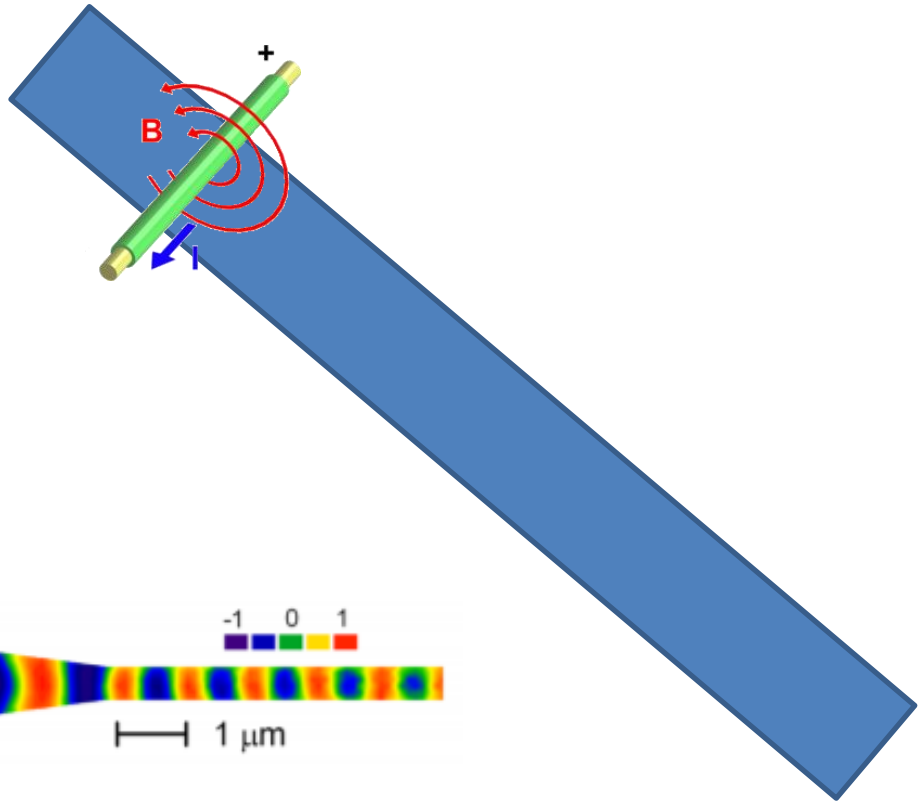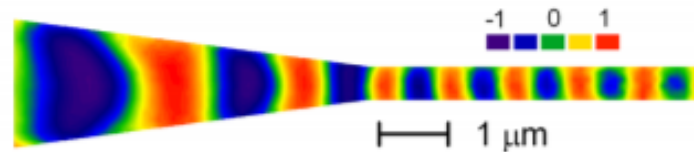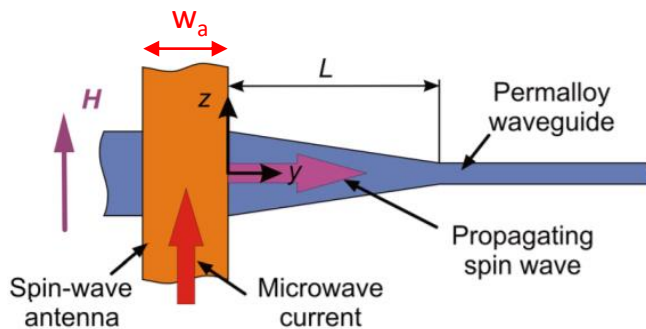
• **External field is necessary**

Kittel formula

$$f = \frac{\gamma}{2\pi} \sqrt{H(H + M_S)}$$

γ ：Gyromagnetic ratio
H ：External field
M_S ：Saturation magnetization

H_{ext}

m

H_{ac}
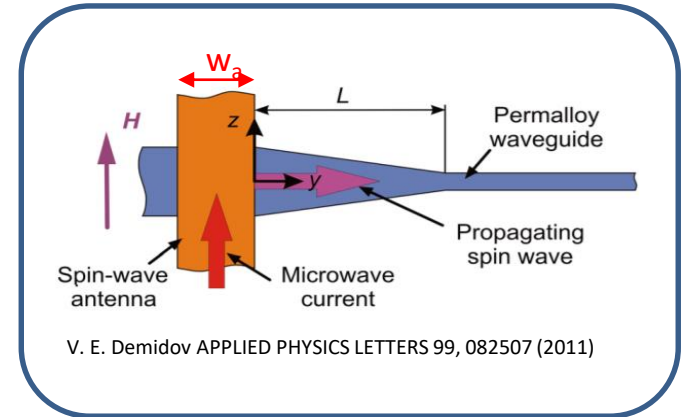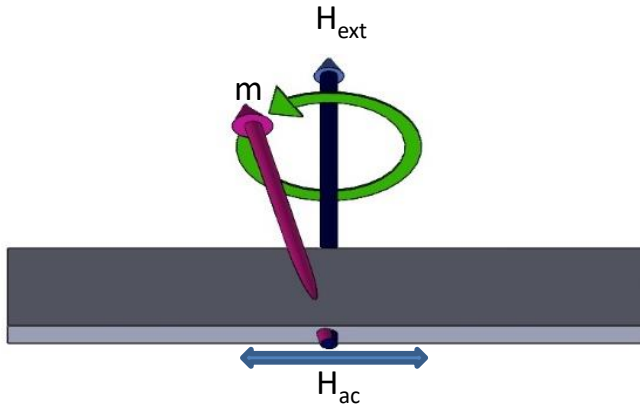
V. E. Demidov APPLIED PHYSICS LETTERS 99, 082507 (2011)
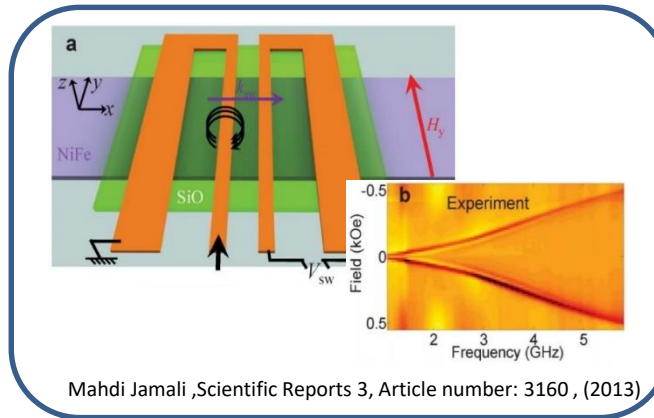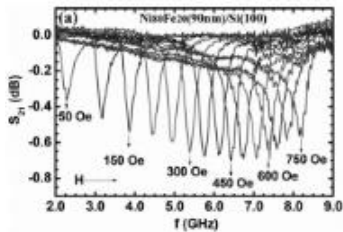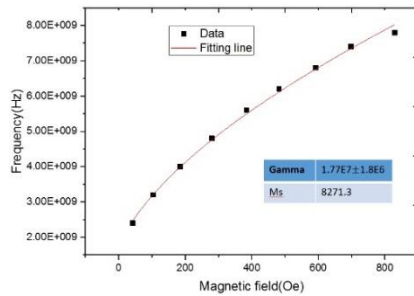
Mahdi Jamali ,Scientific Reports 3, Article number: 3160 , (2013)
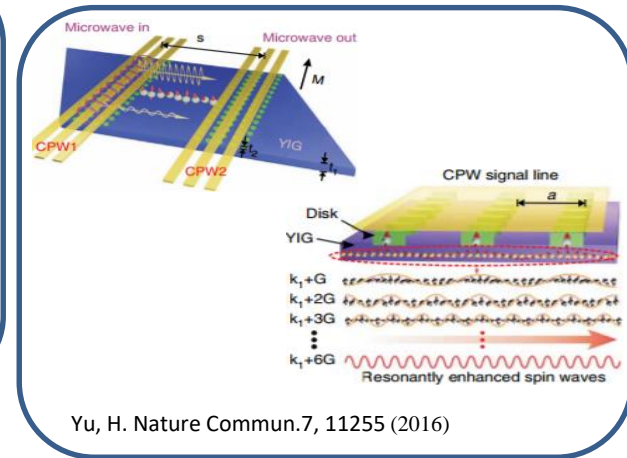
Yu, H. Nature Commun.7, 11255 (2016)

Magnetic vortex motion

Resonant amplification of vortex-core oscillations by coherent magnetic-field pulses

Young-Sang Yu, Dong-Soo Han, Myoung-Woo Yoo, Ki-Suk Lee, Youn-Seok Choi, Hyunsung Jung, Jehyun Lee, Mi-Young Im, Peter Fischer & Sang-Koog Kim ✉

Thiele's equation

$$\bar{\bar{M}}\ddot{\boldsymbol{X}} - \boldsymbol{G} \times \dot{\boldsymbol{X}} - \bar{\bar{D}}\dot{\boldsymbol{X}} + \boldsymbol{F} = 0$$

G: the gyroforce vector
D: the damping tensor

Figure 1: Concept of resonant amplification of vortex oscillations by coherent serial pulses.

Figure 2: Sample geometry for time-resolved soft X-ray microscopy measurement.

Figure 3: (a) Amplification and (b) damping of vortex oscillations.

Micromagnetic simulation

500Oe   250Oe   0Oe

H_{ext}

M_{Z+} / M_S

1

0

-1

M_{Z+} / M_S

1

0

-1

$H_{Z\ AC}$
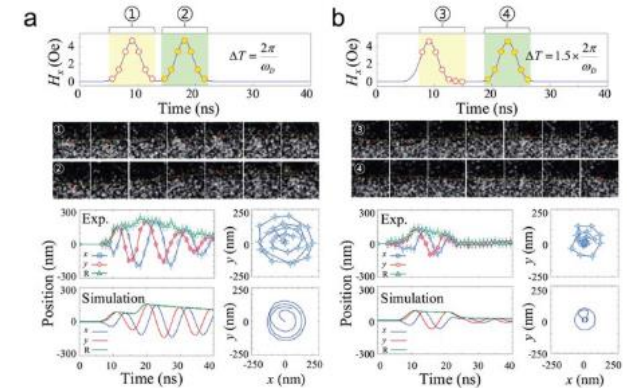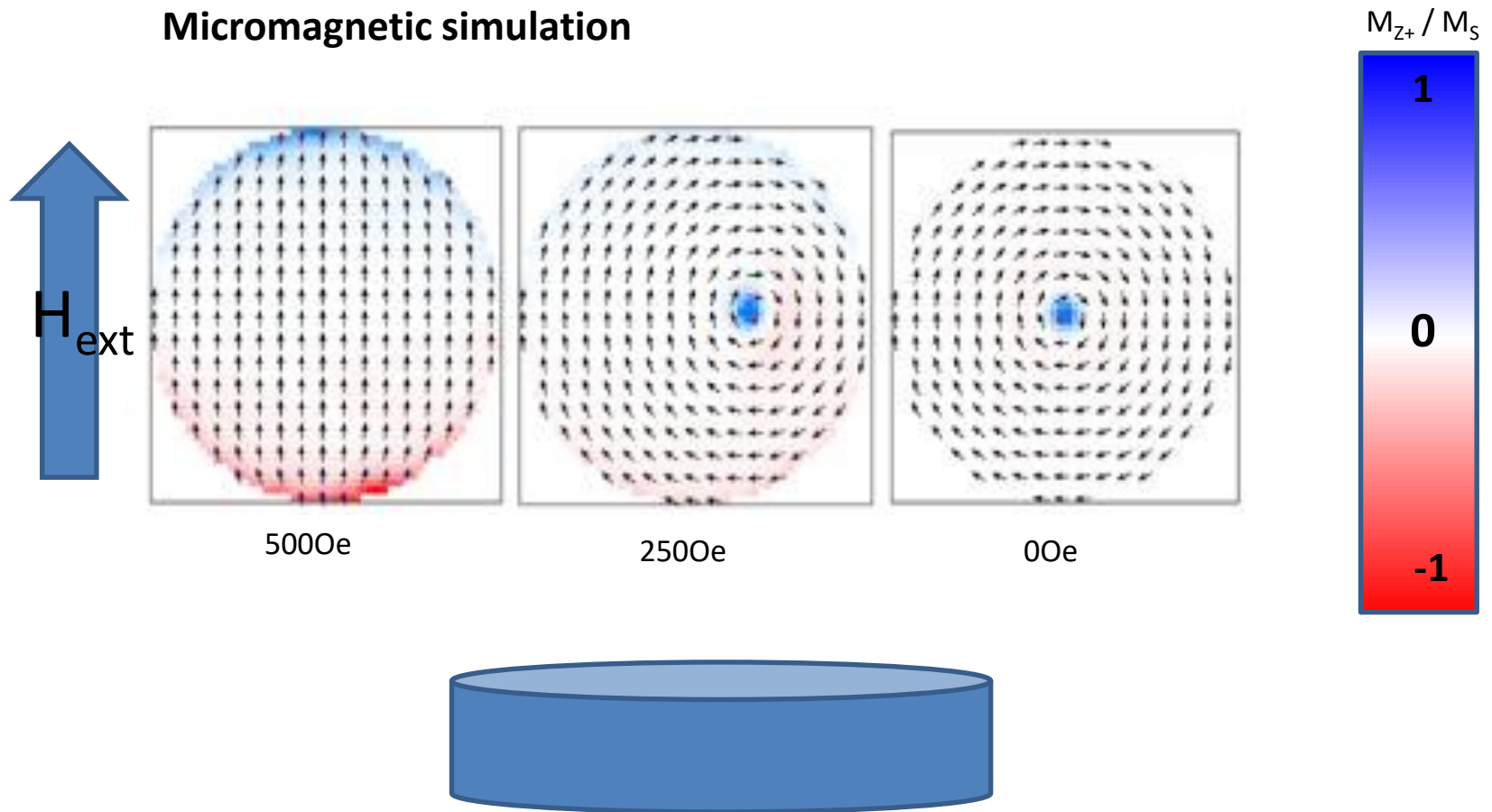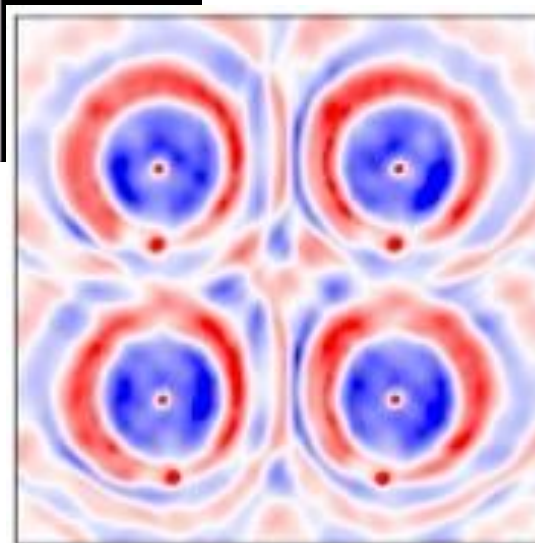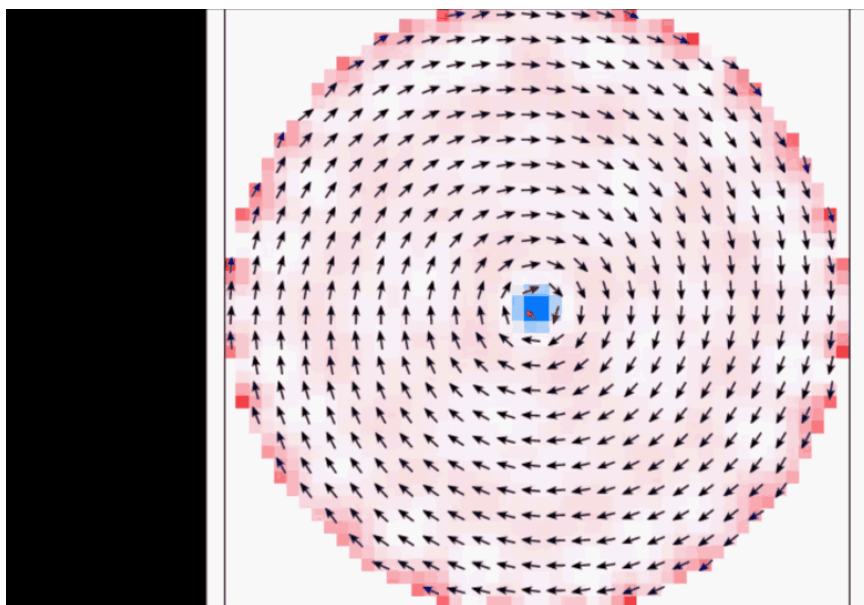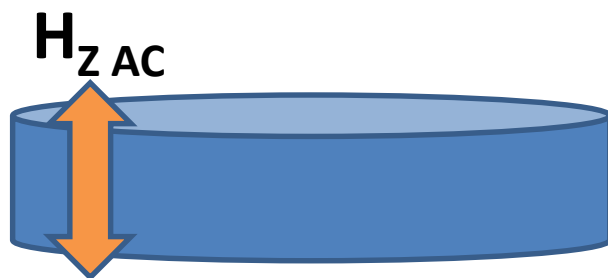
Sample fabrication
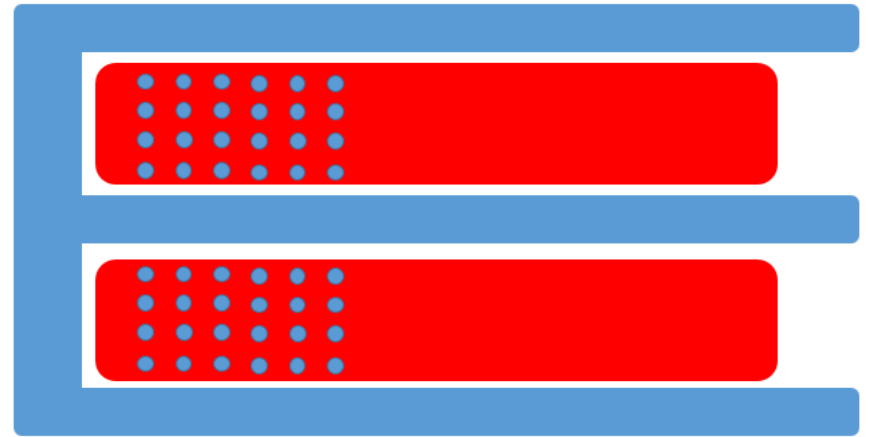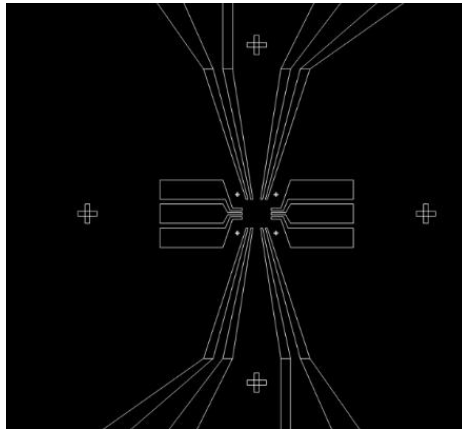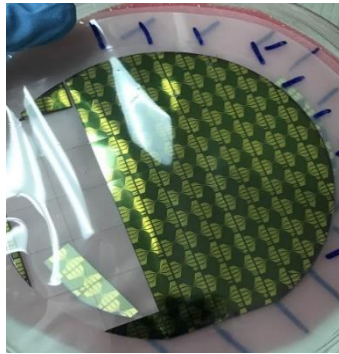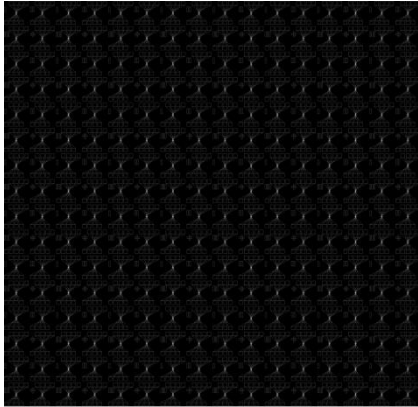
R=500nm

Oscillating vortex cores of permalloy (NiFe) disk array by microwave
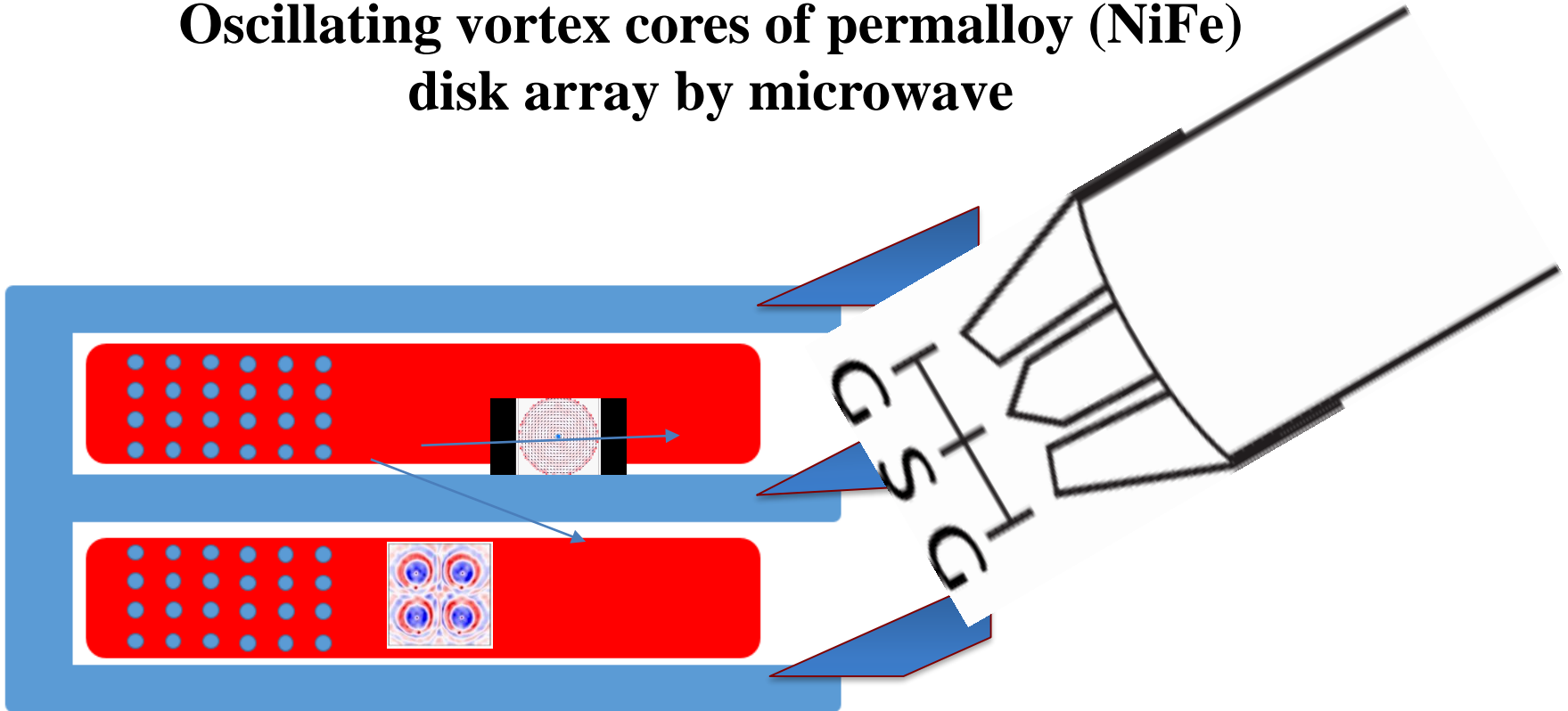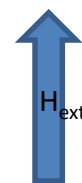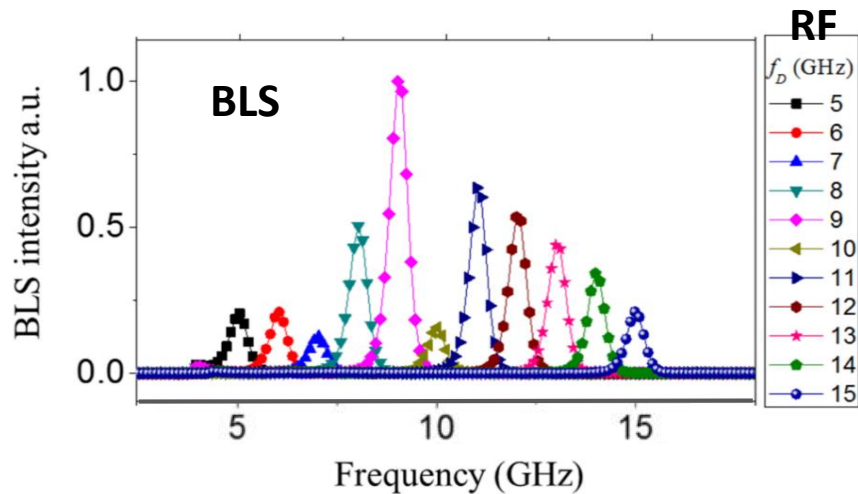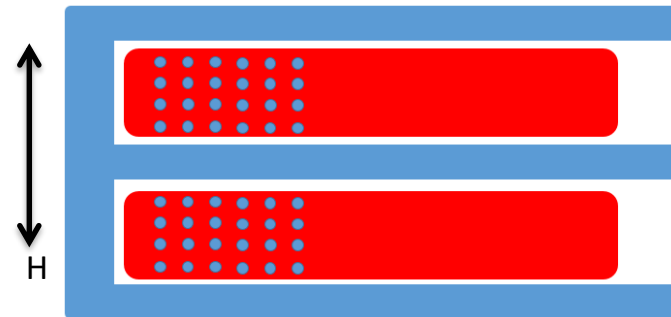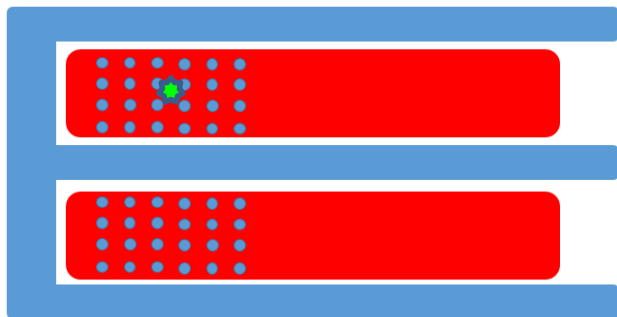
Brillouin light scattering (BLS)
magnon detection and measurement

$$\hbar \vec{k}_{out} = \hbar \vec{k}_{in} + \hbar \vec{k}_{sw}$$

$$h\nu_{out} = h\nu_{in} + h\nu_{sw}$$

magnon

$$h\nu_{out} = h\nu_{in} - h\nu_{sw}$$

$$\hbar \vec{k}_{out} = \hbar \vec{k}_{in} + \hbar \vec{k}_{sw}$$
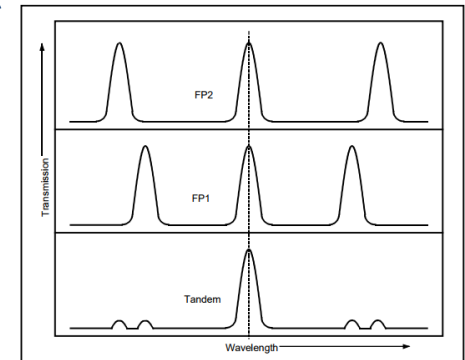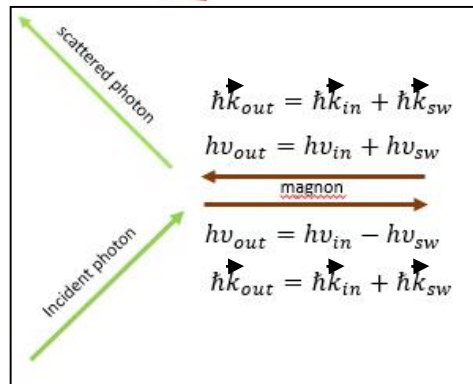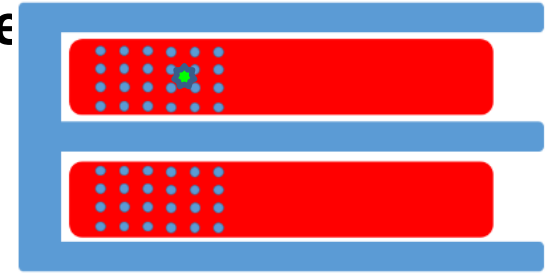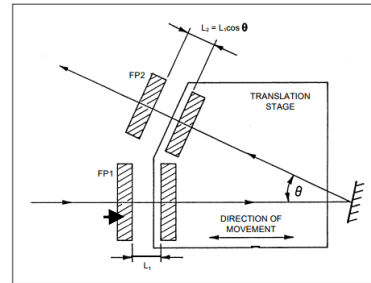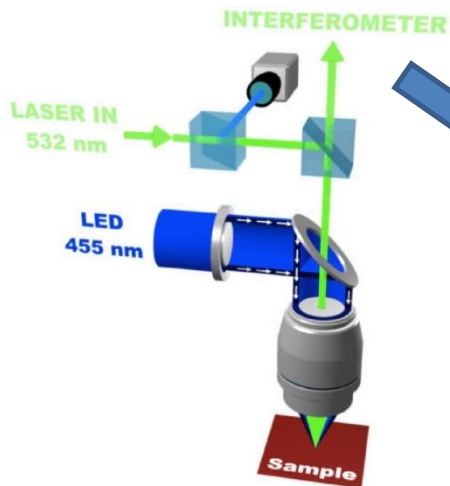
Frequency modulated spin waves generation
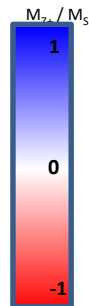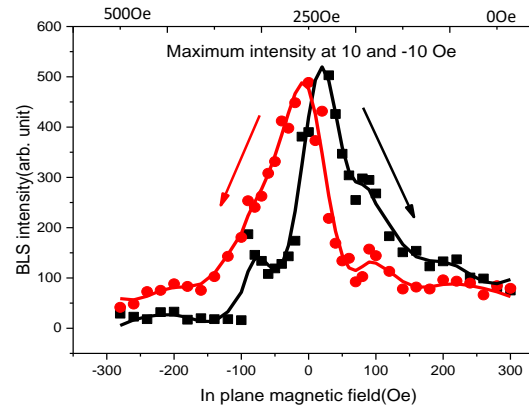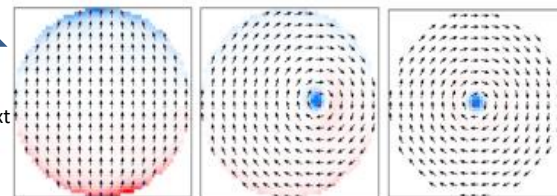
spin wave propagation (by BLS)

Decay length ~ 900 nm

$10\mu m$

$2\mu m$

286.0

200.2

100.1

0.000
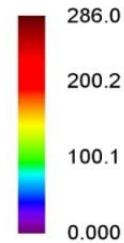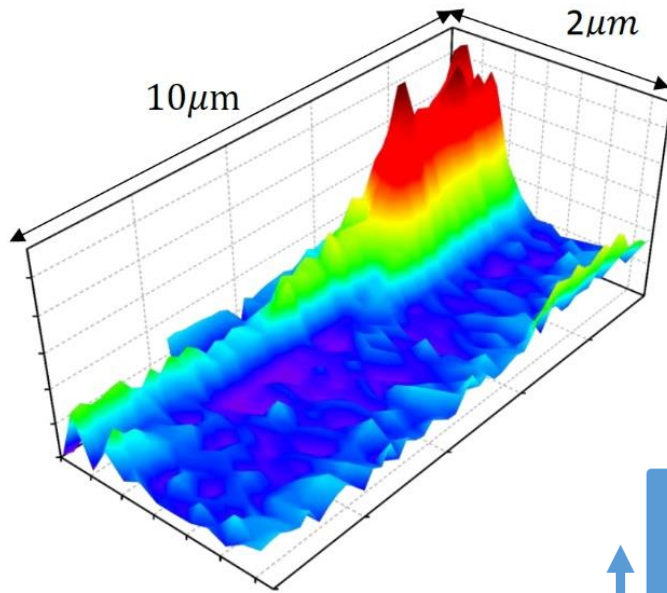
BLS intensity

(arb. unit)
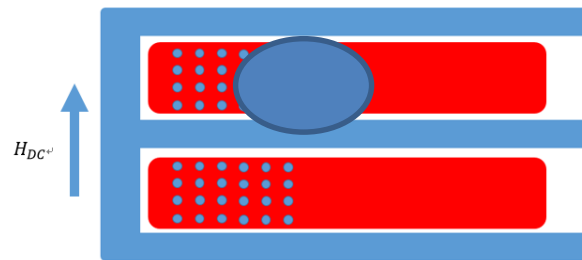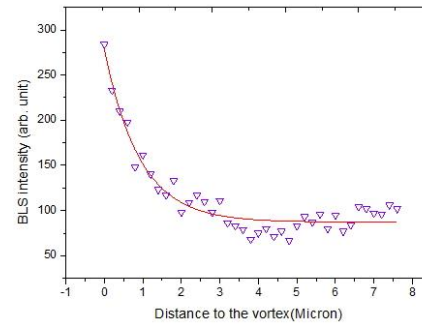
Electrical property measurement (Anisotropic magnetoresistance, AMR)

L>T>P
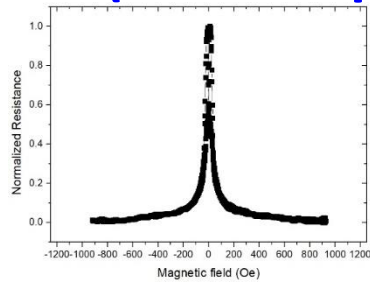
$$\rho(\varphi) = \rho_\perp + (\rho_\parallel - \rho_\perp)\cos^2\varphi$$
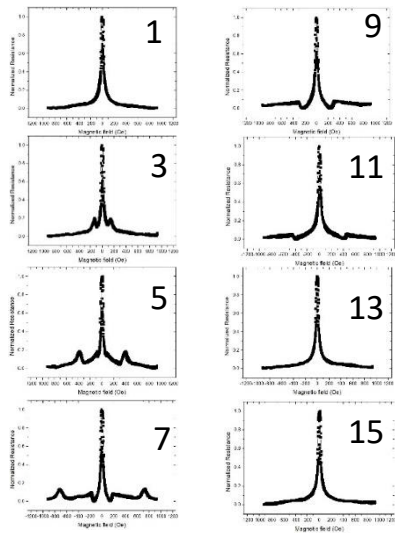
$$f = \frac{\gamma}{2\pi}\sqrt{H(H + M_S)}$$

The magneto-resistance (MR) results with varying frequencies of our sample. The dark line is the FMR signal which is well fitted by the Kittel equation while the white line should be the spin wave signal.
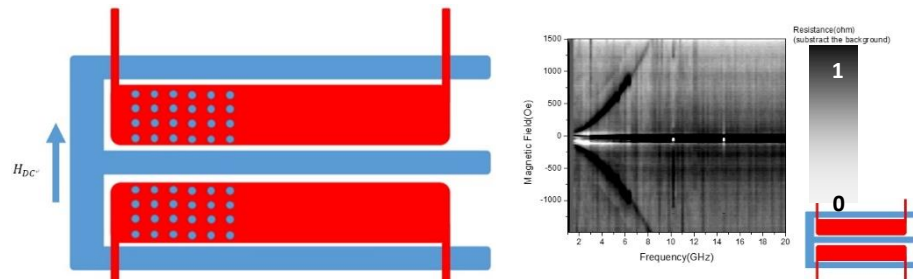
Summary

- DW oscillation with resonance frequency as high as 2.92 GHz and the resonance frequency can be tuned by the width of protrusion.

- The higher resonance frequency for the narrow trap is due to the steeper potential landscape which enhances the restoring force on the pinned DW.

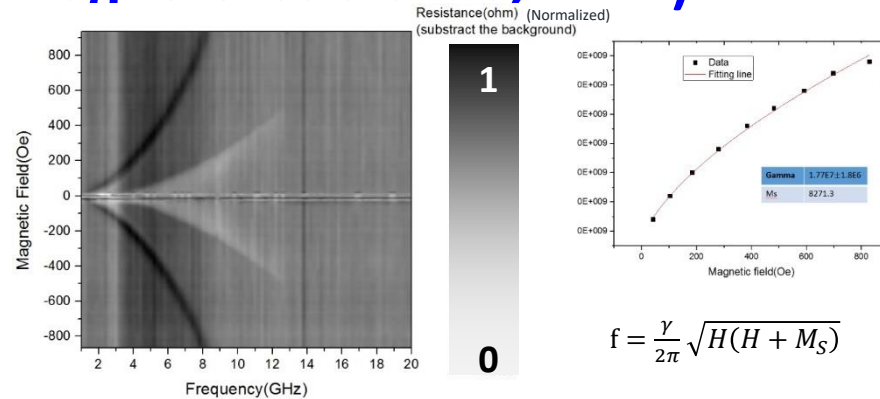- For the domain wall oscillations induced by injection of a dc current investigated, the observed peak in *dV/dI* associated with the reversible change of magnetoresistance is attributed to the reversible motion of the DW.

Topological insulator

Topological insulators

- A **topological insulator** is a material conducting on its boundary but behaves as an insulator in its bulk.

- The conducting channel(s) are guaranteed by time-reversal symmetry, topologically protected, will not be affected by local impurities etc, and thus robust.

Why the word 'topological'?

- Topological order:
a pattern of long-range quantum entanglement in quantum states, can be described by a new set of quantum numbers, such as ground state degeneracy, quasiparticle fractional statistics, edge states, topological entropy, etc.

- Landau symmetry breaking

  describes classical orders in materials. But it failed to describe the chiral spin state, which was proposed (but failed) to explain HTS.
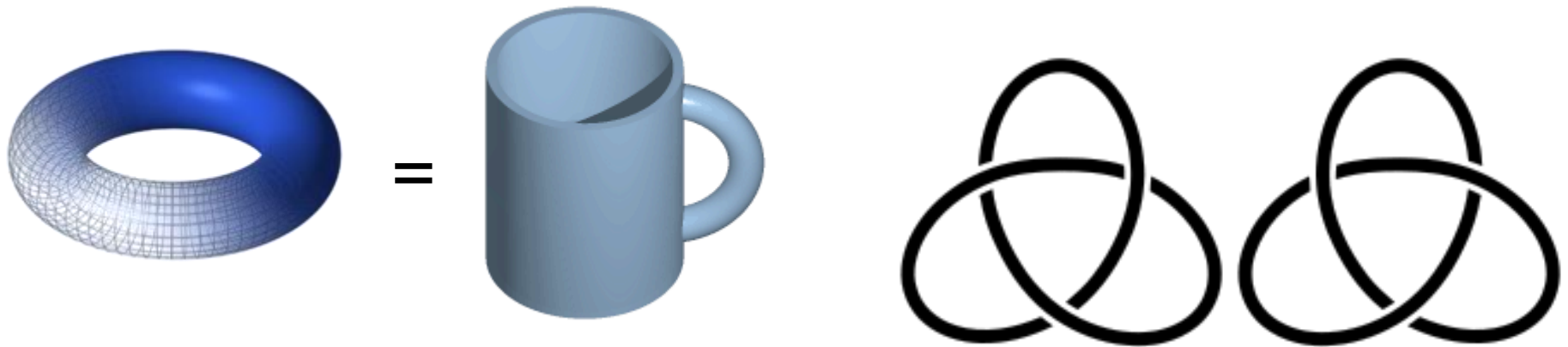
- Z_2 topological quantum number
- Chern numbers (陳省身) explains Quantum Hall Effect (from Foucault pendulum to Chern numbers)

$$1/2\pi \int_s K \, dA = 2 \, (1 - g)$$

How to become a topological insulator?
Or, how to cross from an intrinsic insulator to a topological insulator?
Or, how to build the edge conducting states?

- Spin-orbit effect
- Lattice constant adjustment

To get inversion states and Dirac cone on the boundary.

- Carriers in these states have their spin locked at a right-angle to their momentum. At a given energy the only other available electronic states have opposite spin, so scattering is strongly suppressed and conduction on the surface is nearly dissipationless.
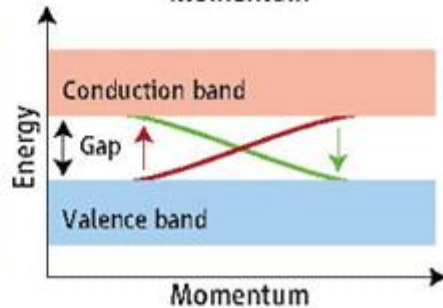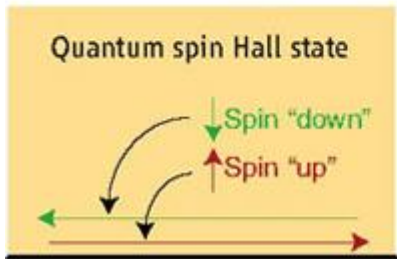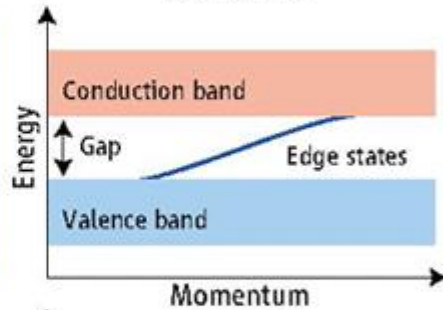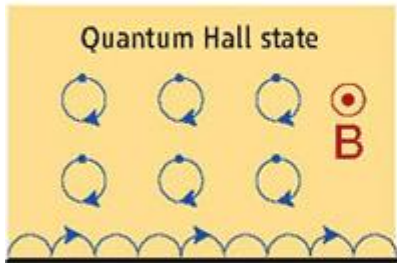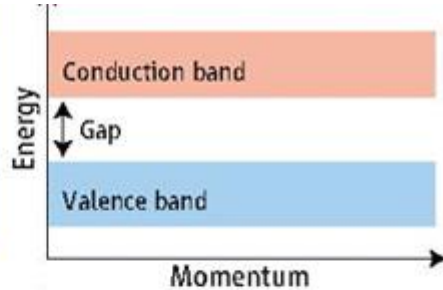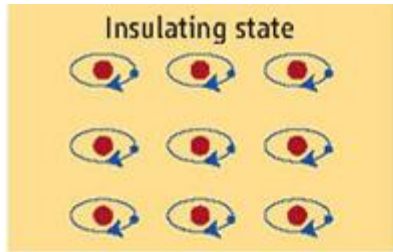
- States of matter. (**Top**) Electrons in an insulator are bound in localized orbitals (left) and have an energy gap (right) separating the occupied valence band from the empty conduction band. (**Middle**) A two-dimensional quantum Hall state in a strong magnetic field has a bulk energy gap like an insulator but permits electrical conduction in one-dimensional "one way" edge states along the sample boundary. (**Bottom**) The quantum spin Hall state at zero magnetic field also has a bulk energy gap but allows conduction in spin-filtered edge states.

A zoo of Hall effects

- Hall effect --- $B \perp I$, $V \perp I$

$$R_H = \frac{-n\mu_e^2 + p\mu_h^2}{e(n\mu_e + p\mu_h)^2}$$

- Anomalous (Extra-ordinary) Hall effect ---
  extra voltage proportional to magnetization

- Planar Hall effect --- in-plane field, $V \perp I$

- (Integer) Quantum Hall effect ---
  $B \perp I$, $V \perp I$ in 2D electron gas

$$\sigma = \nu \, \frac{e^2}{h},$$

- Fractional quantum Hall effect ---
  electrons bind magnetic flux lines

- Spin Hall effect --- $B = 0$, $V \perp I$

- Quantum spin Hall effect --- 2D topological insulator

- Quantum anomalous Hall effect
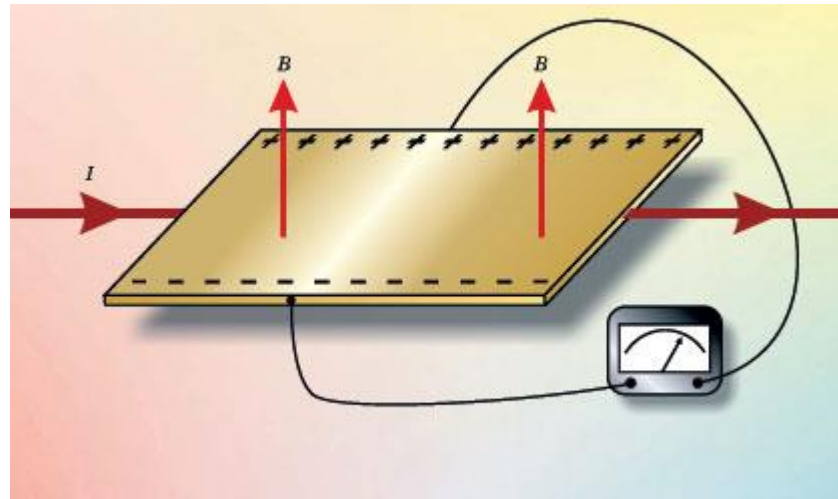
Edwin Hall's 1878 experiment was the first demonstration of the Hall effect. A magnetic field *B* normal to a gold leaf exerts a Lorentz force on a current *I* flowing longitudinally along the leaf. That force separates charges and builds up a transverse "Hall voltage" between the conductor's lateral edges. Hall detected this transverse voltage with a voltmeter that spanned the conductor's two edges.

PhysicsToday, Aug 2003, p38
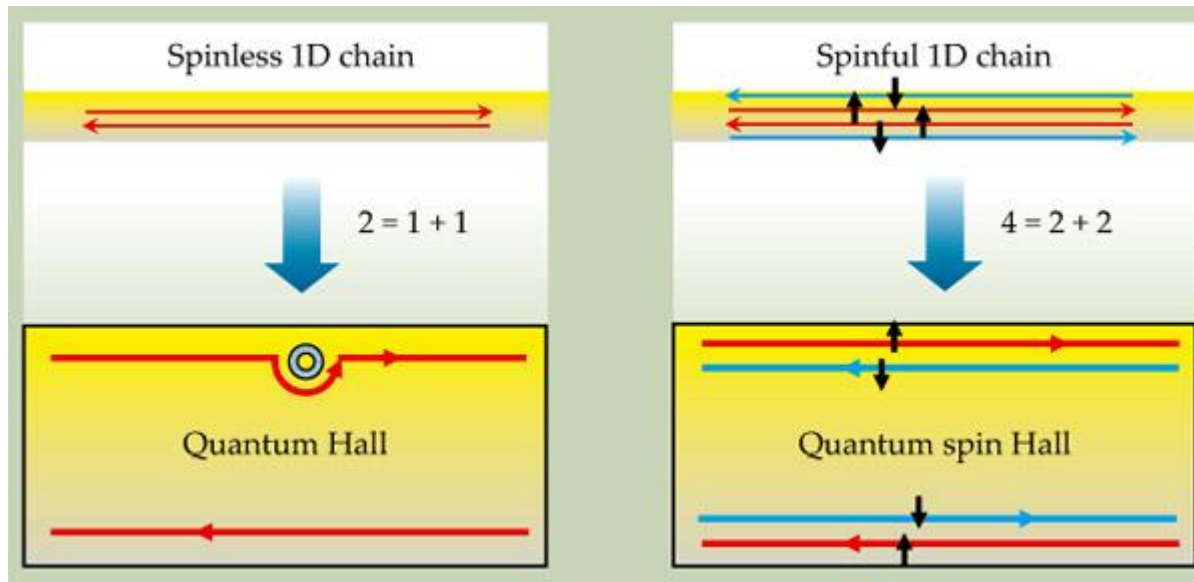
Figure 1. Spatial separation is at the heart of both the quantum Hall (QH) and the quantum spin Hall (QSH) effects. **(a)** A spinless one-dimensional system has both a forward and a backward mover. Those two basic degrees of freedom are spatially separated in a QH bar, as illustrated by the symbolic equation "2 = 1 + 1." The upper edge contains only a forward mover and the lower edge has only a backward mover. The states are robust: They will go around an impurity without scattering. **(b)** A spinful 1D system has four basic channels, which are spatially separated in a QSH bar: The upper edge contains a forward mover with up spin and a backward mover with down spin, and conversely for the lower edge. That separation is illustrated by the symbolic equation "4 = 2 + 2."
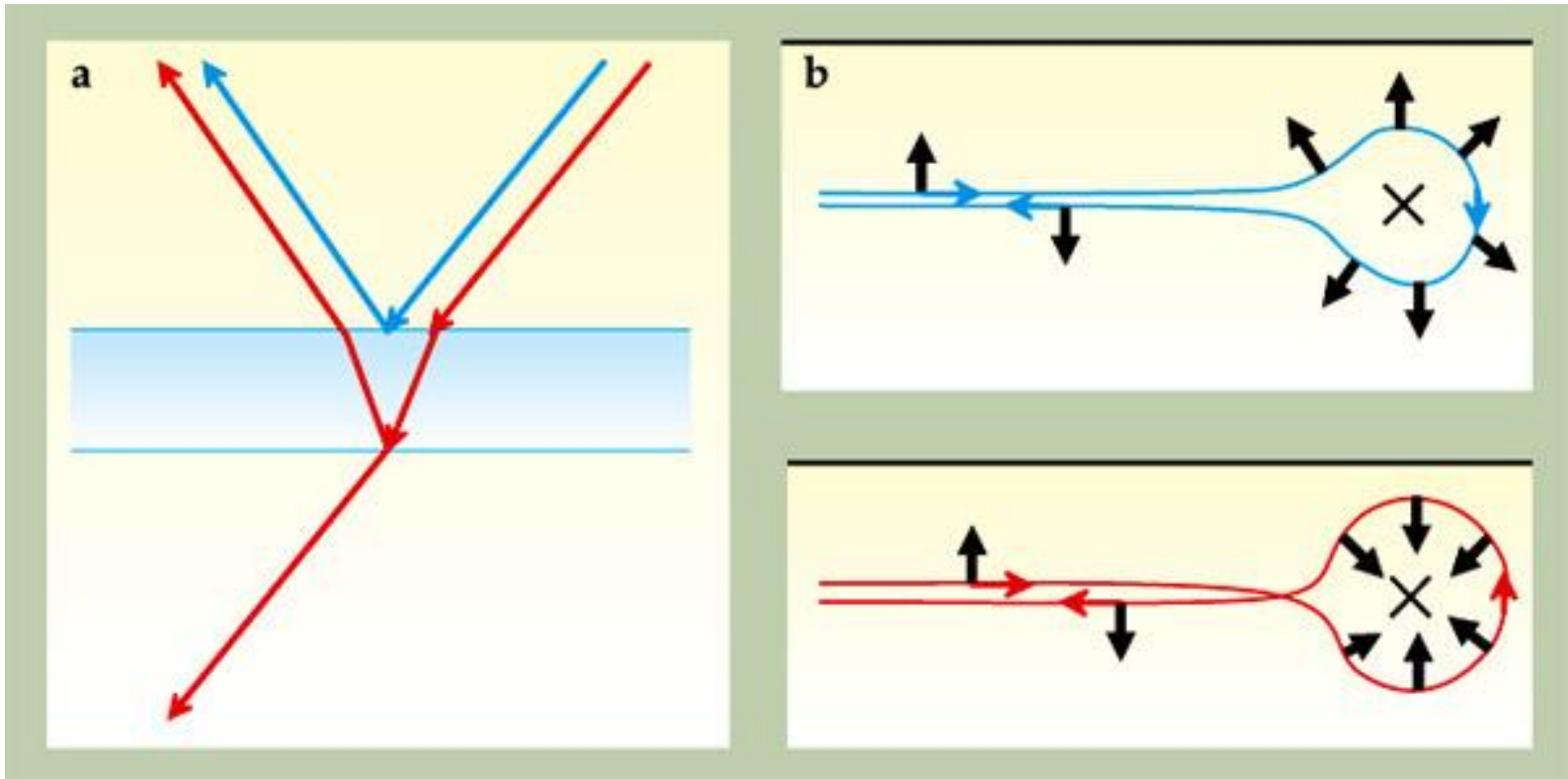
Figure 2. (a) On a lens with antireflection coating, light waves reflected by the top (blue line) and the bottom (red line) surfaces interfere destructively, which leads to suppressed reflection. **(b)**A quantum spin Hall edge state can be scattered in two directions by a nonmagnetic impurity. Going clockwise along the blue curve, the spin rotates by π; counterclockwise along the red curve, by $-\pi$. A quantum mechanical phase factor of -1 associated with that difference of 2π leads to destructive interference of the two paths—the backscattering of electrons is suppressed in a way similar to that of photons off the antireflection coating.

Figure 3. Mercury telluride quantum wells are two-dimensional topological insulators. **(a)** The behavior of a mercury telluride–cadmium telluride quantum well depends on the thickness d of the HgTe layer. Here the blue curve shows the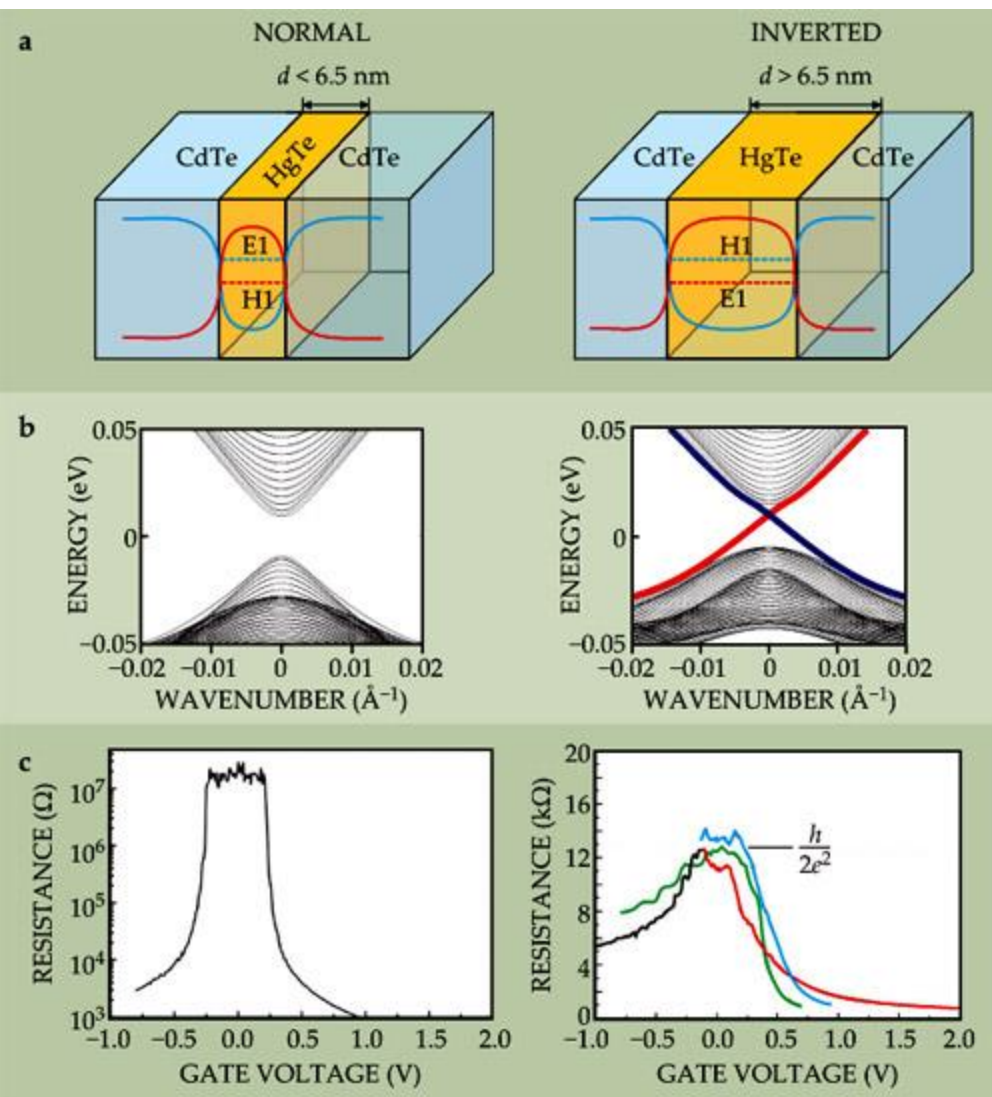 potential-energy well experienced by electrons in the conduction band; the red curve is the barrier for holes in the valence band. Electrons and holes are trapped laterally by those potentials but are free in the other two dimensions. For quantum wells thinner than a critical thickness $d_c \simeq 6.5$ nm, the energy of the lowest-energy conduction subband, labeled E1, is higher than that of the highest-energy valence band, labeled H1. But for $d > d_c$, those electron and hole bands are inverted. **(b)** The energy spectra of the quantum wells. The thin quantum well has an insulating energy gap, but inside the gap in the thick quantum well are edge states, shown by red and blue lines. **(c)** Experimentally measured resistance of thin and thick quantum wells, plotted against the voltage applied to a gate electrode to change the chemical potential. The thin quantum well has a nearly infinite resistance within the gap, whereas the thick quantum well has a quantized resistance plateau at $R = h/2e^2$, due to the perfectly conducting edge states. Moreover, the resistance plateau is the same for samples with different widths, from 0.5 μm (red) to 1.0 μm (blue), proof that only the edges are conducting.
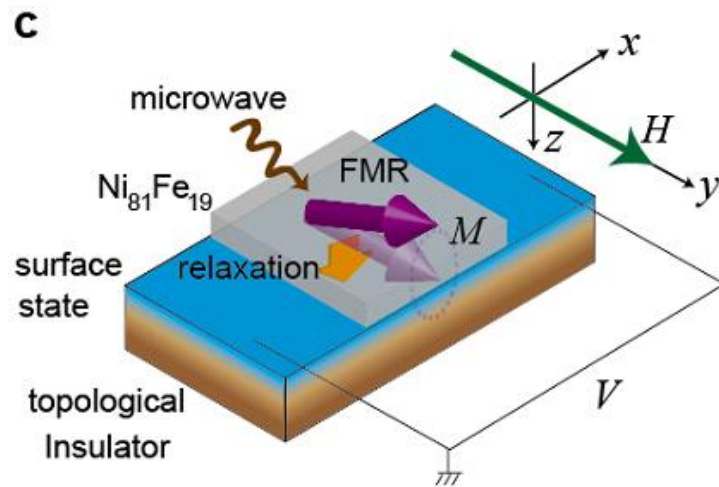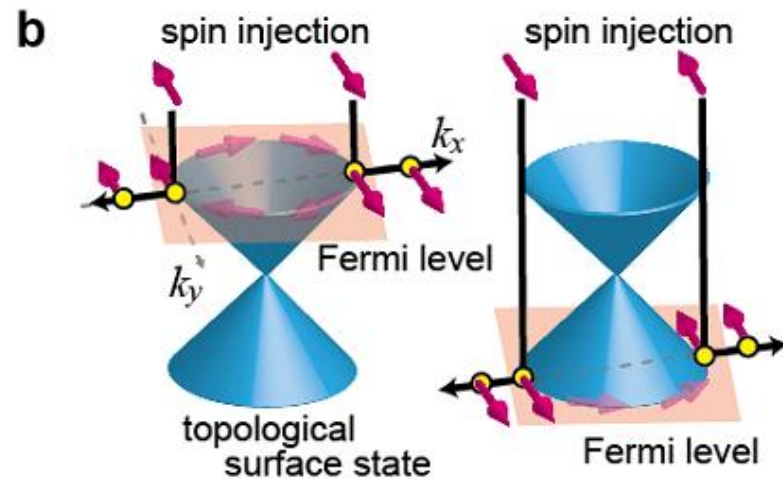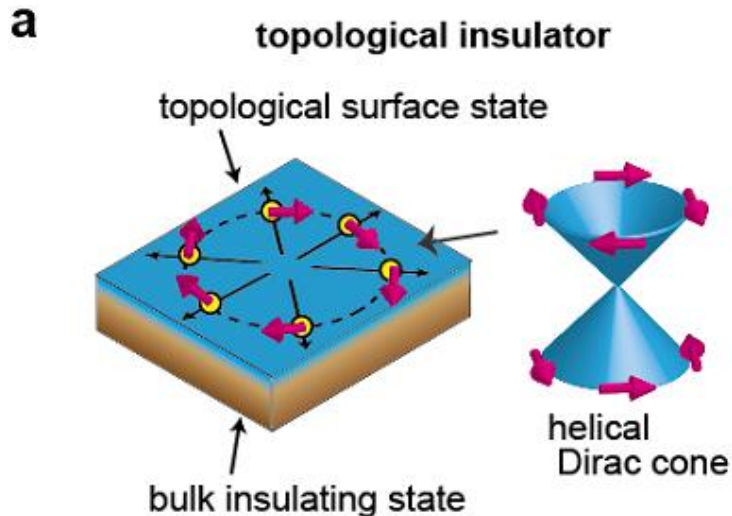
Angle Resolved Photo Emission Spectroscopy (ARPES)

Fig. 1. Electronic band structure of undoped Bi_2Se_3 measured by ARPES. (**A**) The bulk conduction band (BCB), bulk valence band (BVB), and surface-state band (SSB) are indicated, along with the Fermi energy (E_F), the bottom of the BCB (E_B), and the Dirac point (E_D). (**B**) Constant-energy contours of the band structure show the SSB evolution from the Dirac point to a hexagonal shape (green dashed lines). (**C**) Band structure along the K-Γ-K direction, where Γ is the center of the hexagonal surface Brillouin zone (BZ), and the K and M points [see (D)] are the vertex and midpoint of the side of the BZ, respectively (14). The BCB bottom is ~190 meV above E_D and 150 meV below E_F. (**D**) Photon energy–dependent FS maps (symmetrized according to the crystal symmetry). Blue dashed lines around the BCB FS pocket indicate their different shapes.
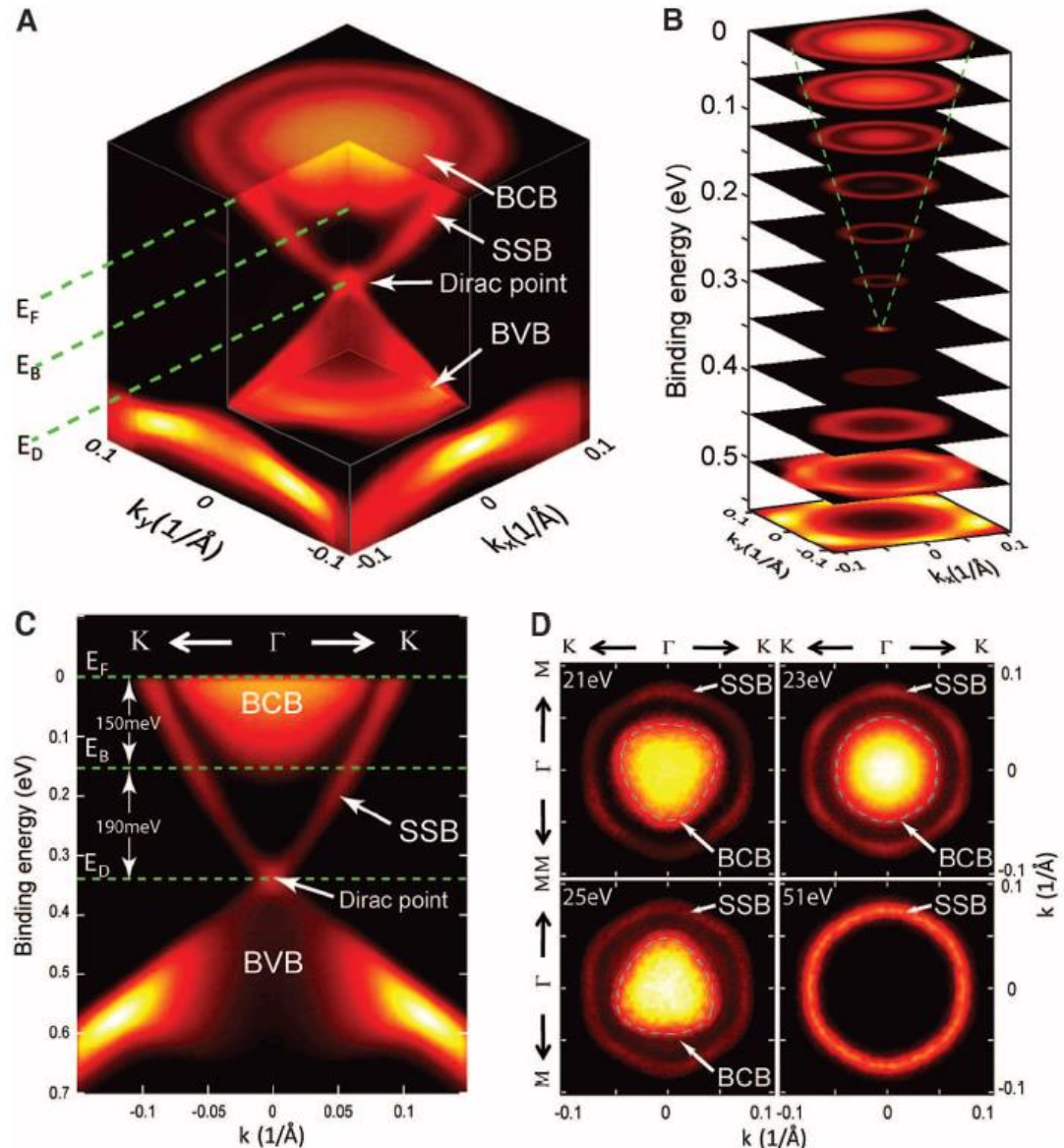
3 D topological insulators: Bi_2Sb_3, Bi_2Se_3, Bi_2Te_3, Sb_2Te_3. There is optical proof of the Dirac cone, but no transport evidence.

M. Z. Hasan, C. L. Kane

SCIENCE 329, 659 (2010)

Topological insulators for Spintronic

a topological insulator

topological surface state

helical Dirac cone

bulk insulating state

b spin injection — spin injection

k_x

k_y

Fermi level

topological surface state

Fermi level

c microwave

$Ni_{81}Fe_{19}$

FMR

M

surface state

relaxation

topological Insulator

x

z

H

y

V

A. TIs have topologically-protected metallic surface states.

spin-momentum locking: Conduction electrons states behave as Dirac fermions.

B. i.e. direction of the e-motion determines its spin direction.

C. if a spin imbalance is induced in the surface state by spin pumping, a charge current Jc is expected to show up along the "Hall" direction defined by Jc ∥ (z×σ)

Shiomi et. al., arXiv1312.7091 (2013).

Spin Chemical Potential Bias Induced Surface Current Evidenced by Spin Pumping into Topological Insulator Bi$_2$Te$_3$

Faris Basheer Abdulahad, Jin-Han Lin, Yung Liou, Wen-Kai Chiu, Liang-Juan Chang, Ming-Yi Kao, Jun-Zhi Liang, Dung-Shing Hung, and Shang-Fan Lee
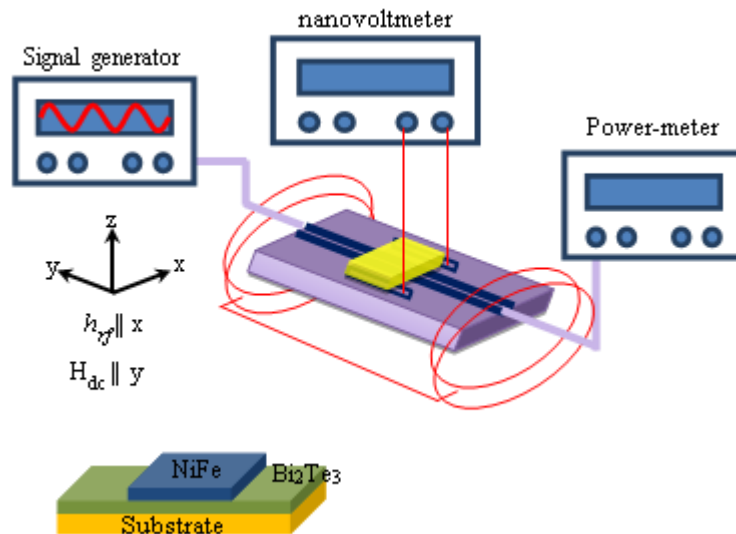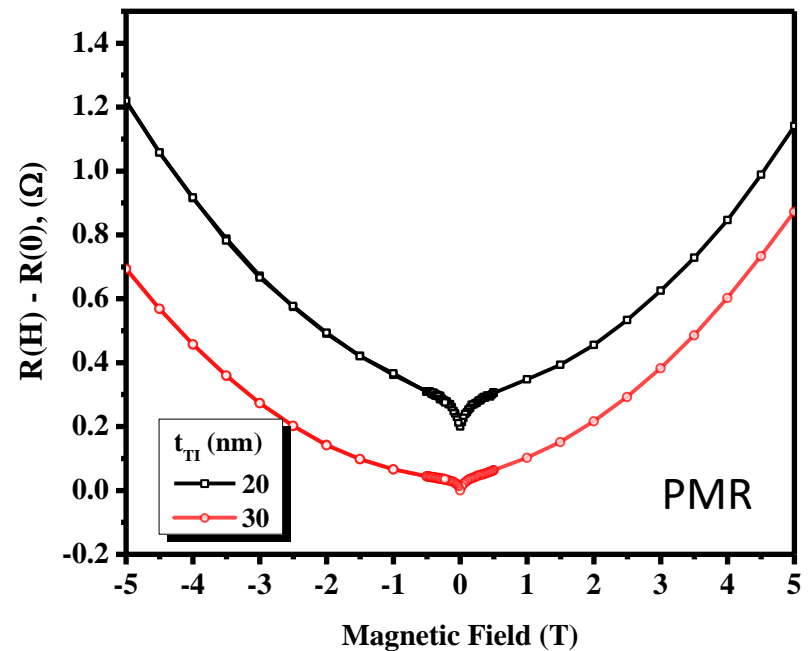
Transport measurements on Bi$_2$Te$_3$ films grown on sapphire (0001)

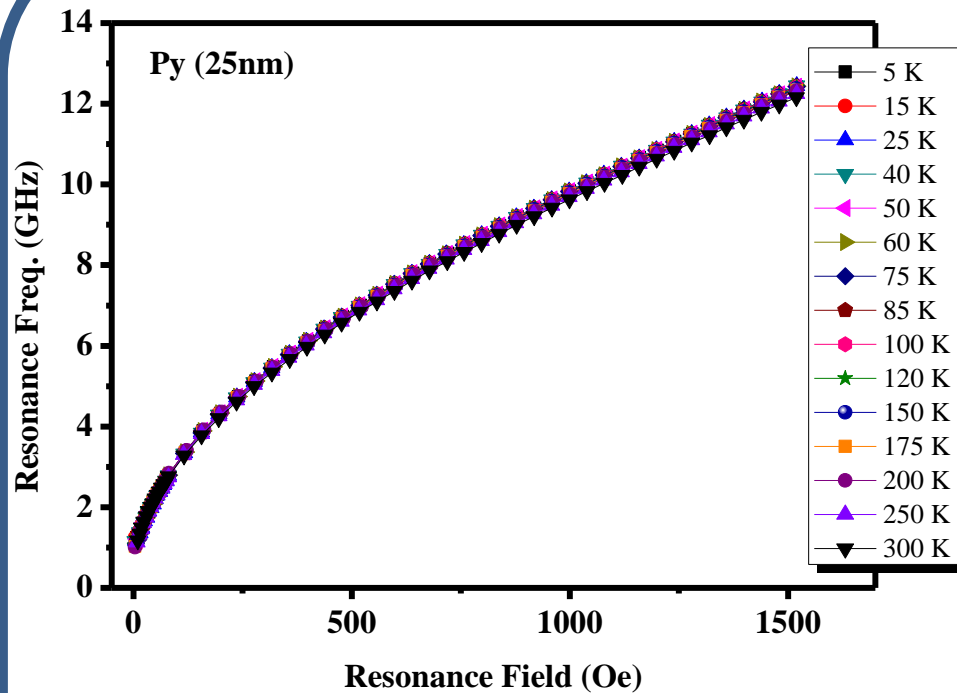t_{TI} = 30 nm

CB
E_F
SS
VB
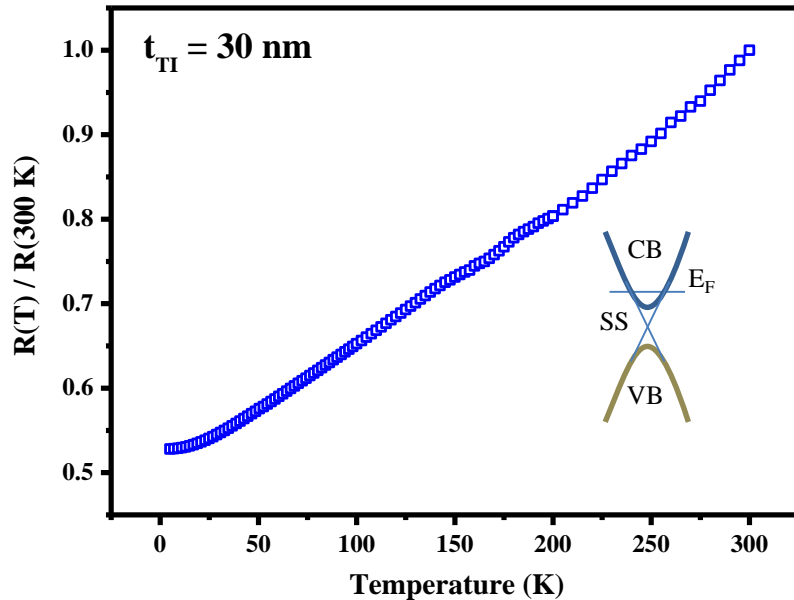
Temperature dependence of normalized resistivity for 30 nm sample measured under zero magnetic field. Inset shows the schematic illustration of the Fermi level.
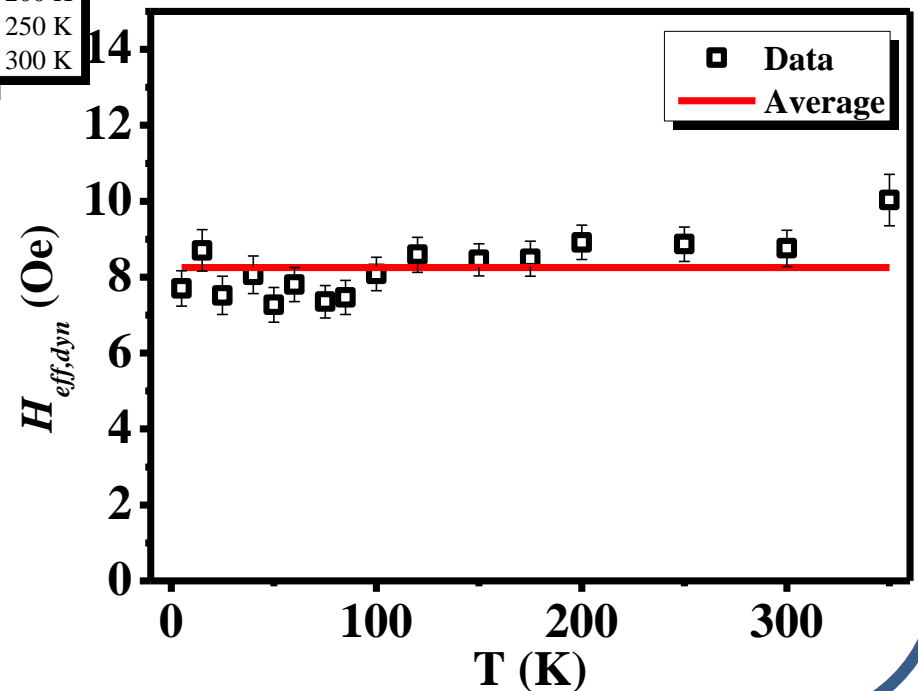
Magnetic field dependence of normalized resistivity for 20 nm (black) and 30 nm (red) samples at T = 5 K. The black curve is shifted for clarity.

t_{TI} (nm)
20
30

PMR

FMR for Py (25nm) single layer

Py (25nm)

Resonance Freq. (GHz) vs Resonance Field (Oe)

Legend:
- 5 K
- 15 K
- 25 K
- 40 K
- 50 K
- 60 K
- 75 K
- 85 K
- 100 K
- 120 K
- 150 K
- 175 K
- 200 K
- 250 K
- 300 K

$$f_{res} = \frac{\gamma}{2\pi}\sqrt{H_{\mathrm{FMR}}\left(H_{\mathrm{FMR}} + 4\pi M_S\right)}$$

$H_{eff,dyn}$ (Oe) vs T (K)

- Data
- Average

FMR for Bi$_2$Te$_3$/Py Bilayers
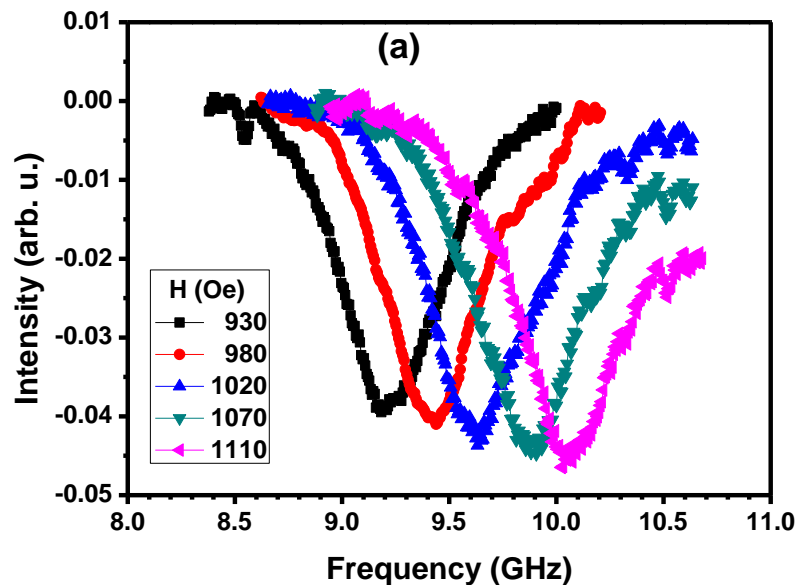
Temperature dependence measurements of FMR show upper left shift compared to single Py layers.
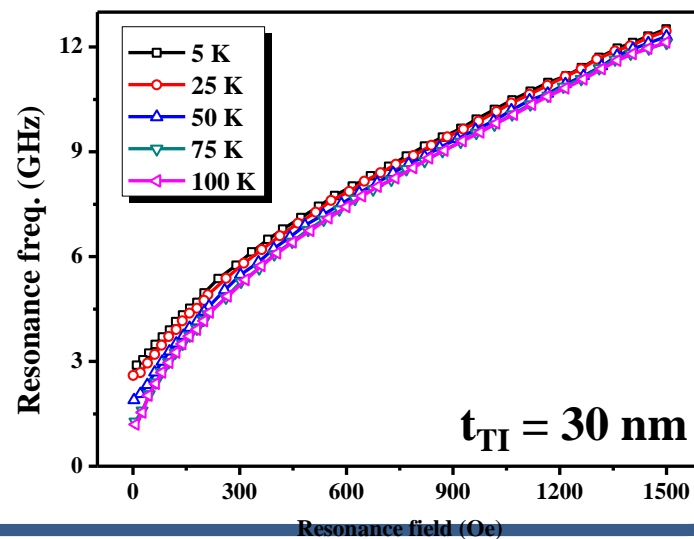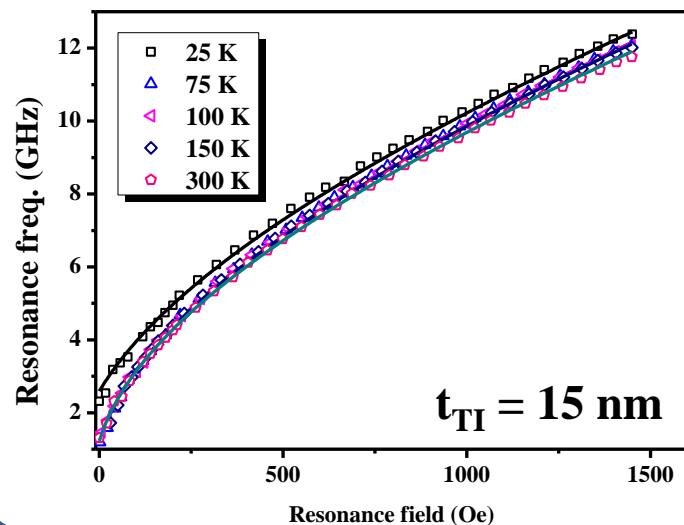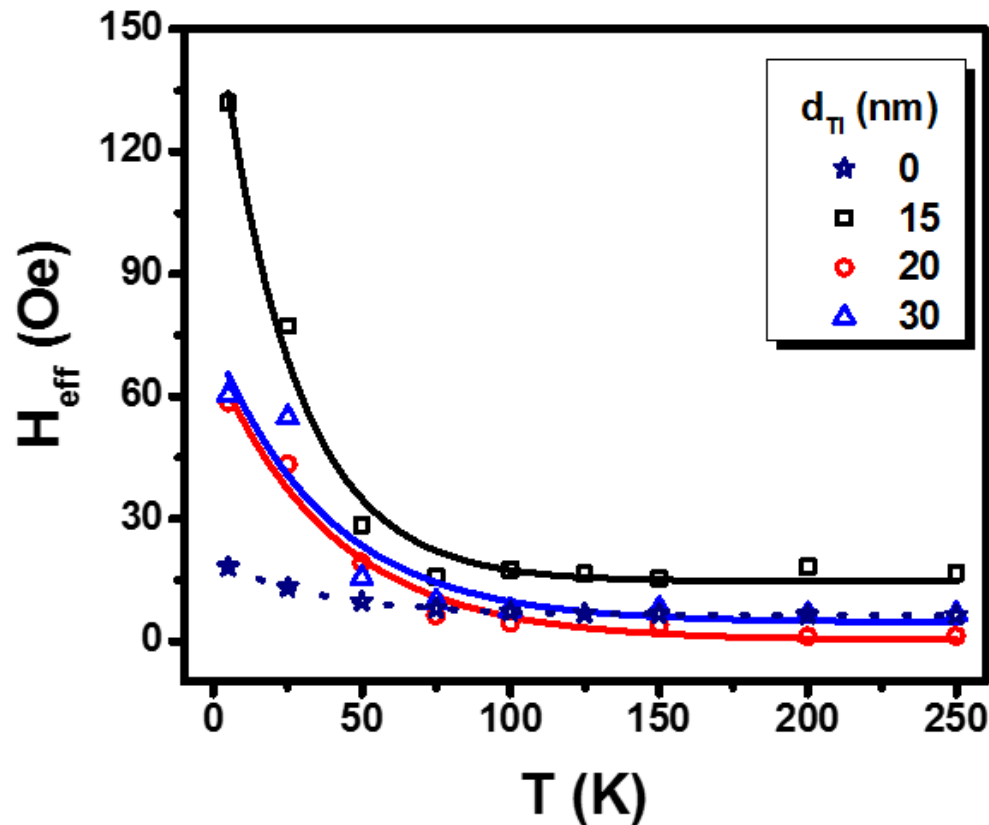
Possible effects:

- FM-anisotropy
- proximity effect
- FM/TI exchange coupling.

$$f_{res} = \frac{\gamma}{2\pi} \sqrt{(H_0 + H_{eff})\left((H_0 + H_{eff}) + 4\pi M_s\right)}$$

Temperature dependence of the effective field for the reference sample and 15, 20, and 30 nm Bi_2Te_3 samples.
Solid lines are exponential fits.

Bi₂Te₃/Py Bilayers

Bi₂Te₃ thickness dependence of FMR

Bi$_2$Te$_3$/Py Bilayers

H$_{eff}$ for Bi$_2$Te$_3$ thickness dependence

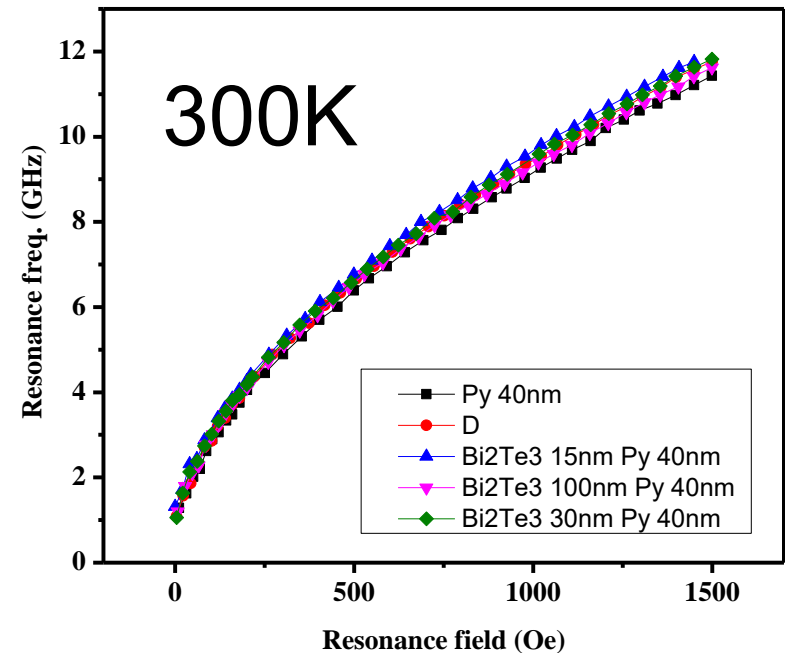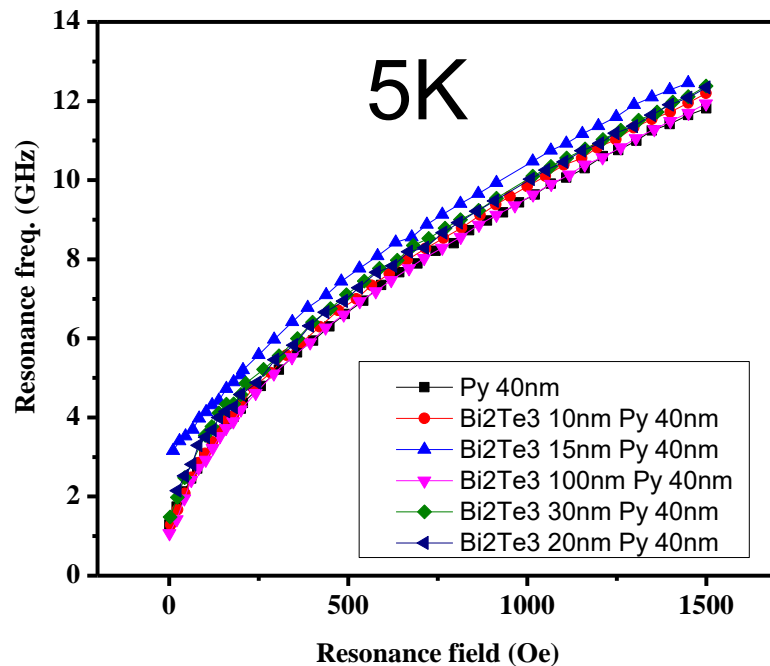|	$\Upsilon=1.8887E7$; M$_s$=8863.2 Oe (5K) $\Upsilon=1.88264E7$; M$_s$=8271.3 Oe (300K)	
	5K	300K
Py (40nm)	18.26 $\pm$1 Oe	6.64 $\pm$1 Oe
Bi$_2$Te$_3$ (10nm)/ Py (40nm)	27.79 $\pm$3.6 Oe	22.16 $\pm$3.43 Oe
Bi$_2$Te$_3$ (15nm)/ Py (40nm)	132$\pm$5.5Oe	44$\pm$5.4Oe
Bi$_2$Te$_3$ (20nm)/ Py (40nm)	58.5$\pm$4.25Oe	-
Bi$_2$Te$_3$ (30nm)/ Py (40nm)	60.344$\pm$5.5Oe	29$\pm$3.7Oe
Bi$_2$Te$_3$ (100nm)/ Py (40nm)	12.17$\pm$1.1 Oe	19.8$\pm$1.9 Oe

Summary

1. Large H_{eff} due to the spin pumping effect was observed for different Bi_2Te_3 thin films.

2. H_{eff} has a maximum value around t_{TI} = 15nm.

3. H_{eff} decreases with temperature exponentially; characteristic temperature T_0 ~ 25-33 K is on the energy scale of 2.5 meV.
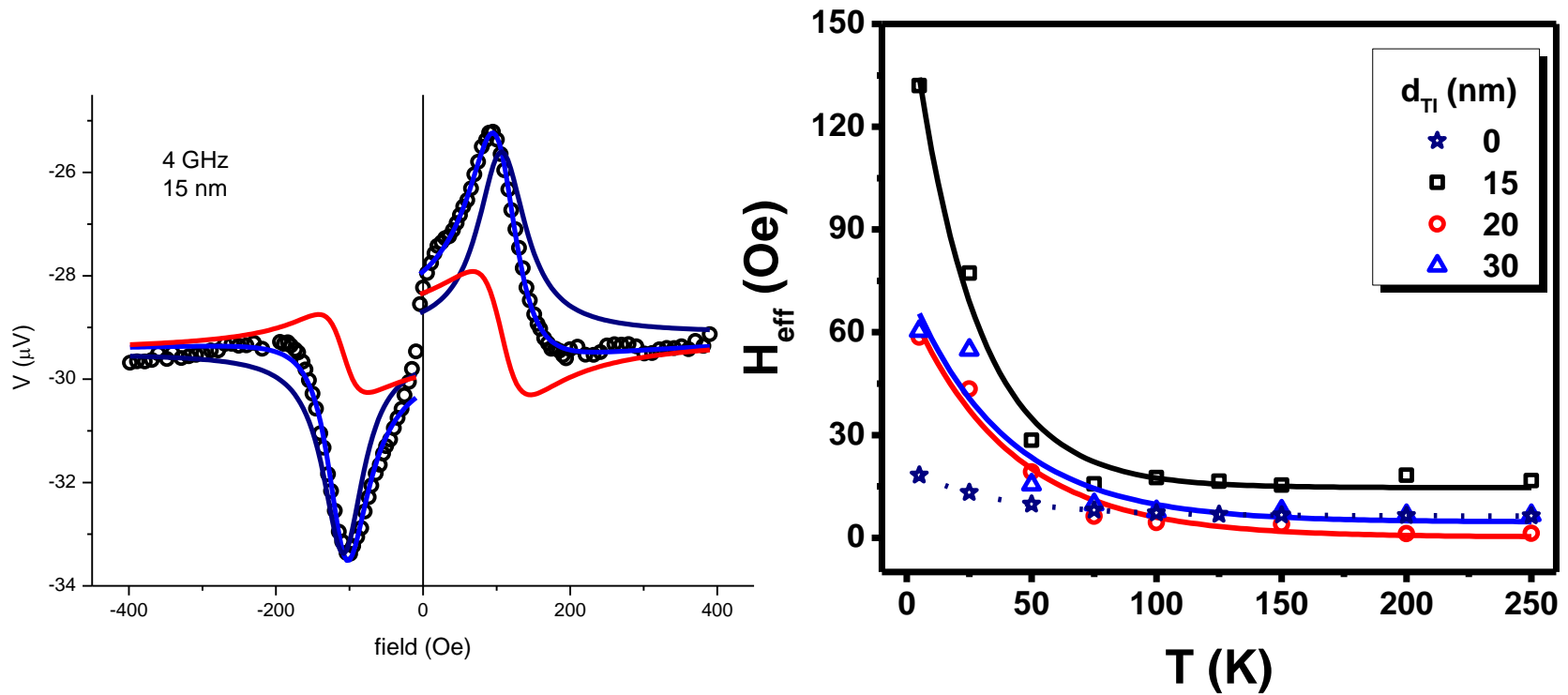
We observed an exchange coupling between NiFe and TI surface. The strength of this coupling decay with increasing temperature with a characteristic temperature ~25K, or ~2.2 meV.

Topological insulators and topological superconductors
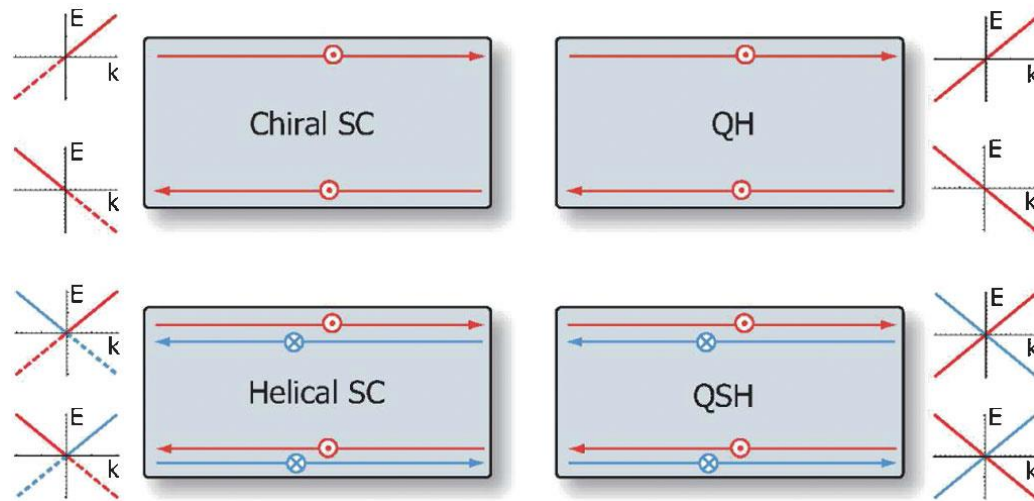
Schematic comparison of 2D chiral superconductor and QH states. In both systems, TR symmetry is broken and the edge states carry a definite chirality. (Bottom row) Schematic comparison of 2D TR invariant topological superconductor and QSH insulator. Both systems preserve TR symmetry and have a helical pair of edge states, where opposite spin states counterpropagate. The dashed lines show that the edge states of the superconductors are Majorana fermions so that the E<0 part of the quasiparticle spectrum is redundant. In terms of the edge state degrees of freedom, we have symbolically QSH = (QH)^2 = (helical SC)^2 = (chiral SC)^4.
From Qi, Hughes et al., 2009a.

Summary

- Giant Magnetoresistance, Tunneling Magnetoresistance
- Spin Transfer Torque
- Pure Spin current (no net charge current)
  - Spin Hall, Inverse Spin Hall effects
  - Spin Pumping effect
  - Spin Seebeck effect
- Micro and nano Magnetics
- Spin pumping into Topological Insulator, Topological Superconductor
- Spin logic
- Skyrmion

- Is Spintronics the next generation technology beyond 2020?

Is there better candidate in sight?

Spin Hall Magnetoresistance

Spintronics has evolved in many aspects other than material developments, including effects like Giant Magnetoresistance, Tunneling Magnetoresistance, Spin Transfer Torque, Spin Hall, Spin Pumping, Inverse Spin Hall, and more. The underlying idea was to investigate and manipulate the electron spin degree of freedom in addition to its charge in transport phenomena. However, charge transport is usually accompanied by Joule heating problem as the sizes of the electronics continue to shrink. Thus, devices that manipulate pure spin currents can be highly beneficial compared to traditional charge-based electronics. We now have "spin caloritronics", where one exploits the interaction between heat transport and the charge/spin carriers.

Spin caloritronic effect, such as spin Seebeck effect, has attracted a great deal of attention recently. The difference in the chemical potentials of the spin-up and the spin-down electrons can cause a pure spin current. This pure spin current can be detected by Pt strips via the inverse spin-Hall effect. In most cases such studies have been made on ferromagnetic thin films on substrates. The mechanism of spin Seebeck effect has evolved from the above-mentioned intrinsic difference in the spin chemical potentials when it was first reported experimentally to magnon-phonon interaction through the substrate in recent publication. We use patterned ferromagnetic thin film to demonstrate the profound effect of a substrate on the spin-dependent thermal transport [1]. With different sample patterns and on varying the direction of temperature gradient, both longitudinal and transverse thermal voltages exhibit asymmetric instead of symmetric spin dependence. This unexpected behavior is due to an out-of-plane temperature gradient imposed by the thermal conduction through the substrate and the mixture of the anomalous Nernst effects. Only with substrate-free samples have we determined the intrinsic spin-dependent thermal transport with characteristics and field sensitivity similar to those of anisotropic magnetoresistance effect.